Structural Plasticity and Network Dynamics in the Dorsal Hippocampus - Accumbal Circuitry

Vadim Koren

Thesis submitted for the degree of Doctor of Philosophy

St. John's College

University of Oxford

Trinity Term 2018

Abstract

Structural Plasticity and Network Dynamics in the Dorsal Hippocampus - Accumbal Circuitry

Vadim Koren, St. John's College

Thesis submitted for the degree of Doctor of Philosophy, Trinity Term 2018

The dorsal hippocampus has been implicated in the encoding of contextual information with particular involvement in spatial navigation. The nucleus accumbens is thought to promote the translation of higher order cognitive modalities into motor function directives. The dorsal hippocampus-accumbal circuitry has been postulated to promote the acquisition, consolidation and reinstatement of context specific reward seeking behaviour. However, the corresponding anatomical connectivity and physiological underpinnings of the translation of spatial representations into behavioural directives have not yet been established. This thesis entails the first study of the hippocampal dCA1-accumbal pathway whereby two complementary approaches were employed.

Synaptic plasticity mechanisms, believed to underly experience dependent functional adaptations in the hippocampus and nucleus accumbens, have been shown to correlate with structural changes in dendritic spine morphology. For the sake of their study, invasive techniques have been established, however have been shown to incur significant damage to associated circuitries, rendering insights into structural plasticity in deep brain regions challenging. This thesis entails the first full in vitro and in vivo proof of principle of a new approach toward minimally invasive high resolution deep brain imaging of dendritic spines utilising adaptive optics and holographic light propagation through a single optical fibre, thinner than a human hair. This technology reduces the footprint and thus resulting tissue damage by two orders of magnitude while maintaining diffraction limited resolution. This work might facilitate future investigations of structural synaptic plasticity in deep brain circuitries such as the hippocampal dCA1-accumbal pathway (supervisor: Prof. Dr. Nigel Emptage).

There has been indication that spatial information guided behaviour might be dependent on a functionally intact integrated dorsal hippocampus - accumbal circuitry. In order to study the downstream effect of dorsal hippocampal spatial information processing on the network dynamics of the accumbal circuitry, large scale multichannel electrophysiological recordings combined with optogenetic stimulation were employed simultaneously in both structures. dCA1 pyramidal cell long range projections were shown to mono-synaptically drive the activity of parvalbumin expressing interneurones in the NAc which in turn orchestrate the activity of medium spiny neurons through feed forward inhibition in a context dependent manner. This facilitates the selective activity of discrete medium spiny neuron cohorts and supports the translation of neural representations of space into spatial appetitive behaviour. Furthermore, this work might help to conceptualise how the nucleus accumbens can act as a gateway for converging and potentially competing input from different corticolimbic systems (supervisor: Ass. Prof. Dr. David Dupret).

Acknowledgements

Firstly, I would like to thank my supervisors Prof. Dr. Nigel J. Emptage and Ass. Prof. Dr. David Dupret. Their joint guidance and leadership allowed me not only to learn and apply a wide range of state-of-the-art experimental techniques at the cutting edge of scientific research, but also to grow professionally as well as personally.

In addition, I would like to express gratitude to the members of the two groups established by Nigel and David, for all their support and help over the past few years. Special thanks go to Dr. Stephanie Trouche in David's lab as well as to Dr. Sebastian Vasquez-Lopez in Nigel's lab for their collaboration on the two projects, which resulted in manuscripts currently under review (Trouche, Koren et al. 2019; Vasquez-Lopez, Koren et al. 2018).[1] Furthermore, this work would not have been possible without the help of many others, most notably Dr. Natalie M. Doig, Dr. Tommas J. Ellender, Dr. Vítor Lopes-dos-Santos, Dr. Pavel V. Perestenko, Dr. Mohamady El-Gaby, Dr. Gido van de Ven as well as Dr. Zahid Padamsey and Dr. Martin Plöschner, who have contributed so much[1]. Finally, I would also like to thank Prof. Dr. Tomas Cizmar, Prof. Dr. Peter J. Magill and Ass. Prof. Dr. Andrew Sharott for their external collaboration on these projects.

In addition, I would like to thank the members of the MRC BNDU as well as the wider Department of Pharmacology for the productive scientific atmosphere. I am grateful to the support staff, in particular to Jane Janson and Liz Norman. I thank Ass. Prof. Dr. Andrew Sharott and Prof. Dr. Martin Booth for helpful comments on my Transfer of Status report and my Confirmation of Status presentation. My DPhil studies have been funded by a Medical Research Council Doctoral Training Award and St John's College.

1 all respective individual contributions are acknowledged explicitly whenever first introduced/referenced in the thesis

Contents

Figures

Table

Abbreviations

AAV	Adeno-associated virus
AOD	Acousto-optic deflector
ArchT	Archaerhodopsin-T
BLA	Basolateral amygdala
BNDU	MRC Brain Neural Dynamics Unit Oxford
CAG	Cre-inducible promoter
CaM	Calmodulin
CaMKII	Ca2+/calmodulin-dependent protein kinase II
CCD	Charge coupled device
ChR2	Channelrhodopsin2
CPP	Conditioned Place Preference
CPU	Central processing unit
CR	Calretinin
Cre	Tyrosine recombinase enzyme
D1/D2	Dopamines receptors
DAPI	4',6-diamidino-2-phenylindole
Dbscan	Density-based spatial clustering of applications with noise
dCA1	CA1 region of the dorsal hippocampus
DIO	LoxP recognition sites
DPhil	Doctor of Philosophy
DM	Dichroic mirror
DMD	Digital micro-mirror device
DREADDs	Designer receptor exclusively activated by designer drugs
dSub	Dorsal Subiculum
EEG	Electroencephalography
EF1a	Cre-inducible promoter
EPSP	Excitatory postsynaptic potential
flex	LoxP recognition sites
FlpO	Recombinase
fMRI	Functional magnetic resonance imaging
(p)FSIs	(Putative) fast spiking interneurons
GABA	γ-Aminobutyric acid
GCaMP	Engineered protein consisting of a per-mutated Green Fluorescent Protein, Calmodulin and M13 peptide
(E)GFP	(Enhanced) green fluorescent protein
GLM	Generalised linear model
GPU	Graphics processing unit
GRIN	Lens gradient-index lens
HEPES	(4-(2-hydroxyethyl)-1-piperazine ethanesulfonic acid
HPc	Hippocampus
ISI	Inter-spike-interval
IPSP	Inhibitory postsynaptic potential
Jaws	Red shifted cruxhalorhodopsin
LED	light-emitting diode
LFP	Local field potential
LoxP	Cre dependent recombination site
LTD	Long-term depression
LTP	Long-term potentiation
mCherry	Red fluorescent protein
MMF	**M**ultimode fibre
MO	Microscope objective
(p)MSNs	(Putative) medium spiny neurons in the NAc
NA	Numerical aperture
NAc	Nucleus Accumbens
NPBS	Non-polarising beam splitter
NPY	neural protein
OI	Optical isolator
PB	0.1 M phosphate buffer
PBS	0.1 M phosphate-buffered saline
PBS	Polarising beam-splitter
PBS-T	PBS with 0.25 % Triton X-100
PC	Principal cells
PCA	Principle component analysis
PFA	Paraformaldehyde
PFC	Prefrontal cortex
PMT	Photo multiplier tubes
PMF	Polarisation maintaining fibre
PV(+)	Parvalbumin (expressing)
PYR	Pyramidal cells
RMS	Root mean square
SD	Standard deviation
SE	Standard error
SEM	Standard error of the mean
SLM	Spatial light modulator
SMF	**S**inglemode fibre
SST	Somatostatin
STDP	spike-timing-dependent potential
(p)TANs	(Putative) tonically active neurons
Thy1	Thymus cell antigen 1
TM	Tranformation matrix
VTA	Ventral tegmental area
WGA	Wheat-germ agglutinin
WPRE	WHP post transcriptional response element
(E)YFP	(Enhanced) yellow fluorescent protein

CHAPTER 1: GENERAL INTRODUCTION

1.1) Development and structural/functional integration of subcortical brain structures

The development of the vertebrate nervous system begins with the neural induction: the structural specialisation of the ectoderm at the gastrula stage of embryonic development (Spemann & Mangold 1924). During the subsequent process of neurulation, this structure goes on to alter its morphology to give rise to the neural tube. This process is facilitated by inter-cellular cohesion mechanisms and represents the first spatial tissue organisation. The thereby established axial directionality allows for the following molecular gradient triggered development of distinct cellular identities along the axis of the tissue (anterior-posterior patterning). With continued structural growth and differentiation, the neural tube formation derives the prosencephalon (forebrain), the mesencephalon (midbrain) and the rhombencephalon (hindbrain) (summerised well by Evans et al. 2012). The prosencephalon gives rise to the telencephalon, which in turn develops into the neocortex, archicortex (including hippocampus), paleocortex and the diencephalon which begets diverse structures such as the striatum (including nucleus accumbens). The mesencephalon, metencephalon and myelencephalon (the derivates of the rhombencephalon) finally, give rise to neuronal structures such as the thalamic structures, the midbrain, the cerebellum as well as the medulla.

The structural specialisation of neuronal tissue is accompanied by the functional diversification of individual cells. Not only do different neuronal cell types arise through genetic differentiation, they do so also through functional dedication to distinct operational tasks. Hereby, functional cohorts of neurons integrate into higher order entities of purposeful information relay and processing: circuitries. The early architecture of brain circuits, i.e. the connectivity between differentiated brain cells, is cued by the topical distribution of molecular signals in the extracellular matrix, which enables axonal guidance over long distances and thus a first crude and unrefined wiring of local processing units into the larger context of the

global brain circuitry. Once rudimentary neuronal connectivity is established, electrical inter-cellular communication becomes available as the substrate for further activity-dependent refinement of the information relay architecture in interaction with the environment and in accordance with its requirements. This developmental process explains a fundamental principle of the organisational dichotomy of the neural circuitry in the brain: the disintegration of information into local processing units and their concomitant integration through long range projections.

Traditionally, different brain regions have been ascribed to perform distinct tasks in accordance with the principle of spatial disintegration of information processing. This notion however has been shown to fall short in explaining various physiological and pathophysiological phenomena, that arise from the systemic spatio-temporal integration of neuronal activity between multiple local circuitries. Not only does their integration through long range projections functionally amount to more than "the sum of its parts", but it has also been demonstrated that the intrinsic structural architecture of a given local circuitry cannot be fully understood in isolation, without knowledge of its extrinsic connectivity (Brown et al. 2009). Finally, even after the structural hardwiring during the initial developmental stages, activity dependent synaptic plasticity continues to provide a way to optimise an animal's capacity to process information in accordance with changing environmental requirements through the modulation of the functional network dynamics (Brown et al. 2009). As Leong et al. so accurately put it: "[…] In order to understand how function and behaviour are generated within a circuitry, the mutual interdependence of neural activity and its corresponding structural correlate have to be studied. One of the biggest challenges facing contemporary neuroscience is to provide an integrated mechanistic model of the spatiotemporal activity pattern within the wider scope of large-scale brain wide interactions." (Leong et al. 2016)

1.2) Neural circuitry for reward

1.2.1) Structural synaptic plasticity in the neural circuitry for reward

Some principles of such integrated spatio-temporal dynamics of large scale interactions between subcortical structures and their structural correlate can be illustrated on the example of the brain reward circuitry. This neuronal system is involved in the processing of valence related information and has been subject of extensive research over the past decades. Multiple neuronal structures are hereby involved, most notably the nucleus accumbens (NAc), the amygdala, the ventral tegmental area (VTA), the prefrontal cortex (PFC) as well as the hippocampus (HPc). Traditionally, those brain regions have been ascribed to perform distinct tasks: the hippocampus was associated with mnemonic performance, the amygdala with emotions, the ventral tegmental area with motivation, the prefrontal cortex with cognition and the nucleus accumbens with appetitive behaviour. Together, they constitute the so-called mesolimbic system and are imperative in the recognition, evaluation, motivation and storage of information associated with reward (Russo and Nestler, 2013). Furthermore, addictive substances are thought to act at different regulatory levers of this circuitry, effectively highjacking the system (Ron et al. 2016).

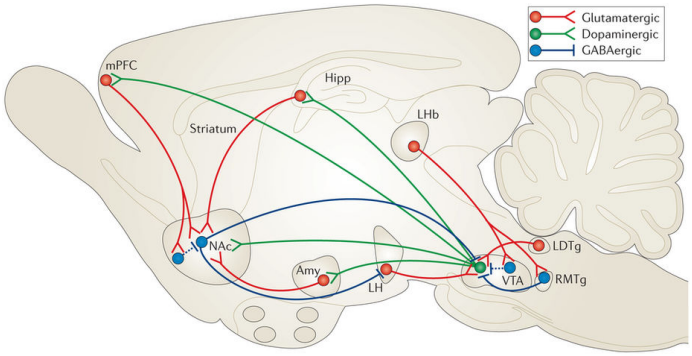

Fig. 1.1: Neural circuitry for reward: mesolimbic system consisting of the nucleus accumbens (NAc), the amygdala, the ventral tegmental area (VTA), the prefrontal cortex (PFC) and the hippocampus (HPc) with the corresponding most prominent glutamatergic, dopaminergic and GABAergic long range projections (adapted from Russo and Nestler, 2013)

In the study of structural synaptic plasticity, the HPc has served as the main model structure due to the relative simple preparation of its in-vitro tissue cultures allowing for direct optical, pharmacological and electrophysiological access to a highly organised connectivity architecture among separated neuronal populations. The hereby facilitated synaptic

manipulation ultimately led to the discovery of long term potentiation (LTP) at the Schaffer collaterals in 1973 (Bliss et al. 1973a, Bliss et al. 1973b, Bliss et al. 2007). LTP like modulations of synaptic efficacy have been demonstrated in alive animals and implicated as physiological correlates of mnemonic processing (Whitlock et al. 2006, Gruart et al. 2006). In addition to LTP, further synaptic plasticity mechanisms were described, most notably long term depression (LTD) (Dudek et al. 1992), excitatory post-synaptic potential (EPSP) spike potentiation (Abraham et al. 1985) and spike-timing-dependent plasticity (STDP) (Dan et al. 2004) (summarised well by Neves et al. 2008). Whilst in vitro research has been imperative in the elucidation of the molecular substrate of synaptic plasticity (Malenka et al. 2004), in order to explore physiological, behaviourally relevant synaptic plasticity, in vivo approaches had to be developed. Significantly, synaptic plasticity mechanisms such as LTP and LTD are correlated with structural alterations in the morphology of dendritic spines, which are postsynaptic membrane specialisations harbouring the excitatory synaptic apparatus (Harris et al. 1989, Takumi et al. 1999, Petralia et al. 1999, Bosch et al. 2012, Engert et al. 1999, Maletic-Savatic et al. 1999). This allows for a quantifiable read-out of synaptic plasticity on a large scale, provided that optical access can be achieved. Multiple different experimental approaches have been established to provide optical access to subcortical brain structures, most notably the mechanical aspiration (i.e. removal) of overlying tissue and the insertion of optical probes such as microscope objectives (Dombeck et al. 2010), graded index (GRIN) lenses (Barretto et al. 2011, Resendez et al. 2016) or fibre bundles (Szabo et al. 2014) (Vasquez-Lopez, Koren et al. 2018).

Importantly, early stage pathologies of neurological conditions such as Alzheimer's and Parkinsons have been correlated with structural changes in dendritic spine morphology in various deep brain structures, most notably the HPc and the striatum (Auffret et al. 2009, Moolman et al. 2004, Villalba and Smith 2018, Smith et al. 2009; Vasquez-Lopez, Koren et al.

2018). These findings underscore the need for the relation of acute structural changes in dendritic spine morphology within those networks to ongoing behavioural and experimental conditions in order to understand the intricate relationship between neuronal activity and its structural correlate. Such studies have been conducted mostly in superficial and easily accessible neuronal structures such as the peripheral nervous system (Kerschensteiner et al. 2005, Bareyre et al. 2005) and the cortical layers (Tsai et al. 2004, McLellan et al 2003, Meyer-Luehmann et al. 2008)(summerised by Barretto et al. 2011). Unfortunately, due to reasons, which will be discussed later, so far only few studies were able to provide results of this kind in the aforementioned deep brain structures, and the ones that did, focused mainly on structures immediately below the cortex. Nevertheless, some notable advances have been made in the exploration of a few disease models on a sub cellular level in deep brain structures in vivo. Structural changes of dendritic spines due to epileptic seizures for instance were investigated with the aforementioned technical approaches not only in the cortex (Rensing et al. 2005), but also in the hippocampal structure (Mizrahi et al 2004) and were shown to correlate with the severity and quantity of the episodes (Misgeld et al. 2006). Barretto et al. went one step further and imaged dendritic arbours and cerebral microvasculature not only in the HPc, but also in the striatum (Barretto et al. 2011). They were able to study glioma angiogenesis and to establish biomarkers such as vessel size and blood-flow speed. All in all however, the field of in vivo structural synaptic plasticity imaging in deep brain structures remains severely limited by the associated technical challenges.

Finally, while great advances in the functional imaging of neuronal cell population activity have been made with the aforementioned invasive optical probes as well (Sheffield et al. 2015, Jennings et al. 2015), their large footprint usually does not permit the recording of

multiple deep brain structures simultaneously, necessitating the employment of electrophysiological recording techniques such as described in the following.

1.2) Information relay in the neural circuitry for reward

Improvements in electrophysiological in-vivo recording technology (e.g. multisite recordings through independently moveable tetrodes) have made it possible to gain insight into the integrated workings and functional interactions between individual structures of the mesolimbic system during animal behaviour (summarised well by Russo et al. 2013). Hereby, the experimental manipulation of individual cross-structural pathways allowed for the correlation of the interdependence of different brain structures and its corresponding effect on the behavioural output. This methodology helps to transcend the restrictions of the "roles" traditionally assigned to the respective brain regions, enabling the study of the dialectic interrelation between information processing units in the wider context of brain wide information relay.

Various studies using genetic knock-outs, pharmacological intervention and lesions have shown that dopamine neurons in the VTA are essential in the generation of reward induced motivational states and learning (Berridge et al. 2009; Flagel et al. 2011; Ikemoto and Bonci 2014; Ilango et al. 2014; Schultz 2007; Schultz 2013) (Han X et al. 2017). Behavioural and electrophysiological read-out allowed for the correlation of those cells' activity with predicted and acquired rewards and the resulting behavioural adaptations (Han X et al. 2017). While stimulation of VTA dopaminergic neurons was sufficient to drive intracranial self-stimulation in rats (Adamantidis et al. 2011; Kim et al. 2012; Pascoli et al. 2015; Witten et al. 2011)(Han et al. 2017), it has only been due to an integrated network approach that the functional effect of those neurons on downstream target circuitries and the behavioural modulation of those projections could be delineated. The VTA projects to multiple brain regions, notably the NAc, amygdala and HPc. The VTA-NAc pathway provides the information of valence in the

initiation of guided behavioural output through transient and phasic release of dopamine in the NAc (Sombers et al. 2009). Stimulation of VTA-NAc axonal projections within the NAc leads to reinforcement of appetitive behaviour (Han et al. 2017). Acute administration of most addictive substances leads to a down regulation of this input (Koob and Volkow, 2010). As for the VTA-HPc pathway, Dr. Colin McNamara in the Dupret lab has recently shown that stimulating VTA-hippocampal dCA1 projections leads to strengthened reward guided performance in a spatial memory task. The release of dopamine in the dCA1 supported the reactivation of environment specific cell assemblies during sleep following memory acquisition, and their reinstatement in subsequent trials (McNamara et al. 2014). Finally, VTA-amygdala projections are responsible for most of dopamine release within the amygdala (Bjorklund and Dunnett, 2007). Pharmacological inhibition of those projections as well as pharmacological interference with dopaminergic neurotransmitter release or receptor function in the amygdala detrimentally affects the animal's ability to perform in fear conditioning tasks (Nader and LeDoux, 1999; Guarraci et al. 1999, 2000; Greba and Kokkinidis, 2000; Greba et al. 2001; Fadok et al. 2009) (Cho and Fudge, 2009). As such, VTA dopaminergic cell activity can orchestrate differential behaviourally relevant modulation of downstream functional network dynamics depending on the respective output circuitry. With an appropriately designed experimental set-up that allows for the effective dissection of the physiological and behavioural role of a pathway, these downstream effects can thus be studied in isolation.

While exemplifying task-dependent downstream effect specificity, VTA long range projections are mainly dopaminergic and as such not representative of the vast majority of neurotransmitter based signalling within the global brain circuitry. Dopaminergic neurons possess unique qualities such as the interconnection through electrical synapses and the diffuse neurotransmitter release into the extracellular space by specialised axonal terminals. This allows for the synchronised release of large quantities of dopamine within the downstream structures (Vandecasteele et al. 2005, Glimcher 2011, Brown et al. 1997). This

mode of information relay can be contrasted with the point-to-point long-range glutamatergic signalling employed by structures such as the amygdala, which projects prominently to the NAc and the HPc. This spatial and temporal precision in information relay allows for a more selective and specific regulation of the downstream network physiology. The amygdala is thought to be imperative in the formation of associative fear and reward memories (Russo et al. 2013). Multiple studies have shown that the optogenetic stimulation of the amygdala leads to the initiation and consolidation of fear associations and avoidance behaviour (Johansen et al. 2010, Huff et al. 2013) (LaLumiere 2014). Similarly to the VTA, the stimulation of projections from the amygdala to the NAc promotes reward cued behaviour, while their inhibition has the reverse effect (Stuber et al. 2012). Summarised well by LaLumiere (LaLumiere 2014), optogenetic stimulation of amygdala projections to the ventral HPc increased anxiety symptoms (Felix-Ortiz et al. 2014) and their silencing decreased the same. Importantly, this work also used electrophysiological means to investigate the physiological effect of the pathway stimulation. By doing so, these projections were not only shown to directly target hippocampal pyramidal cells, but also to recruit an indirect feed forward mechanism through the activation of local inhibitory interneurons. A similar mechanism will be investigated within the scope of this thesis in the interaction between the dorsal HPc and the NAc.

The structural and functional characteristics of these two brain regions, the HPc and the NAc, will be discussed further in the following.

1.3) Hippocampus

Hippocampus structural architecture

The three-layered archicortex, which is one of the derivates of the telencephalon, encompasses the hippocampal formation. This "seahorse"-shaped structure is formed through the inward folding of the cerebral cortex, which thins out from its generic six-layered architecture. The hippocampal formation is composed of three distinct structures: the dentate gyrus, the CA layers (CA1, CA2 and CA3; hippocampus proper) as well as the subiculum (van Strien et al. 2009). The three layers corresponding to each of the structures exhibit architectural differences in accordance with their respective functional role. The most superficial layer contains the apical dendrites of hippocampal cells and is the layer which integrates and provides external input from adjacent hippocampal subregions to the local cell cohort. In the subiculum and dentate gyrus this layer is called stratum moleculare, while in the CA formations the same layer has multiple sublayers called the stratum lacunosum moleculare, stratum radiatum and stratum lucidum (not present in CA1 and CA2, van Strien et al. 2009). The next-deeper layer is called stratum pyramidale in the CA formations as well as the subiculum and granule layer in the dentate gyrus. This layer contains the cell bodies of the principal cells and interneurons of the hippocampal sub-formations and is dedicated to the

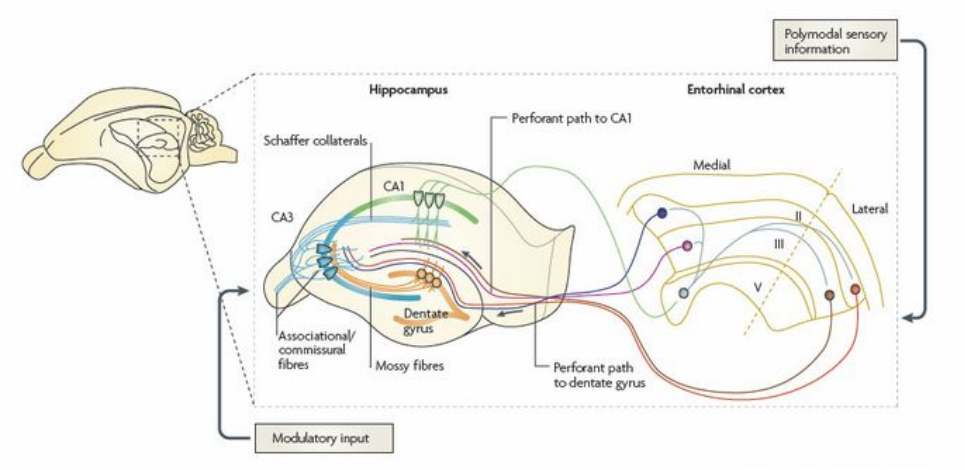

Fig. 1.2: Hippocampal structural architecture. The hippocampal formation is composed of three distinct structures: the dentate gyrus, the CA layers (CA1, CA2 and CA3) and the subiculum. The main afferent input to the hippocampal formation comes from the entorhinal cortex, whereby its pyramidal cells project to the subiculum, which in turn innervates mostly the dentate gyrus. The dentate gyrus projections, referred to as mossy fibres, connect to the CA3, which itself then innervates the CA1 (Neves et al. 2008)

local processing of the largely unidirectional information stream passed through the hierarchically structured hippocampal formation. The deepest layer contains afferent and efferent axons and interneurons. In the hippocampal CA formations, this layer is called stratum oriens, in the dentate gyrus it's the hilus (summerised well by van Strien et al. 2009).

This hippocampal circuitry has been extensively studied in the past 100 years due to its clear hierarchical organisation (so-called "three-synaptic"), which allows for a differential approach in the study of the information relay through the hippocampal formation. The main afferent input to the hippocampal formation comes from the entorhinal cortex, whereby its pyramidal cells project to the subiculum, which in turn innervates mostly the dentate gyrus. The dentate gyrus projections, referred to as mossy fibres, connect to the CA3, which itself then innervates the CA1 through so called Schaffer collaterals (ipsiateral) and commissural fibres (contralateral) (Amaral and Witter, 1989, Sun et al. 2014). Furthermore, the CA1 receives multiple further inputs from sources like the entorhinal cortex (Steward and Scoville, 1976) or the medial septum (Freund and Antal, 1988; Gulyas et al. 1990, Sun et al. 2014). Apart from targeting pyramidal cells, this mostly excitatory input has been described by Prof. Klausberger and Prof. Somogyi in Oxford to engage in differential feed forward inhibition of CA1 pyramidal cells through exerting control over various interneuron types (Klausberger and Somogyi, 2008) (summerised well by Sun et al. 2014). This motif of spatio-temporally tuned close-knit inhibitory control imposed over a large low firing neuronal populations will be discussed again later in this thesis.

Hippocampal CA1 functional role

Due to their marked structural differences, the proposed function of the CA1 structure has been contrasted to that of the CA3 in the HPc-dependent processing of mnemonic information (Treves, 2004). While the CA3 formation is distinguished through a high incidence of recurrent excitatory connectivity within its population of principal cells and hence has been

suggested to serve the purpose of auto associative pattern completion (Marr, 1971, McNaughton and Morris 1987, Norman and O'Reilly 2003; Rolls 2007, Hasselmo 2011), the CA1 exhibits only little such connectivity among its pyramidal cell cohort. For this reason and due to the fact that it receives input not only from the CA3 but also from the medial entorhinal cortex, the CA1 has been postulated to function as a crossroad between the two allowing for a comparative juxtaposition between the respective engram representations (Gray 1982; Hasselmo and Schnell 1994, Hasselmo 2011). Such representations in the CA1 have most commonly been investigated in the context of spatial information processing (Farovik et al. 2010), and extensively so over the past decades ever since the initial description of place cells in rats (O'Keefe et al 1971, O'Keefe, et al. 1976). Hereby, the firing rate of a large proportion of principal cells in the CA1 has been shown to be modulated by the animal's position in space, so much so, that the animal's movement within an enclosed environment could be inferred solely based on the activity profile of a few dozen pyramidal cells (Wilson and McNaughton 1993) (Ahmed and Mehta 2009). These early observations have since been complemented by various evidence correlating the CA1 neuronal rate code to the processing of other information modalities such as temporal (Kesner, 1998; Levy, 1996; Lisman, 1999; Rolls and Kesner, 2006), episodic (Manns et al. 2007) or valence related (Xia et al. 2017) in nature (summerised well by Hoge and Kesner 2007). Notwithstanding the contention in the field regarding the underlying principles of hippocampal functionality, the basic consensus remains that CA1 is involved in the encoding of contextual information. This is corroborated by studies that show cue dependent conditioning to be HPc independent whilst the functional impairment of the HPc/CA1 formation is sufficient to disturb the integration and retrieval of contextual memory (Phillips and LeDoux 1992, Phillips and LeDoux 1994).

Hippocampal (CA1) synaptic plasticity

The three-synaptic circuit architecture predestined the HPc not only to serve in the functional study of information relay, but also to become the most widely used brain structure in the

study of synaptic plasticity processes. As already described earlier, the in vitro preparation of hippocampal slice cultures has significantly facilitated the understanding of molecular processes underlying synaptic plasticity, leading to the discovery of LTP and LTD among others. These changes in the efficacy of single synapses were shown to be associated with corresponding morphological changes in the respective postsynaptic membrane specialisation, the dendritic spines (Harris et al. 1989, Takumi et al. 1999, Petralia et al. 1999, Bosch et al. 2012, Engert et al. 1999, Maletic-Savatic et al. 1999). Although in vitro preparations have enabled much of our understanding of the mechanistic and functional underpinning of structural synaptic plasticity (Malenka et al. 2004), understanding the relationship between the hippocampal functional activity and its structural correlate ultimately necessitates the correlation of acute structural changes in dendritic spine morphology within the HPc to ongoing behaviour. Prominent studies have demonstrated imaging of dendritic spines in the hippocampal formation in anaesthetised and freely behaving rodents (Mizrahi et al. 2004, Baretto et al. 2009, Gu et al. 2014) (Attardo et al. 2015). Especially the dorsal CA1 region, due to its layered architecture parallel to the cranium and its proximity to the brain surface has been a popular choice in such investigations. In chronic preparations, dendritic spines in the dorsal CA1 have been shown to be structurally plastic, being formed and erased at low rates (Gu et al. 2014). These results have been further confirmed and served in the attempt to computationally model the dendritic spine turn-over that suggests a mean synaptic lifetime within the pyramidal cell population of the dorsal CA1 in mice of approximately 1-2 weeks (Attardo et al. 2015) These findings correspond with widely held beliefs about the ephemeral nature of HPc dependency in memory retrieval (Varela et al. 2016) and further substantiate the notion that mnemonic engrams within the dorsal CA1 are represented by cell cohorts formed through the corresponding alterations in synaptic efficacies.

1.4) Nucleus Accumbens

Nucleus Accumbens structural architecture

The nucleus accumbens (NAc) is situated in the ventral part of the striatum and was first anatomically and functionally described about four decades ago (Heimer & Wilson 1975, Mogenson et al. 1980) based predominantly on its local expression of distinct neuropeptides (Groenewegen et al. 1987, 1999; Zaborszky et al. 1985; Zahm & Heimer 1990) (Floresco et al. 2014). The NAc can be structurally compartmentalised into two sub-formations, referred to as the core (lateral) and shell (medial) of the NAc (Zahm and Brog 1992), whereby this distinction is based on the differential composition of cell types as well as connectivity architecture (Groenewegen et al. 1991; Zahm 2000, 2008) (Floresco et al. 2014). The core as well as the shell cells mostly comprise of GABAergic inhibitory medium spiny neurons (MSNs, about 95%), expressing either D1 or D2 dopaminergic receptors; some MSNs expressing both are mainly confined to the shell. Apart from a differential biomarker expression, marked morphological distinctions of the MSNs in the shell relative to the core include a reduced dendritic arborisation as well as fewer spines. Similarly to hippocampal pyramidal cells, MSNs are highly interconnected (Koos et al. 2004) and in addition are also subject to differential inhibitory control by interneurons in the NAc (Koos and Tepper 2018). Apart from MSNs, the NAc consists of GABAergic interneurons (comprising approx. 2% of cells) and cholinergic interneurons (approx. 1%), both aspiny. Being the main efferent projecting neurons of the NAc, MSNs in the shell target the VTA, the ventral palladium, amygdala and hypothalamus, while core MSNs innervate the globus pallidus and substantia nigra, all structures associated with reward guided behaviour (Meredith et al. 1992, Koob and Volkow, 2010). Afferent input to the NAc is mainly excitatory and comes predominantly from the prefrontal cortex, basolateral amygdala and the HPc. Hereby, these inputs have been shown to have a prevalence to innervate the same target cells in the NAc (Britt et al. 2012,

Floresco et al. 2001b, French & Totterdell 2003, O'Donnell & Grace 1994) (Floresco 2015). As Stan B. Floresco so accurately put it: "[…] as individual NAc neurons receive converging (and potentially competing) information from different sources, the intrinsic connectivity of these circuits would necessitate a certain biasing or gating mechanism that could permit information processed by one system to have a preferential influence over behaviour via the NAc."

Nucleus Accumbens functional role

In accordance with this statement, the NAc has been postulated to constitute a gateway, which translates higher order cognitive functions via input from cortical/limbic brain regions into behavioural modulation via its output towards subcortical motor function-related brain areas. Hereby, it functions as a integrator between diverse, potentially competing cues to bias behavioural output according to the animals needs (Floresco 2015). In this process, the two NAc compartmentalisations, the core and the shell, have been proposed to serve two distinct functionalities. The core has been implicated in the facilitation of the execution of reward seeking behaviour, whereas the shell has been demonstrated to be instrumental in the functional association of motivational environmental cues with the corresponding reward (Chiara 2002; Russo et al. 2010)(Rutherford et al. 2011). In addition, GABAergic MSNs expressing D1 receptors have been shown to be functionally different to D2 receptors expressing MSNs (Russo and Nestler 2013, Chiara et al. 2002). The former support reward seeking behaviour, while the later are instrumental in the expression of aversion (Calipari et al. 2016). GABAergic interneurons and cholinergic interneurons, which comprise the rest of the neurons in the NAc, while all together only constituting less than 5% of the cells, also have a potentially strong impact on the animals behavioural output. The activation of the cholinergic interneurons for instance has been shown to promote reward seeking behaviour

(Witten et al. 2010) (Russo and Nestler 2013). The instrumental role of a subset of GABAergic interneurons in the NAc will be elucidated as part of this thesis.

Nucleus Accumbens synaptic plasticity

Similar to the hippocampal dorsal CA1 structure, neuronal plasticity is believed to underly long-term changes in the NAc-dependent behavioural output modulation. This neuronal plasticity is again relying on alterations in synaptic strength, which in turn are associated with changes in dendritic spine morphology (Everitt and Robbins 2005; Voorn et al. 2004) (Turner et al. 2018). Drugs of abuse are believed to highjack synaptic plasticity processes in the NAc and thus have been instrumental in the study of reward seeking behaviour as well as its maladaptation. Such substances, in addition to having been shown to rely in their effect upon altered synaptic efficacy in the NAc (Hyman et al. 2006; Kauer and Malenka 2007)(Ji et al. 2012), have been demonstrated to induce changes in dendritic spine morphology of MSNs in the NAc (Nestler 2001, Robinson and Kolb 1999, Robinson et al. 2001).(Norrholm et al. 2015). Apart from artificially induced structural synaptic plasticity, changes in spine density within the MSN population in the NAc have also been linked to the animal's behaviour under physiological conditions, such as chronic and social defeat stress (Christoffel et al. 2011; Muhammad et al. 2012) (Russo and Nestler 2013). In addition, there has been indication that structural synaptic plasticity is differentially affected by substances of abuse and stress in MSNs expressing D1 versus D2 receptors (Mendoza et al. 2016) as well as in the core versus the shell of the NAc (Robinson and Kolb 1999; Robinson et al. 2001). Relating acute structural changes in dendritic spine morphology within the NAc to appetitive behaviour might help to understand this intricate relationship between NAc functional activity and its structural correlate.

1.5) Hippocampal accumbal circuitry

Structural study

As already stated, afferent input to the NAc is mainly excitatory and comes predominantly from the prefrontal cortex, basolateral amygdala and the HPc. While in humans the hippocampal CA input to the NAc remains to be shown (Kahn et al. 2013), in rodents, this input has been exclusively studied pertaining to the ventral part of the HPc (MacAskill et al. 2012). This thesis will entail the first anatomical description of the dorsal hippocampal (CA1) -accumbal pathway.

Although significant advances have been made in the study of structural synaptic plasticity in vivo in the dorsal HPc, the NAc has not yet been subject to such investigations. While endoscopic approaches have been developed to circumvent the challenges associated with long distance image reconstruction through brain tissue (due to its complex refractive index distribution)(Vasquez-Lopez, Koren et al. 2018), there is a significant caveat: the tissue damage incurred by the aforementioned invasive strategies to gain optical access to sub cellular deep brain processes, is relatively extensive as well as proximate to the imaging site (Tang et al. 2016). It has been shown however, that even minimal and remote damage to the brain causes significantly altered spine turnover dynamics (Xu et al. 2007). Therefore, if such processes are to be investigated, the footprint of the imaging probe and hence the volume of tissue damage incurred should ideally be reduced to any extent that may be reconciled with the preservation of diffraction-limited imaging performance (Vasquez-Lopez, Koren et al. 2018). Over the past decade, efforts have been made to use spatial light modulation to focus scattered light to generate diffraction limited focal points at depths significantly greater than is possible with ballistic light (Sylvian et al. 2017). This new generation of imaging techniques might provide optical access to sub-cellular processes in deep brain regions such as the NAc beyond the reach of traditional means. This thesis will entail one such possible approach in

the form of a novel minimally invasive approach toward high resolution deep-brain imaging through a graphics processing unit (GPU) processing enabled micro-endoscope prototype. Hereby, recent advances in adaptive optics and parallel computing are used in a highly optimised statistical application process to enable image reconstruction with diffraction limited resolution but with a footprint up to 100 times smaller than comparable technologies. This technology will be applied in vitro and in vivo to the HPc and striatum. The results presented here form the basis of a manuscript currently under review (Vasquez-Lopez, Koren et al. 2018).

Functional study

In humans, while the corresponding hippocampal-accumbal circuitry remains to be established (Kahn et al. 2013), various attempts have been made to functionally analyse the relation between those two structures on the basis of findings made in rodents. Such attempts involved most notably functional magnetic resonance imaging (fMRI, Knutson et al. 2001), which, by exploiting spontaneous low-frequency modulations in the signal, allowed to determine a functional correlation between the HPc and NAc indicative of a convergent connectivity between the two (Kahn et al. 2013). The main drawback of this technology is its poor temporal resolution. Another approach, more suitable to uncover HPc-NAc circuit-level interactions, consisted of the use of intracranial electroencephalography (EEG, Cohen et al. 2009, Axmacher et al. 2010). Axmacher et al. were able to record in the HPc and NAc in patients with depression and epilepsy, establishing an indirect measure of temporal correlation in the response latency of those two structures during a standardised memory task. A major drawback in this study was the fact that the HPc and the NAc were recorded in two different sets of patients (as there is no condition that would clinically justify a simultaneous recording of the HPc and NAc in humans), thus not allowing for a direct measure of correlated activity.

Still, as suggested by Axmacher et al., this approach might serve as a bridge between fMRI in humans and electrophysiological means employed in rodents.

In rodents, the ventral hippocampus-accumbal pathway has been described to innervate MSNs in the NAc, and although it is thought to be comparatively weak (MacAskill et al. 2012), ventral hippocampal pyramidal cells have nevertheless been shown to significantly modulate the activity profile of NAc MSNs (Ciocchi et al. 2015; Goto and O'Donnell, 2001) (Trouche, Koren et al. 2019). In contrast, even though there has been work suggesting a correlation between the activity of dorsal hippocampal pyramidal cells and NAc MSNs (Tabuchi et al. 2000; Lansink et al. 2012; Sjulson et al. 2017) (Trouche, Koren et al. 2019), there has been little evidence presented so far to the effect of a direct influence of the former structure onto the later. Nevertheless, due to the respective traditionally assigned roles of the two brain regions, the hippocampus-accumbal circuitry has been postulated to promote the acquisition, consolidation and reinstatement of context specific reward seeking behaviour (Lindon et al. 2010, Britt et al. 2012, Chersi et al. 2015). In particular, the dorsal hippocampal CA1 region, which is implicated in the mnemonic representation of spatial information (Leutgeb et al. 2005; O'Keefe and Dostrovsky, 1971; Wilson and McNaughton, 1993) was hereby the focus of attention. Considering the output of the NAc, which indirectly modulates motor function through its projections to the basal ganglia, if this circuitry was to be demonstrated to exist, it would indeed stand to reason that it could be involved in the translation of spatial information into goal directed behaviour. However, the corresponding anatomical connectivity and physiological underpinning of the promotion of spatial mnemonic representations into appetitive behavioural directives have not yet been established (Trouche, Koren et al. 2019). One circumstance potentially corroborating the existence of such a pathway is that certain dorsal HPc-dependent mnemonic tasks have been demonstrated to be affected by

physiological impairment of the NAc circuitry (Annett et al. 1989; Mogenson et al. 1980; Schacter et al. 1989). This is an indicator that spatial information guided behaviour might be dependent on the intact spatiotemporal network dynamics within integrated dorsal hippocampal accumbal circuitry (Trouche, Koren et al. 2018). As already stated earlier in this chapter, an appropriately designed experimental set-up might allow for the effective dissection of the physiological and behavioural role of the downstream dependencies of dorsal hippocampal spatial information processing in the NAc. This thesis will entail the first physiological description of the dorsal hippocampal-accumbal pathway and will reference some behavioural results obtained by Dr. Stephanie Trouche in David Dupret's lab, which together form the basis of a manuscript currently under review.

1.6) Overview

The dorsal HPc and the NAc are integral in the processing of contextual information and the translation of higher order cognitive faculties into motor function. This thesis entails the first description of an integrated dorsal CA1 accumbal circuitry, which is ideally poised to be involved in the translation of spatial information into reward seeking behavioural directives.

Both those structures comprise of a highly plastic network architecture that allows the organism to adapt its mnemonic processes and behavioural strategies to changing environmental needs. This plasticity is associated with sub-cellular structural changes in dendritic spine morphology. Over the past two decades a new research-field emerged aiming to visualise fundamental sub-cellular mechanisms in the nervous system during physiological as well as patho-physiological processes. Early stage pathologies of neurological conditions such as Alzheimer's and Parkinson's have been demonstrated to correlate with structural changes in dendritic spine morphology in the HPc and the striatum. In order to study these under acute and especially chronic conditions in vivo, various invasive probes and operative

strategies were developed to gain optical access to sub-cortical brain regions (Vasquez-Lopez, Koren et al. 2018). While being met with great interest by the scientific community, these novel possibilities of deep brain imaging suffer from intrinsic limitations: relying on Fourier based light relay, they are subject to an inherent trade-off between their foot-print size (and hence the incurred tissue damage) and the achievable image resolution. In order to enable high resolution deep brain imaging with minimal disturbance to the associated neural circuitry in subcortical neuronal networks such as the dCA1-accumbal pathway, we used adaptive optics to gain holographic control over the light propagation through a single 50 μmeter core optical fibre, thinner than a human hair (Vasquez-Lopez, Koren et al. 2018). By doing so, we were able to reduce the endoscope footprint by two orders of magnitude compared to other invasive techniques, which achieve similar, diffraction limited resolutions. This novel approach has been only recently enabled by advances made in the field of parallel computing and adaptive optics. The results entailed in this thesis constitute the first proof of principle of this technology in vitro and in vivo, demonstrating its performance in the high resolution structural image acquisition of axonal boutons and dendritic spines, the pre- and post-synaptic cell membrane specialisations (Vasquez-Lopez, Koren et al. 2018). This work shall serve as the first stepping stone in the ongoing progress of this technology and highlight a route to achieving minimally invasive high-resolution optical access to deep-brain synaptic plasticity processes in awake and behaving animals. It shall demonstrate how future technical advances and improvements upon the current technological state might enable the functional visualisation of neuronal calcium transients (through increased frame rates), imaging in awake and freely behaving animals (through the use of long bending optic fibres), multi-photon image acquisition and other more sophisticated capabilities in the future.

Apart from the structural study of the dorsal HPc and the NAc, their functional physiology has been the subject of much attention in the past decades. This thesis will entail the first functional description of the integrated network dynamics within the dorsal hippocampal CA1 accumbal circuitry. There has been indication that spatially guided behaviour might be dependent on intact information processing within this circuitry. In order to study the downstream dependencies of dorsal hippocampal spatial information processing in the NAc, large scale multichannel electrophysiological recordings were employed simultaneously in both structures in freely moving, behaving mice (Trouche, Koren et al. 2019). In order to account for systemic network interactions between distinct cell types, electrophysiological biomarkers were established as a means for the reliable identification of cell types in the NAc. This approach, together with concomitant optogenetic manipulations, allowed for the further exploration of the functional interactions within the dorsal hippocampal-accumbal circuitry. Hereby, pyramidal cells in the dCA1 were established to predominantly drive the activity of a subset of fast spiking interneurons in the NAc which in turn modulate NAc output through exerting control over MSNs (Trouche, Koren et al. 2019). A first preliminary mechanistic model of the network dynamics in the dCA1-accumbal circuitry will be presented in this thesis. It will among other address two questions. Firstly, how can the dCA1 project a meaningful, comprehensive activity profile to the downstream network of the NAc through sparse connectivity? Secondly, how could the accumbal network potentially integrate multiple such inputs from different brain regions independently from each other? Furthermore, behavioural experiments results obtained in David Dupret's lab will be referenced that investigated the role of this circuitry in context dependent reward seeking behaviour and complement the physiological experiments presented in the following (Trouche, Koren et al. 2019). This study may serve as a first step in the further investigation of this newly discovered circuitry and its function.

1.7) Summary

This thesis represents the first account of the dorsal CA1 - accumbal circuitry in mice, which is ideally poised to underpin the translation of neural representations of space into spatial appetitive behaviour. In order to fully understand how information relay within this circuitry is orchestrated, neural activity as well as its structural correlate need to be studied.

In order to study the downstream effect of dorsal hippocampal spatial information processing on the network dynamics of the NAc, multichannel electrophysiological recordings with concomitant optogenetic stimulation will be employed simultaneously in both structures. This will allow the correlation of dCA1 activity with neural activity of distinct NAc cell types (Trouche, Koren et al. 2019). The experimental objective will be to examine this correlation while optogenetically silencing and stimulating dCA1-NAc projections as well as their post-synaptic targets in the NAc. This will be the first analysis of systemic network interactions between distinct cell types in the dCA1 and the NAc.

In order to be enable the study of structural synaptic plasticity in deep brain circuitries such as the hippocampal dCA1-accumbal pathway, a new minimally invasive high resolution deep brain imaging approach utilising holographic control over light propagation through a single optical fibre will be employed (Vasquez-Lopez, Koren et al. 2018). The experimental objective will be to subject this approach to a standardised and controlled evaluation of its capabilities in the depiction of axonal boutons and dendritic spines in organotypic slice cultures as well as in sub-cortical structures of an anaesthetised mouse. This will represent the first full in vitro and in vivo proof of principle of this technology.

CHAPTER 2: EXPERIMENTAL PROCEDURES

2.1) Structural plasticity in the dorsal hippocampus - accumbal circuitry

Imaging application

The technical details of the optical set-up and the principles of its functionality will be presented in chapter 3.1. In the following, supplementary instructions on the experimental protocol and further procedural aspects will be elaborated upon.

The entire optical system was encapsulated by a frame of blackout hardboard material (Thorlabs) in order to avoid light interference during photo multiplier tubes (PMT) based recording. Before each imaging day, the maximal laser power yield at the output of the polarisation maintaining fibre (PMF) and single-mode fibre (SMF) was controlled for and if necessary adjusted by altering the respective laser source coupling. An optic fibre (Thorlabs, FG050UGA, numerical aperture NA = 0.22) piece was cut anew by means of a fibre cutter, approximately 2-3 cm in length. The fibre length was chosen arbitrarily (no impact on scanning point quality), in sole dependence of its mechanical stability and desired imaging depth within the fluorescently labelled sample. The clean cut on both fibre facets was confirmed with a light microscope and the fibre was washed in ethanol to ensure aseptic conditions. The latter was repeated between any two imaging trials to clean the facets from accumulating dust and organic matter (Figure 2.1). Subsequently, the proximate fibre facet was manually positioned roughly in the focal plane of the aspheric lens (f = 8mm), which was

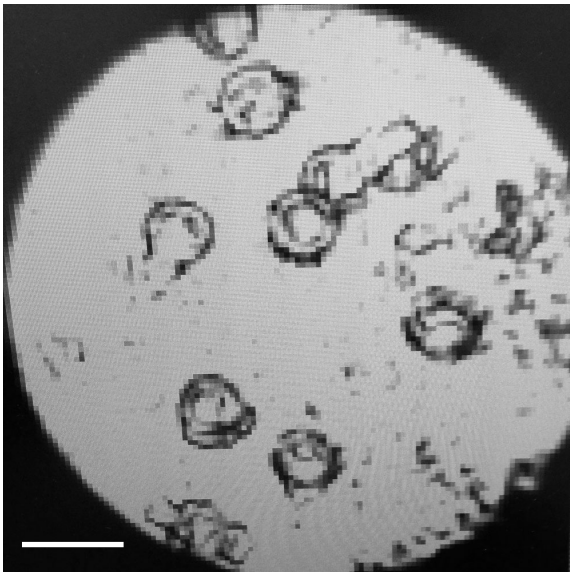

Fig. 2.1: Organic matter accumulation at the distal optic fibre facet after insertion into brain tissue in vivo. Visualised through a microscope objective, single red blood cells are visible to adhere to the fibre tip (scale bar 10 μm)

suspended above it. To ensure ideal alignment, the spatial light modulator (SLM) was used to scan a diffraction limited point in a xy-grating across the proximate fibre facet while the camera (CCD) was used to record the intensity of the overall diffuse signal obtained on the distal side of the optic fibre corresponding to each of the xy coordinates (Figure 2.2a). Using this real-time feedback, the fringes of the proximate optic fibre core were centred and positioned with high precision in focus of the aspheric lens (by altering its xyz positioning). Subsequently, the portable imaging unit was lowered via an automatised hydraulic ramp for the distal fibre facet to be positioned within the focal plane of the microscope objective (MO, Fig. 2.2b). Misalignments in x and y were adjusted for by means of a xy translation stage (Thorlabs), which the portable imaging unit was wholly suspended on. At this stage, the SLM was used to project diffuse light into the proximate optic fibre facet and the CCD to record its output. Using laser power of low intensity and averaging over multiple hundred frames resulted in a clear image of the distal optic fibre, which could be used to provide information about its state in-between imaging sessions just as the light microscope did before the optic fibre was fixated within the optical

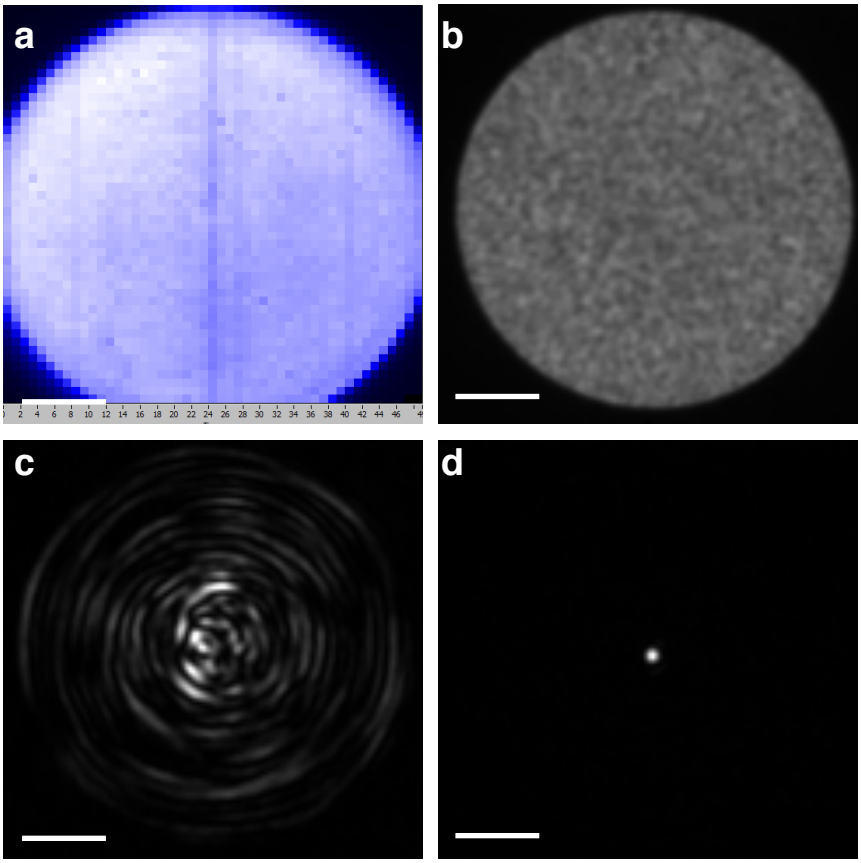

Fig. 2.2: Optical set-up preparation. (**a**) Scan of a diffraction limited point in a xy-grating across the proximate fibre facet while the camera (CCD) was used to record the intensity of the overall diffuse signal obtained on the distal side of the optic fibre (**b**) Distal fibre facet, positioned within the focal plane of the microscope objective (**c**) Interference grating of the optic fibre (MMF) output with the original light phase provided by the SMF (**d**) Projection of a diffraction limited point at the distal end of the optic fibre (scale bar 10 µm)

set-up (Fig. 2.1). In the next step, the interference grating of the optic fibre (MMF) output with the original light phase provided by the SMF as a backdrop within a non-polarising beam splitter (NPBS) was adjusted as seen in Fig. 2.2c. Hereby the ratio between the light intensities provided to the PMF and SMF had to be adjusted as well as the overall laser strength. In order to define the focal plane of the optic fibre based imaging, the imaging unit was raised by the respective distance in z (0-100 µm). In the case of a Z stack calibration, the automatic hydraulic ramp was programmed to allow for an individual transformation matrix to be calculated every 1.5 µm in z, which was then saved to disc. This was usually done overnight, before any given imaging day, as every calibration took approximately 4 min to complete. These preparations should be sufficient to ensure the successful manipulation of the imaging system as described in chapter 3.1.

Software

A GPU accelerated toolbox (open source), developed by Dr. Martin Plöschner and Prof. Dr. Tomas Cizmar (Plöschner et al. 2014), was utilised and adapted. GPU processing constitutes a two orders of magnitude faster implementation of transformation matrix computation (stored in GPU memory) and online holographic projection over the preceding central processing unit (CPU) based versions. The SLM control algorithm is implemented in CUDA C (similar to standard C in process representation), which is then visualised through OpenGL (or any language for programming

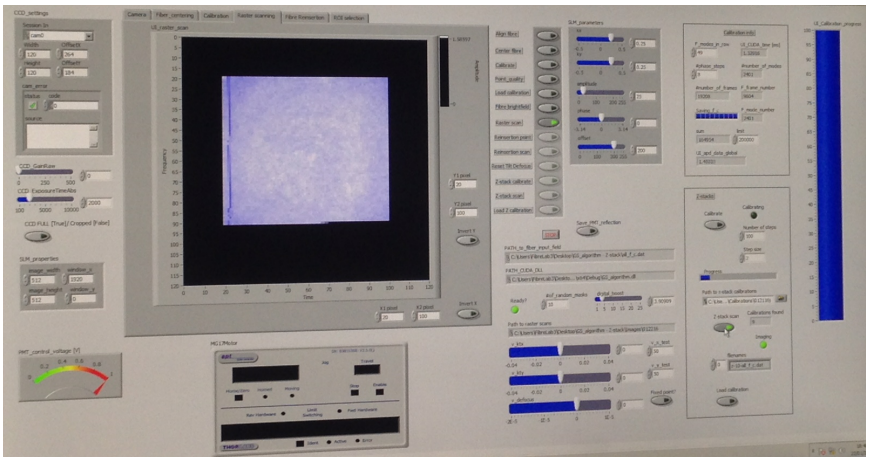

Fig. 2.3: LabView interface for the control of the two operational modes of the optical system: calibration and imaging. It allows the use of the SLM control software in synchrony with its peripherals, such as the PMT or the CCD. Additional features (e.g. Z-stack calibration) can be added if necessary

shader effects). This implementation is wrapped into C code and exported in a format that allows its use by external applications such as the LabView interface seen in Figure 2.3 which was generated by Dr. Martin Plöschner and adapted by Dr. Sebastian Vasquez Lopez and myself (additional features such as the Z-stack calibration capability were added). In order to ensure reproducible synchronisation within the optical system, the hardware utilised should consist of a NVIDIA card (GTX 570/GTX 780), the Basler CCD (piA640-210gm) and the Boulder Nonlinear Systems (BNS 512 × 512) SLM. If any other hardware is to be implemented instead, the system has to be recalibrate anew to ensure in sync functionality (Plöschner et al. 2014)

In vitro imaging

All animal work was carried out in accordance with the Animals (Scientific Procedures) Act, 1986 (UK), and under project and personal licenses approved by the Home Office (UK). Subjects utilised in chapter 3 for the in vitro experiments were male Wistar rats (postnatal day 7). Their hippocampal structure was extracted and coronal slices of 350μm thickness were made. These served in the preparation of organotypic hippocampal slice cultures, whereby they were plated on Millicell inserts (Millipore) and incubated (32-34 C°; 5% CO2; 1-2weeks) before the experiment. For the entire duration of the experiment the slices were submerged in heated ACSF consisting of 120 mM NaCl, 2.5mM KCl, 2mM CaCl2, 1.2mM NaH2PO4, 1mM MgCl2, 26 mM NaHCO3, 11 mM glucose and 25mM HEPES (Sigma Aldrich; pH = 7.2-7.4). In order to reduce photodynamic damage, and thus maintain structural integrity of the specimen between the confocal and the optic fibre imaging 0.2mM ascorbic acid and 1mM Trolox were added. The cells utilised for comparative imaging were dentate granule cells due to their generic morphological simplicity and ease of identification. These were patched (whole cell patching) and loaded with a KGluconate solution with 0.1-0.2 mM Alexa Fluor 488 fluorescent dye (ThermoFisher Scientific; pH = 7.2-7.4). Self-made glass

electrodes were utilised of approximately 16-25 MΩ resistance. After 5 to 10 min that were passed to ensure the sufficient diffusion of the dye through the arborisations of the neuron, the electrode was retracted to allow the cell-membrane patch to reseal. Due to the nature of the experiment it was paramount to keep the external and internal cellular conditions as stable as possible between the two imaging sessions, so as not to impact the structural integrity of the synapses. The cell was firstly imaged in its entirety by means of a confocal microscope (BioRad Radiance 2000) with a 488 nm argon laser. Multiple high resolution (1024 x 1024 pixels) Z-stacks (1μmetre step size) were obtained through a 60x water-immersion objective (0.9 NA; Olympus; Olympus BX50WI microscope). Subsequently, the specimen was transferred underneath the portable imaging unit of the optic fibre system. Repeated insertion of the MMF into the slice allowed for the acquisition of Z-stacks (1.5μmetre step size) through the optic fibre set-up to be compared with the confocal control. (Vasquez-Lopez, Koren et al. 2018; technical assistance Dr. Zahid Padamsey)

In vivo imaging

All animal work was carried out in accordance with the Animals (Scientific Procedures) Act, 1986 (UK), and under project and personal licenses approved by the Home Office (UK). Subjects utilised in chapter 3 for the in vivo experiments were male or female transgenic mice (4–12 weeks old), hetero- or homozygous for the transgene carrying the green fluorescent protein (GFP) under the control of the Thymus cell antigen 1 (Thy1) promoter: Thy1-GFP-M (line 007788, Jackson Laboratories). This mouse line sparsely expresses EGFP in different areas of the brain such as the HPc and the striatum. Animals were administrated dexamethasone (Dexadreson, 4μg), carprofen (Rimadyl, 0.15μg) and atropine (Atrocare, 1μg) through intraperitoneal injection as well as medetomidine (Domitor, 0.5 mg/kg), fentanyl (Sublimaze, 0.05 mg/kg) and midazolam (Hypnovel, 5 mg/kg) to induce anaesthesia. Once depth of anaesthesia was confirmed (foot pinch reflex), the animal's skin was shaven and a

longitudinal incision was made to expose the skull. A small craniotomy of 0.5-1 mm diameter was drilled into the skull (Foredom K.1070, Blackstone Industries, CT, USA) above the right ventral striatum (1.3 mm anterior, 1.0 mm lateral relative to the bregma) and the meninges covering the brain tissue were cleared. A custom-made stainless steel bar was adhered to the bone-structure using dental cement serving thus as stabilising anchor for the placement of the animal underneath the the portable imaging unit of the optic fibre system. The MMF was then slowly lowered (approximately 20 μm/min) into the tissue, while concomitantly performed image acquisition provided a realtime feedback. Once a suitable fluorescently labelled structure came into the field of view, the optic fibre was kept stationary. The structure was subsequently imaged in focus by adjusting the focal plane through the loading of the corresponding calibration. (Vasquez-Lopez, Koren et al. 2018)

Histology

The animals subject to the surgical procedure were anaesthetised with pentobarbital following completion of the experiments and transcardially perfused (0.1 M phosphate buffer saline PBS followed by 4 % paraformaldehyde PFA / 0.1% glutaraldehyde in PBS solution). Brains were extracted and kept in 4% PFA for at least 24 h before slicing (50-70 μm thick coronal slices) and sections were stored in PBS-azide in order to confirm the location of the fibre tract. (Vasquez-Lopez, Koren et al. 2018)

2.2) Network dynamics in the dorsal hippocampus - accumbal circuitry

Subjects

All subjects utilised in chapter 4 were adult male transgenic mice (4–7 months old), heterozygous for the transgene carrying the Tyrosin recombinase enzyme (Cre) driven either by the Ca2+/calmodulin-dependent protein kinase II (CaMKIIa) promoter (Jackson Laboratories, B6.Cg- Tg(CaMK2a-cre)T29-1Stl/J, stock number 005359; RRID: IMSR_JAX: 005359) or by the parvalbumin (PV) promoter (Jackson Laboratories, B6;129P2-Pvalbtm1(cre)Arbr/J, stock number 008069). They were housed together with their litter-mates before the first surgical procedure and individually thereafter. Ad libitum water supply was ensured at all time, food deprivation was administrated (>85% of body weight maintained) as part of more elaborate behavioural testings (not included in the scope of this thesis). A constant 12/12h light/dark cycle (7 a.m. to 7 p.m.) was maintained, while all experimental procedures were conducted during the day-light period. All experiments involving animals were conducted according to the UK Animals (Scientific Procedures) Act 1986 under personal and project licenses issued by the Home Office following ethical review (Trouche, Koren et al. 2019).

Viral vectors

Adeno-associated viral (AAV) vectors utilised within the scope of chapter 4 were encoding for the protein Archaerhodopsin-T (ArchT) fused with the green fluorescent protein (GFP) under the control of a Cre-inducible promoter CAG (AAV2-CAG-flex-ArchT-GFP; titre 2.0e12vg/mL; UNC Vector Core; chapter 4.2) and encoding for the protein Channelrhodopsin2 (hChR2) fused to an enhanced yellow fluorescent protein (EYFP) under the control of a Cre-inducible promoter EF1a (from Prof. Dr. Karl Deisseroth AAV2:EF1a-

DIO-hChR2(H134R)-EYFP-WPRE; titre 2.5e12vg/mL; UNC Vector Core; chapter 4.3). Furthermore, a transgene carrying the FlpO (recombinase) transcript under the control of a Cre dependent promoter (pAAV-EF1a-DIO-FLPo-Myc) was packaged in a high-titre serotype 1 viral vector capable of anterograde trans-synaptic transfer (Zingg et al. 2017) and used in mice together with an AAV encoding for the proton pump ArchT merged to an enhanced fluorescent marker EGFP under the control of a promoter whose expression was dependent on the presence of FlpO (pAAV-EF1a-fDIO-ArchT-EGFP; 9.6e12vg/mL; UNC Vector Core; chapter 4.4). The volume per injections site varied between 400nl and 500nl and was injected at a rate of approximately 100 nl/min utilising a hand-made glass micropipette as described previously (Cetin et al. 2006; Trouche, Koren et al. 2019).

Histology

All animals subject to surgical procedures were anaesthetised with pentobarbital following completion of the experiments and transcardially perfused (0.1 M phosphate buffer saline PBS followed by 4 % PFA / 0.1% glutaraldehyde in PBS solution). Brains were extracted and any chronically implanted probes were removed. The brains were kept in 4% PFA for at least 24 h before slicing (50-70 μm thick coronal slices) and sections were stored in PBS-azide in order to confirm the probe placement (not shown here). Optionally, sections were prepared for the immuno-histochemistry procedures involving the anatomical confirmation of cell types and axonal tracing. This work was performed in accordance with published methodology (McNamara et al. 2014).

Micro-drive implant

Mice were implanted with a custom-made micro-drive with twelve independently moveable tetrodes, each hand-made out of 4 tungsten wires (12 μm diameter, California Fine Wire), i.e.

48 channels in total. The anterior-posterior and medial-lateral positioning of each tetrode was determined by its setting within a plastic frame with the only degree of freedom in the ventral-dorsal axis. The movement of each tetrode along this axis was controlled by means of a M1.0 screw (O'Neill et al. 2008, Dupret et al. 2010). Six tetrodes were targeting the NAc in the ventral striatum and another six the dorsal hippocampal CA1 layer, both in the right hemisphere. Optionally, the drive also contained a stationary optic fibre (230 μm diameter, Doris Lenses) for light induced optogenetic stimulation, implanted above the NAc. Both the distance between neighbouring tetrodes and their distance to the optic fibre was approximately 0.4 mm (McNamara et al. 2014).

Surgical procedures

Each animal was subjected to maximally two surgical procedures (viral vector injections followed by a micro drive implantation at least 7 days apart), complemented by appropriate recovery periods. Surgery was conducted under deep anaesthesia administrated by means of isoflurane (0.5–3.5 % oxygen gas mixture 2 l/min) accompanied by analgesia (0.1 mg/kg vetergesic) provision before and after the procedure. Once depth of anaesthesia was confirmed, the animal's skin was shaven and a longitudinal incision was made to expose the skull. Two small craniotomies of 0.5-1 mm diameter were drilled into the skull above the dorsal HPc and ventral striatum and the meninges covering the brain tissue were cleared. Viral vector injection as well as initial tetrode/optic fibre placement was targeted to the stereotaxic coordinates of the NAc (relative to bregma: 1.6 mm anterior, 1.1 mm lateral, 3.8 mm ventral) and dCA1 (relative to bregma: 2 mm posterior, 1.7 mm lateral, 1.1 mm ventral). The chronic micro-drive implants were adhered to the bone-structure using dental cement and further secured with multiple screws placed into the bone plate above the cerebellum, serving thus as stabilising anchors (as well as the ground reference for the electrophysiological recordings).

The point of contact between the brain and the implanted tetrodes/optic fibre was covered with protective paraffin wax.

Experimental protocol

After the recovery period of at least one week that followed the surgical procedures, mice were handled and familiarised with the experimentalist as well as the experimental surrounding. For approximately one week the animals were connected to the recording system for 2-3 hours daily and were able to move freely in an open-field enclosures (the familiar environment). The monitoring of the raw local field potential (LFP) trace signals picked up by the tetrodes allowed the guidance of the careful lowering of the tetrodes to their optimal recording position within the pyramidal layer of the dCA1 and within the NAc. On the morning of each recording day thereafter tetrodes were lowered in search of multi-unit spiking activity into the pyramidal cell layer of the CA1 as well as NAc. Tetrodes were not moved for at least 2h before recordings started. At the end of each recording day, dCA1 tetrodes were raised in order to to spare the pyramidal cell layer from unnecessary mechanical damage overnight. The specific behavioural tasks the animals were subjected to will only find limited mentioning in this thesis and are only in so far relevant as the animals were exposed to different enclosures, which they were able to explore as distinct contextual environments. The length of the behavioural protocols varied between 30 min and approximately 5 hours.

Data acquisition and processing

Each channel's signal was buffered, amplified (RHD2164, Intan Technologies, gain x1000), band pass filtered (0.09 Hz to 7.60 kHz) and digitalised (20 kHz) using a single integrated circuit located on the head of the animal. The signal was transmitted offline and aligned with the registered analog position tracking and laser pulse time stamps. To track the location of

the animal, three light-emitting diodes (LEDs) were attached to the micro-drive and captured at 25Hz by an overhead camera (McNamara et al. 2014, Trouche, Koren et al. 2019).

Spike detection and unit isolation

The electrophysiological traces were subsequently band pass filtered (800 Hz to 5 kHz) and single extracellular discharges (spike detection through thresholding the root mean square RMS power spectrum using a 0.2-ms sliding window) were then assigned as belonging to discrete neurons through automatic principle component analysis (PCA, KlustaKwik) followed by manual spike sorting (based on waveform parameters and spike train dynamics). This was done in accordance to the previously published methodology (McNamara et al. 2014).

Light delivery

A 561-nm diode pumped solid-state laser (Laser 2000, Ringstead) was used to deliver light to the NAc of CaMKII dCA1::ArchT-GFP mice (chapter 4.3) and the NAc of PV dCA1→NAc::ArchT-GFP mice (chapter 4.5) through a long bending optic fiber and a rotary joint (Doric Lenses). In addition, a 473-nm diode-pumped solid-state laser (Laser 2000, Ringstead) was used to deliver light to the NAc (~20 mW) of PV NAc::ChR2-eYFP mice (chapter 4.4). The final optic fibers (on the animal end) were coupled to the implanted fiber using an M3 connector. CaMKII dCA1::ArchT-GFP mice received a single light pulse 10 min in duration. The NAc of PV dCA1→NAc ::ArchT-GFP mice received trains of 20 light pulses 30 seconds in duration with probabilistic intervals of 10-20 seconds in between over an entire period of the 15 min long exploratory recording session. PV NAc::ChR2- eYFP mice received a train of approximately 750 light pulses 10 ms in duration with probabilistic intervals of 1-4

seconds in between over an entire period of approx 20 min in order to optogenetically identify tagged PV+ interneurons (Trouche, Koren et al. 2019).

Analysis

Analytics that were applied in chapter 4, such as the NAc cell type discrimination based on extracted parameterised spike waveform features in chapter 4.2, the short latency spike time correlation analysis through population cross-correlograms in chapter 4.3 or the generalised linear model (GLM) for the prediction of the activity profile of NAc cells from a given dCA1 principal cell input in chapter 4.5, will be introduced in detail in the Results section. Some standard analytical tools, commonly used in the field, however will be utilised without further note and therefore, will be briefly mentioned here with reference to the used methodology: For the purpose of depicting spike train dynamics and firing properties of single neurons, mean firing rates, auto-correllograms and inter-spike-interval (ISI) distributions were used. A neuron's mean firing rate is defined as its total number of spikes divided by the recorded time period. A neuron's auto-correllogram is defined by its discharge probability before and after it has already spiked (spike numbers pre and post each spike are time-binned and normalised by total number of spikes). A neuron's ISI distribution defines the probable time period this neuron will remain silent between two adjacent discharges (all inter-spike-intervals are time-binned and normalised by their total number, then plotted on a logarithmic scale) (Gido van de Ven DPhil thesis).

Statistics

The means of two sets of observations were compared with a two-sample t-test or, if they were obtained from the same set, with a paired t-test (see chapter 4.5). Reported group data are mean ± standard error of the mean (SEM), unless stated otherwise.

CHAPTER 3: STRUCTURAL PLASTICITY IN THE DORSAL HIPPOCAMPUS - ACCUMBAL CIRCUITRY

3.1) Introduction

Pyramidal cells in the dorsal HPc have been demonstrated to provide a spatial representation of locomotion trajectories (O'Keefe et al. 1971, Morris et al. 1982, Pfeiffer et al. 2013). Newly acquired spatial representations are consolidated during subsequent sleep through recurrent reactivation of the respective neuronal assemblies (O'Neill et al. 2010), accompanied by corresponding structural network changes on a synaptic level. While the ventral HPc has been shown to project to the NAc, which indirectly modulates motor output through its projections to the basal ganglia, the dorsal HPc has not (my Transfer Report 2015). The dorsal hippocampal accumbal pathway, which will be anatomically delineated in the next chapter, is ideally poised to be involved in the translation of spatial mnemonic representations into appetitive behavioural directives. Structural plasticity of single dendritic spines has been shown to underlie experience dependent functional adaptations in both hippocampal and accumbal neural networks (Attardo et al. 2015, Ligang et al. 2014, Luscher et al. 2010). Chronic image acquisition in-vivo of those sub-cellular changes and their correlation with the animal's behaviour without the disturbance of the associated local circuitry however has remained challenging due to a general lack of means for minimally invasive high resolution optical access (Vasquez-Lopez, Koren et al. 2018).

Diverse multi-photon microscopy and gradient-index lens preparations have been trialed to overcome this limitation (Mizrahi et al. 2004, Barretto et al. 2009, Dombeck et al. 2010). The necessary aspiration of overlaying tissue (standardly ranging from 1.5mm to 3mm in diameter) however, incurs significant structural and systemic damage to the brain physiology (especially in mice), casting doubt on experimental results as well as preventing those

investigations to advance into deeper brain regions such as the NAc (Vasquez-Lopez, Koren et al. 2018). In collaboration with Prof. Dr. Tomas Cižmár (University of Dundee) a device was developed for in-vivo high resolution endoscopy through a single multimode optical fibre (core 50µm in diameter). This allows for spatially controllable light delivery and fluorescent image acquisition with a footprint two orders of magnitude smaller than any preceding technology of similar resolution performance (Plöschner et al. 2015). Hence, this method might offer an alternative approach for the investigation of synaptic plasticity deep within the brain. This device is relatively inexpensive and could be incorporated in standard experimental set-ups routinely used in the scientific field for optogenetic manipulations. Similarly, it could be used in conjunction with other recording modalities such as electrophysiological tetrode recordings (see chapter 4).

The goal of this project was to showcase the capabilities and limitations of this novel approach toward high resolution deep brain imaging. The optical set-up and its functionality was to be demonstrated and its imaging properties were to be subjected to a standardised and controlled evaluation in vitro (in order to established a reference framework) as well as in vivo. The latter was to take place within sub-cortical structures in the brain of an anaesthetised mouse. Furthermore, the incurred damage to the overlying brain tissue in the in vivo preparation was to be assessed. Ultimately, this study should serve as the first cornerstone in the ongoing progress of this technology and highlight a route to achieving minimally invasive high-resolution optical access to sub-cellular structural and functional processes in deep brain regions of alive and possibly behaving animals.

3.2) Geometry and function of optical set-up

The anatomical delineation of the long range projections from principal cells in the dorsal hippocampal CA1 region to the NAc in the ventral striatum will follow in chapter 4. These

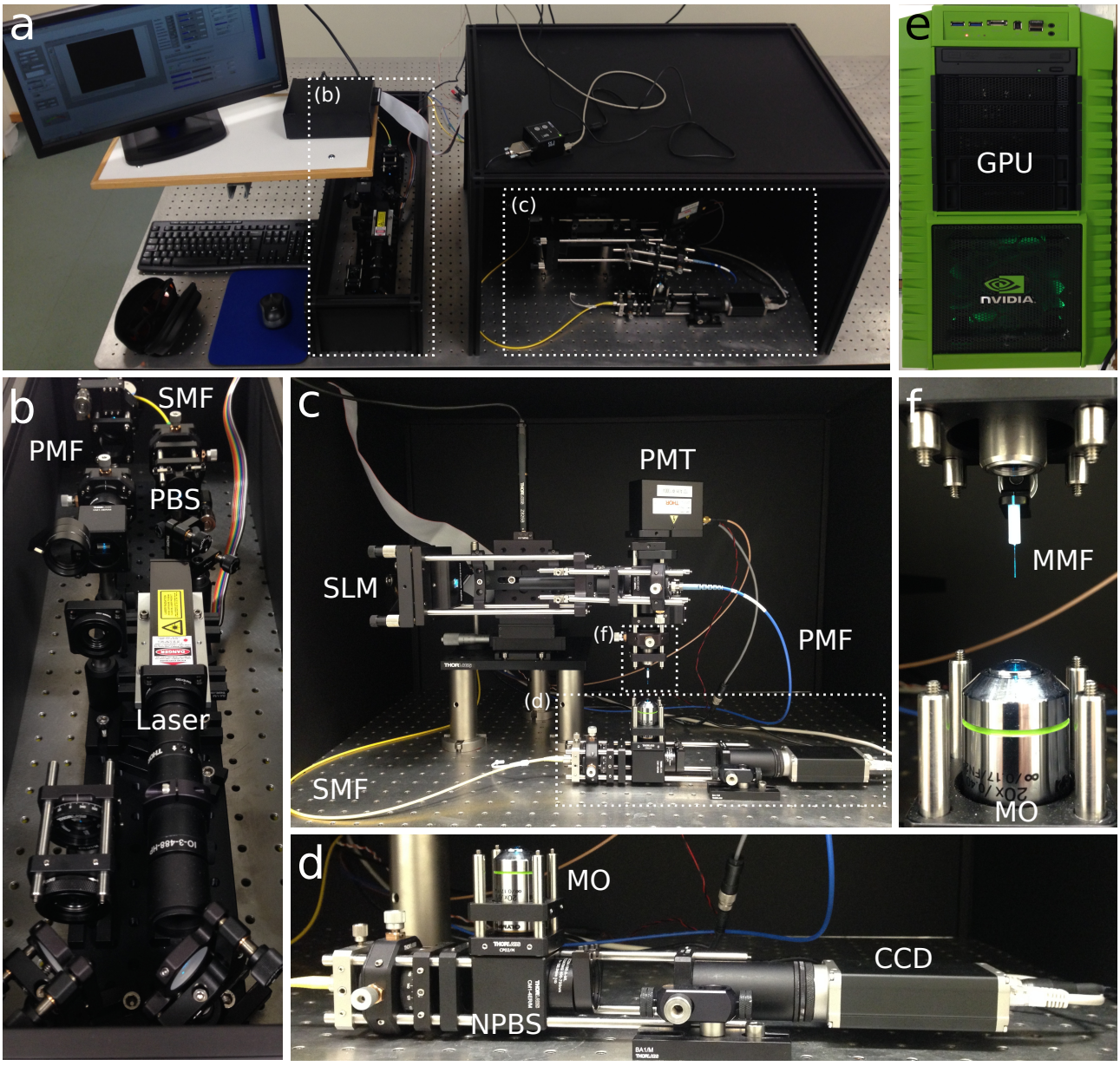

Figure 3.1: Optical system configuration (**a**) Instrumentation for high resolution fluorescent optical fibre micro-endoscopy suspended on a floating table encapsulated by a frame of blackout hardboard material (**b**) Source unit: Laser and polarising beam-splitter (PBS) (**c**) Portable imaging unit: polarisation maintaining fibre (PMF), single-mode fibre (SMF), spatial light modulator (SLM) and photo multiplier tubes (PMT) (**d**) Calibration unit: non-polarising beam splitter (NPBS) and charge coupled device (CCD) (**e**) GPU processor (**f**) multimode fibre (MMF) and microscope objective (MO) (**g**) Schematic diagram of the set-up portraying all three opto-mechanical modules and the laser beam path during the calibration (see Plöschner et al. 2015; Transfer Report 2015)

two deep brain structures will serve in the following in the showcasing of the capabilities and limitations of a newly developed approach toward deep brain imaging. Experience-dependent functional adaptations within this neural circuitry correlate with structural synaptic plasticity. In order to monitor those sub-cellular morphological changes, a novel optical geometry was designed to enable the minimally invasive in vivo high resolution image acquisition through a single multimode optical fibre. The purpose of this subchapter is the presentation of the set-up and its functionality.

Experimental geometry

Previous accounts of the application of wavefront-shaping microscopy through optically complex media such as optic fibres, while in theory identifying this technology's potential benefit for deep brain imaging, have failed to demonstrate, firstly, a high enough spatial resolution for the study of structural synaptic plasticity, and secondly, any practical capacity for image acquisition in vivo. To that effect, the optical system configuration had to be optimised if high resolution deep brain imaging in vivo was to be achieved. Apart from various software modifications, this also necessitated a modular built mobile optical geometry to allow for flexible interchange between the operational modes of the system, i.e. calibration and imaging. Thus, the here presented configuration consists of three opto-mechanical modules: the source unit, the portable imaging unit and the calibration unit (Fig. 3.1) (Vasquez-Lopez, Koren et al. 2018).

A monochromatic, linearly polarised light beam (λ = 488 nm, CrystaLaser; power controlled by optical isolator OI) is split and coupled into two separate optical fibres (a polarisation maintaining fibre PMF and a single-mode fibre SMF). The SMF output will be discussed in the context of the calibration of the optical system. Light exiting the PMF is collected, oriented (f = 60mm achromatic doublet, half-wave plate) and applied onto a liquid crystal

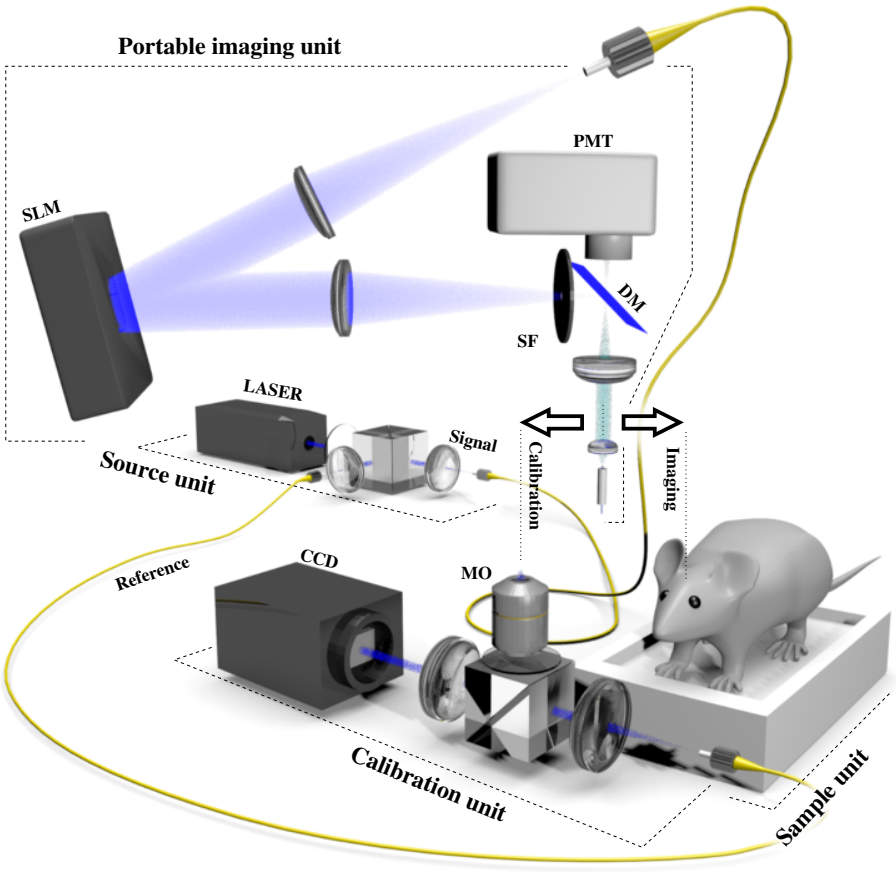

Figure 3.2: Schematic diagram of the set-up portraying all three opto-mechanical units and the laser beam path. The modular built mobile optical geometry allows for flexible interchange between the the calibration- and imaging operational modes of the optical system. Once the transmission matrix is acquired by means of the calibration unit, the microscope objective beneath the MMF is exchanged for a fluorescent probe or neural ex/in vivo tissue respectively. The portable imaging unit is suspended on an automatic hydraulic ramp which allows the targeting of different stereotaxic coordinates relative to the fixed sample unit. The dichroic mirror (DM) separates the SLM output and PMT input, i.e. the backtracked wavelength emitted by the fluorescent sample (diagram made by Prof Dr. Tomas Cizmar and Dr. Martin Plöschner)(Vasquez-Lopez, Koren et al. 2018)

based spatial light modulator (SLM, Meadowlark Optics, segmented 512 by 512) which permits the spatial modulation of the phase and intensity of reflected light (Plöschner et al. 2015). This output is Fourier transformed (f = 100mm plano-convex lens) and projected onto a pinhole to allow solely for its first order diffraction to be further collimated and circularly polarised (quarter-wave plate) (from Vasquez-Lopez, Koren et al. 2018). It is then centred and coupled (f = 50mm plano convex lens, f = 8mm aspheric lens) into the multimode fibre (MMF proximal optic fibre facet, Thorlabs, FG050UGA NA = 0.22) that is to be used for imaging (Plöschner et al. 2015). The light path exiting the distal optic fibre facet of the MMF is dependent upon the mode of operation of the optic geometry described in the following (from Vasquez-Lopez, Koren et al. 2018). The standard experimental protocol consisted of the initial calibration process of the optical system, followed by repeated image acquisition cycles (Fig. 3.2). (my Transfer Report 2015[1]; Vasquez-Lopez, Koren et al. 2018[2])

1: I am the author of this text; originally written/submitted: my Transfer Report 2015; 2: used for paper manuscript write-up 2017; present re-use approved by Prof. Dr. Nigel Emptage

Calibration mode

Collected through a microscope objective (MO, Olympus 20x, NA = 0.4), the MMF's output is linearly polarised (quarter-wave plate) and its field pattern is visualised on a charge coupled device (CCD) chip (Basler pilot piA640-210gm). Hereby, the original light phase provided by the SMF as a backdrop within a non-polarising beam splitter (NPBS, 50:50), serves as a reference signal to infer the phase shifts incurred by the light while propagating through the MMF (Plöschner et al. 2015).

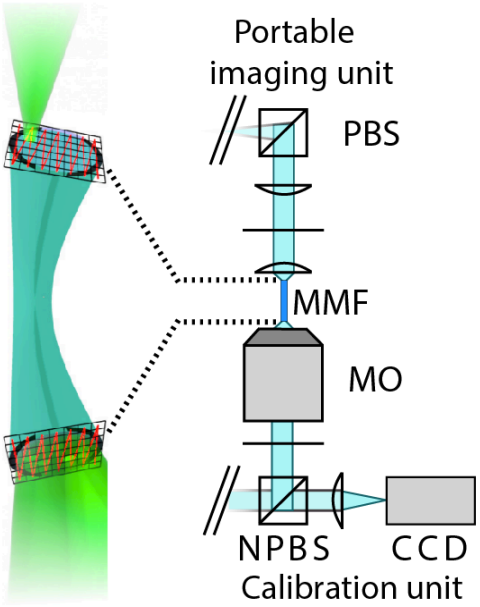

Figure 3.3: The SLM is used to scan a single diffraction limited focal point across the proximate end of the MMF which propagates through the MMF for its field pattern to be registered by the CCD. This allows for the interrelation of all possible inputs with the corresponding outputs and vice versa (part of figure adapted from Martin Plöschner et al. 2015)

Analogous to a Fourier transform performing optical lens, any linear optical system such as a multimode optical fibre can be fully described through a transformation matrix according to its orthogonal geometry. The SLM is used to produce and scan a single diffraction limited focal point across the proximate end of the MMF, generating an orthogonal vector system of 50 by 50 that can be parameterised through x and y coordinates (Plöschner et al. 2015). Each illuminated focal point at the fibre facet propagates through the MMF for its field pattern to be registered by the CCD as an image of 120 by 120 pixels (Fig. 3.3). An additional dimension is added through alterations of the incoming light phase. The resulting linear system describes the correlation between the light-intensity and -phase across the virtual 50 by 50 grid-like segmentation of the proximal fibre facet with its equivalent 120 by 120 segmentation at the distal fibre end. Any possible output, expressed as a complex linear superposition (Fig. 3.4) of the field patterns recorded by the CCD (processed

by GPU, Plöschner et al. 2014), can be produced through a constructive interference of focal points of specified intensity and phase generated by the corresponding SLM diffraction grating (Plöschner et al. 2015). The GPU based processing constitutes a two orders of magnitude faster implementation of transformation matrix computation and online holographic projection over the preceding CPU based versions (Plöschner et al. 2014). This allows for the calibration of the optical system in less than 4 min. (my Transfer Report 2015[1]; Vasquez-Lopez, Koren et al. 2018[2])

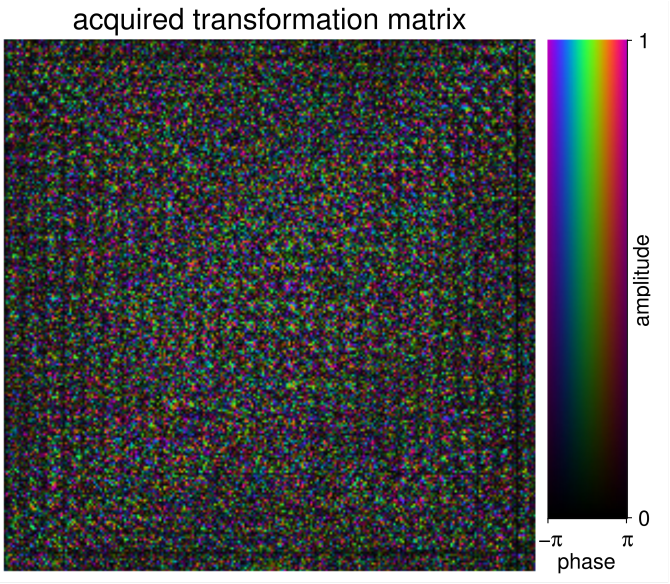

Figure 3.4: Visualisation of acquired transformation matrix (TM). The TM describes the linear system that correlates the light-intensity and -phase across the virtual 50 by 50 grid-like segmentation of the proximal fibre facet with its equivalent 120 by 120 segmentation at the distal fibre end (figure adapted from Martin Plöschner et al. 2015)

Imaging mode

As soon as the optical system is calibrated and the fibre specific transformation matrix established, image acquisition can be conducted immediately thereafter and indefinitely so, provided the relative positioning of the proximate fibre facet within its opto-mechanical frame is not perturbed by external mechanical stress.

Once calibrated, the microscope objective beneath the MMF is exchanged for a fluorescent probe or neural tissue respectively, and the fibre is lowered (Fig. 3.5). The SLM's diffraction grating generates a holographic projection across the proximate fibre facet. This linear superposition of focal points, constructively interferes while propagating through the fibre in order to collimate in a single, diffraction limited focal light-point in short distance of the distal

1: I am the author of this text; originally written/submitted: my Transfer Report 2015; 2: used for paper manuscript write-up 2017; present re-use approved by Prof. Dr. Nigel Emptage

fibre end (Plöschner et al. 2015). With a maximum SLM refresh rate of 204Hz, this point can be used to raster-scan a 75 by 75 orthogonal grid across the fluorescent sample, whereby the emitted wavelength is colluded and backtracked through the fibre. The intensity of this transmitted response signal is registered for each raster scan position by photo multiplier tubes (PMT) and constitutes the pixel value in the acquired 75 by 75 image. (my Transfer Report 2015[1]; Vasquez-Lopez, Koren et al. 2018[2])

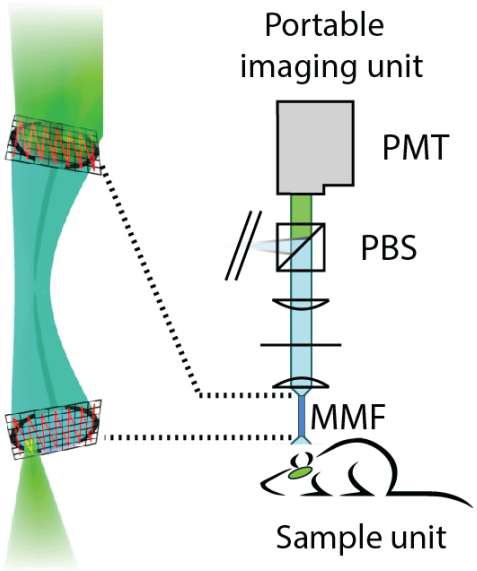

Figure 3.5: The linear superposition of focal points, projected to the proximate fibre facet, constructively interferes while propagating through the fibre in order to collimate in a single diffraction limited focal light-point in short distance of the distal fibre facet (part of figure adapted from Martin Plöschner et al. 2015)

The scanning area underneath the fibre is approximately 50µm x 50µm, could however be increased by adjusting the diameter of the MMF as well as its numerical aperture, which are not per se stipulated by the set-up architecture. Furthermore, multiple calibrations at varying distance from the distal fibre facet permit the subsequent acquisition of a Z-stack. (discussed in the following)

Value proposition

In order to delineate the potential value held by this technology for the scientific community, a brief review of the technical properties of optical devices hitherto available for the purpose of invasive high resolution deep brain imaging in rodents is to follow.

Multiple different experimental approaches have become established practice providing optical access to subcortical brain structures, most notably the mechanical aspiration (i.e. removal) of overlying tissue and the insertion of optical probes such as microscope objectives, graded index (GRIN) lenses or fibre bundles (Vasquez-Lopez, Koren et al. 2018). It has been

1: I am the author of this text; originally written/submitted: my Transfer Report 2015; 2: used for paper manuscript write-up 2017; present re-use approved by Prof. Dr. Nigel Emptage

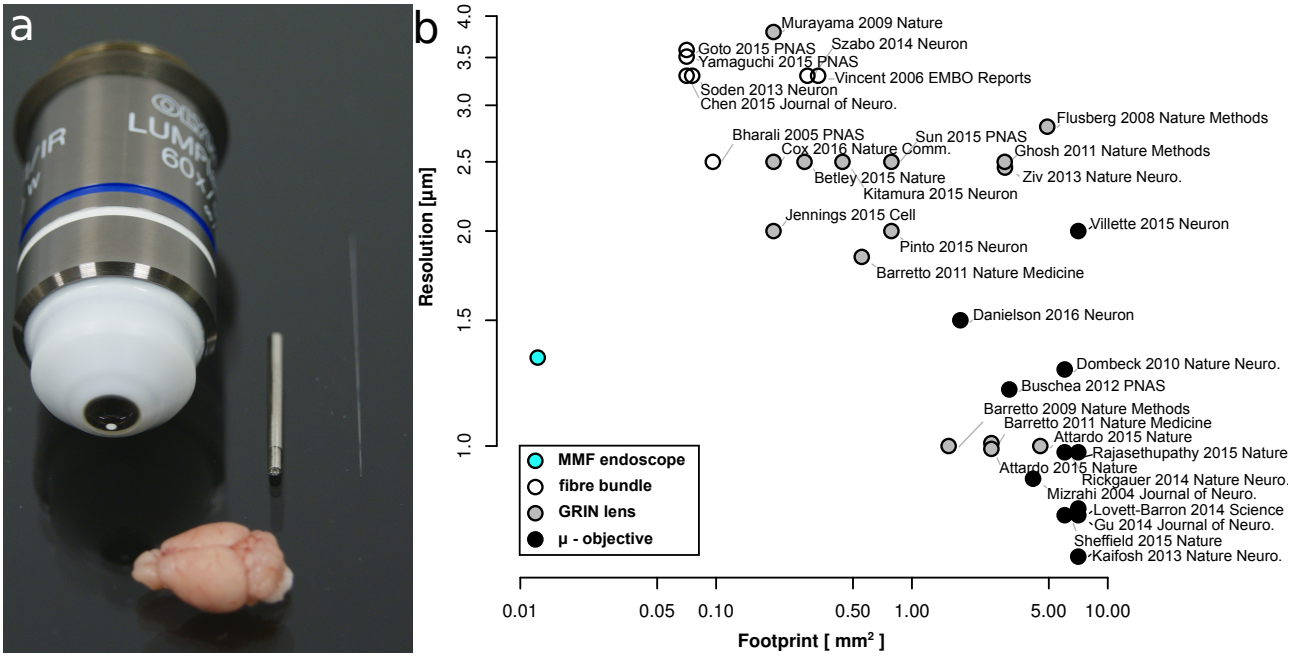

Figure 3.6: Value proposition of the optic fibre base system in the context of other optical devices hitherto available for the purpose of invasive high resolution deep brain imaging in rodents (**a**) Difference in scale of a standard microscope objective (left), a GRIN lens (middle) and a multimode optic fibre MMF (right) next to a perfused mouse brain. The insertion of the former two probes usually necessitates the aspiration of superficial brain structures. (**b**) A representative sample of studies utilising microscope objectives (black), graded index (GRIN) lenses (grey) and fibre bundles (white) was parameterised by the footprint of the respective imaging device and the achieved resolution (plotted on a double logarithmic scale). These are contrasted with the MMF based endoscopic method (blue; diameter 125µm, resolution 1.33µm)(Vasquez-Lopez, Koren et al. 2018)

formerly described, that sub cellular network processes such as structural synaptic plasticity are significantly affected in consequence of invasive surgical procedures even if the tissue damage is incurred peripherally to the site of interest (Xu et al. 2007). Therefore, if such processes are to be investigated, the footprint of the imaging probe and hence the volume of tissue damage incurred should ideally be reduced to any extent that may be reconciled with the preservation of diffraction-limited imaging performance (Vasquez-Lopez, Koren et al. 2018) . Fig. 3.6a depicts the difference in scale of a standard microscope objective, a GRIN lens and an optic fibre (MMF) next to a perfused mouse brain. Noteworthy is that if the fibre had not been positioned to reflect white overhead light projected onto the surface plane, it would not have been visible to the eye on this photograph. Also of note is the mechanically rigid nature of the optical probes currently used for deep brain imaging save the single optic fibre, which is flexible towards external mechanical stress. This feature has the potential to

ultimately provide minimally invasive high-resolution optical access to deep-brain processes in freely behaving animal models (discussed later).

By replacing Fourier-based image relay with a holographic approach, the image acquisition through a single multimode optic fibre allows for the reduction of tissue damage by two orders of magnitude in comparison to optical set-ups of similar resolution (Fig. 3.6b; Vasquez-Lopez, Koren et al. 2018). A representative sample of studies utilising microscope objectives, graded index (GRIN) lenses and fibre bundles was parameterised by the footprint of the respective imaging device and the achieved resolution (see Appendix for full list of references and corresponding parameters used; Vasquez-Lopez, Koren et al. 2018). When plotted on a double logarithmic scale, a clear linear trade-off becomes evident that compromises the relation of the two measures: the less invasive an imaging technique, the less resolved the image. This constraint on imaging modality appears to be independent of the particular technology in use. The reason might lie in the common principle of Fourier-based image relay, which dictates the optical limitations of light propagation within the probes (optic fibre bundles too, usually contain micro-lenses at the imaging facet). This constraint is overcome by the holographic approach utilised by the MMF based endoscopic method. With a diameter of 125µm (50µm core and shell), its resolution is 1.33µm instead of the expected 4-5µm (theoretical resolution based on the NA, the experimental lateral resolution will be explored in the following subchapter).

In this subchapter, a new optical system geometry was introduced, designed to enable the minimally invasive in vivo high resolution image acquisition through a single multimode optical fibre. Its geometric architecture and functionality as well as its potential value to the scientific community were outlined.

3.3) Proof of principle in vitro imaging

The purpose of the present subchapter is the standardised and controlled evaluation of the imaging capabilities of this optical system in vitro, in order to establish a reference framework for future results achieved in vivo.

Resolution measurements

The theoretically attainable lateral resolution of 1.33µm (see Fig. 3.6), that was calculated based on the numerical aperture of the optical fibre (MMF) used here, had to be verified through experimental means. For this purpose, a standard resolution measurement target (USAF-1951 grating) was utilised, whereby the distance between neighbouring fluorescent lines is successively reduced until they become indistinguishable by means of a perpendicular line scan of the optic system (Fig. 3.7a). The lateral resolution of this optic fibre set-up can be estimated to be in the range of 1.31µm-1.47µm (Fig. 3.7b; Vasquez-Lopez, Koren et al. 2018), thus closely corresponding to the optimal resolution achievable with this particular optic fibre (the use of alternative fibres will be discussed later). This experiment was conducted with a 532 nm wavelength laser (CrystaLaser). It stands to reason that the λ=488 nm set-up, used in the following for ex- and in vivo imaging has a marginally superior resolution.

A rough estimate of the axial resolution can be gained by measuring the axial point quality deterioration of the diffraction limited scanning point projected at a proximate distance from the distal optic fibre facet. This can be done by altering the z-axis distance of the microscopy objective (MO) relative to its reference distance used during calibration (not shown) while imaging with the CCD. The system design is susceptible to epi-fluorescent interference due to the nature of single-photon fluorescent excitation. However, if the distance from the distal fibre facet and the MO is varied during calibration process and the multiple calibrations

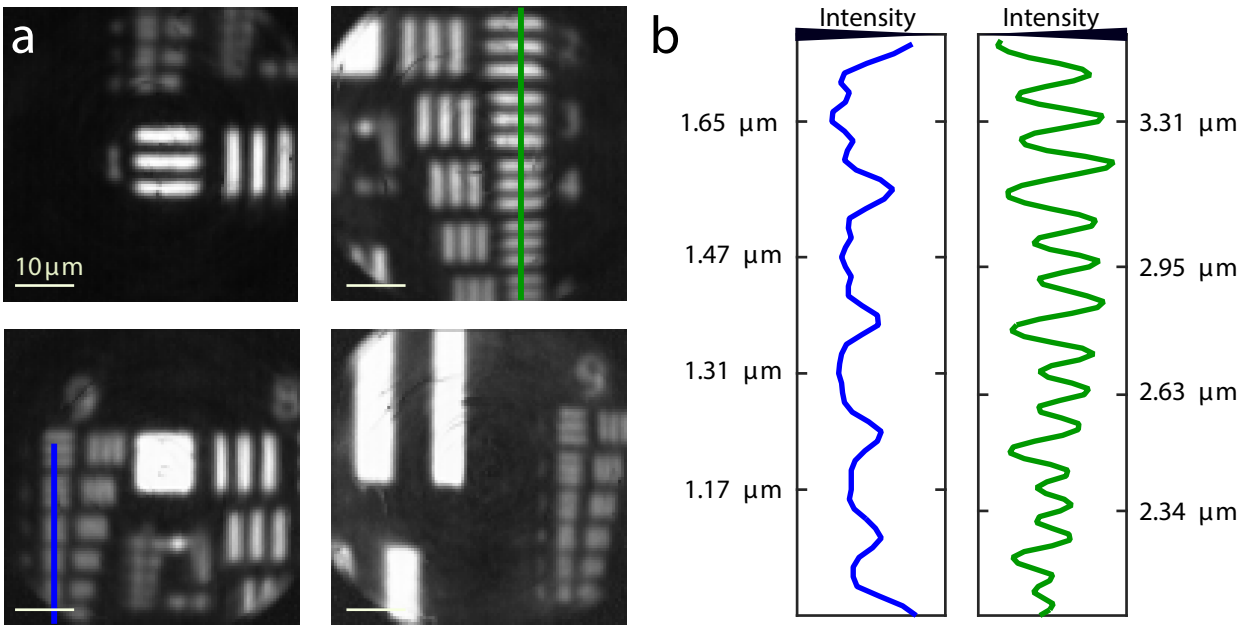

Figure 3.7: Resolution measurement (**a**) A standard resolution measurement target (USAF-1951 grating) was utilised, whereby the distance between neighbouring fluorescent lines is successively reduced until they become indistinguishable by means of a perpendicular line scan of the optic system (scale bar 10 µm). (**b**) The lateral resolution of this optic fibre set-up can be estimated to be in the range of 1.31µm-1.47µm at the wavelength of 532 nm (experiment done by Dr. Sergey Turtaev)(Vasquez-Lopez, Koren et al. 2018)

acquired in this way are loaded in succession during the operational mode of imaging, the acquisition of a Z-stack is possible (see chapter 3.4). This method together with suitable deconvolution algorithms might further improve the image quality as well as allowing three-dimensional reconstructions of fluorescent neuronal structures in tissue.

Fluorescent bead imaging

First proof of principle imaging trials were conducted on fluorescent beads ranging in size from 1.5µm to 3µm. Different preparations were tested to control for the degradation in image quality with varying light scattering properties of the medium. On a solid, non-reflective surface, 1.5µm sized beads were readily resolved and so was the cavity remaining at the junction of several of those small spheres (Fig. 3.8a). This allowed for an additional measure of lateral resolution to be implemented, which relies on a line scan, going through the centres of two neighbouring fluorescent beads (not shown here). This analysis further ascertains the assessment, that the lateral resolution is below 1.5 µm and thus as low as physically possible,

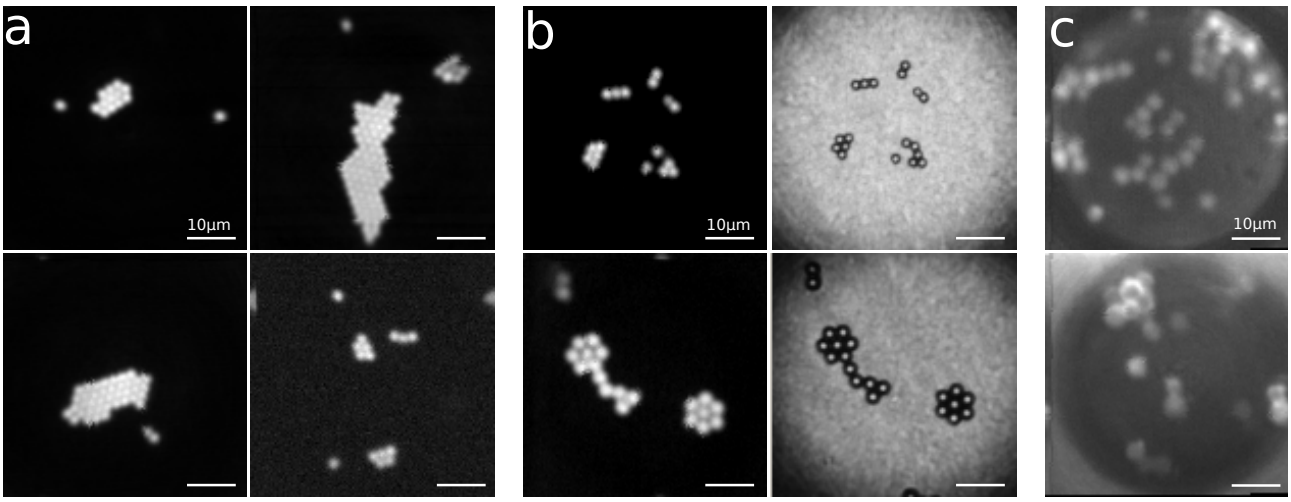

Figure 3.8: Fluorescent bead imaging (**a**) On a solid, non-reflective surface, 1.5µm sized beads were readily resolved as well as the cavity remaining at the junction of several of those small spheres. (**b**) Mounted on a reflective glass cover-slip, the image contrast quickly deteriorates and the noise-to-signal ratio surges. Even under these circumstances however most features of the fluorescent sample are preserved as controlled for by the simultaneous bright-light imaging through the MO from underneath the glass cover-slip. (**c**) Embedded in light scattering agarose gel 3µm small beads were nevertheless clearly distinguishable and so was their physical shape and their spatial relationship to each other (scale bars 10µm, experiment done together with Dr. Sebastian Vasquez Lopez)(Vasquez-Lopez, Koren et al. 2018)

limited only by the optical properties of the optic fibre. Mounted on a reflective glass cover-slip, the image contrast quickly deteriorated and the noise-to-signal ratio surged (Fig. 3.8b). Even under these circumstances however most features of the fluorescent sample were preserved as controlled for by the simultaneous bright-light imaging through the MO from underneath the glass cover-slip (Fig. 3.8b). Furthermore, even when embedded in light scattering agarose gel 3µm small beads were nevertheless clearly distinguishable and so was their physical shape and their spatial orientation to each other (Fig. 3.8c).

Hereby, one limitation of the present optical set-up becomes evident: although the surrounding medium of the fluorescently labeled probe does impact the image quality, it is not accounted for during the calibration of the system. While it is conceivable to perform the calibration through a glass cover slip or agarose gel, this would not be practical once imaging is to be performed in deep brain tissue in vivo. Alternative calibration procedures might rectify this shortcoming in the future, involving an online adjustment of the point scanning process within the tissue (Caravaca-Aguirre et al. 2013).

In vitro imaging

For the purpose of an accurate and controllable evaluation of the performance of the optical system in resolving neuronal sub-cellular structures, an in-vitro set-up was developed that allowed for the imaging of the same fluorescently labeled neurons through the fibre as well as a standard confocal microscope. Organotypic hippocampal brain slices were cultured and prepared from the rat HPc. Single dentate granule neurons, chosen due to their simplistic cellular morphology, were loaded with fluorescent dye (2 mM Alexa Fluor 488) using a whole-cell patch clamp method. After sufficient time (5-10 min) was provided for its diffusion within the cell and hence adequate labelling of the neuronal arbours, the cell was imaged in it's entirety by means of a confocal microscope (BioRad Radiance 2000, 488 nm argon laser, Olympus BX50WI microscope). Hereby a 60x water-immersion objective (0.9 NA; Olympus) was used to acquire four Z-stacks encompassing the different parts of the cell. The concatenated image of the projections of the Z-stacks is seen in Fig. 3.9a. The cell body, the dendritic arbour as well as the extensive axonal structure are visible in their entirety and are fully resolved. Subsequently, the same living slice was transferred underneath the calibrated portable imaging unit of the optic fibre system, that was lowered into the slice, once for the imaging of the axon and once for the dendrites (Vasquez-Lopez, Koren et al. 2018).

Imaging studies of neuronal plasticity primarily focus on the visualisation of structural changes in dendritic spines and axonal boutons, which are the pre- and postsynaptic specialisations of neuronal synapses (Crowe et al. 2014; Vasquez-Lopez, Koren et al. 2018). Hence, the accuracy and reliability of the depiction of those structures by means of the MMF system had to be demonstrated, if the system was to constitute a viable alternative to the already established high resolution deep brain imaging approaches. As evident in Fig 3.9b-e, both the axonal boutons as well as dendritic spines can be identified and individually

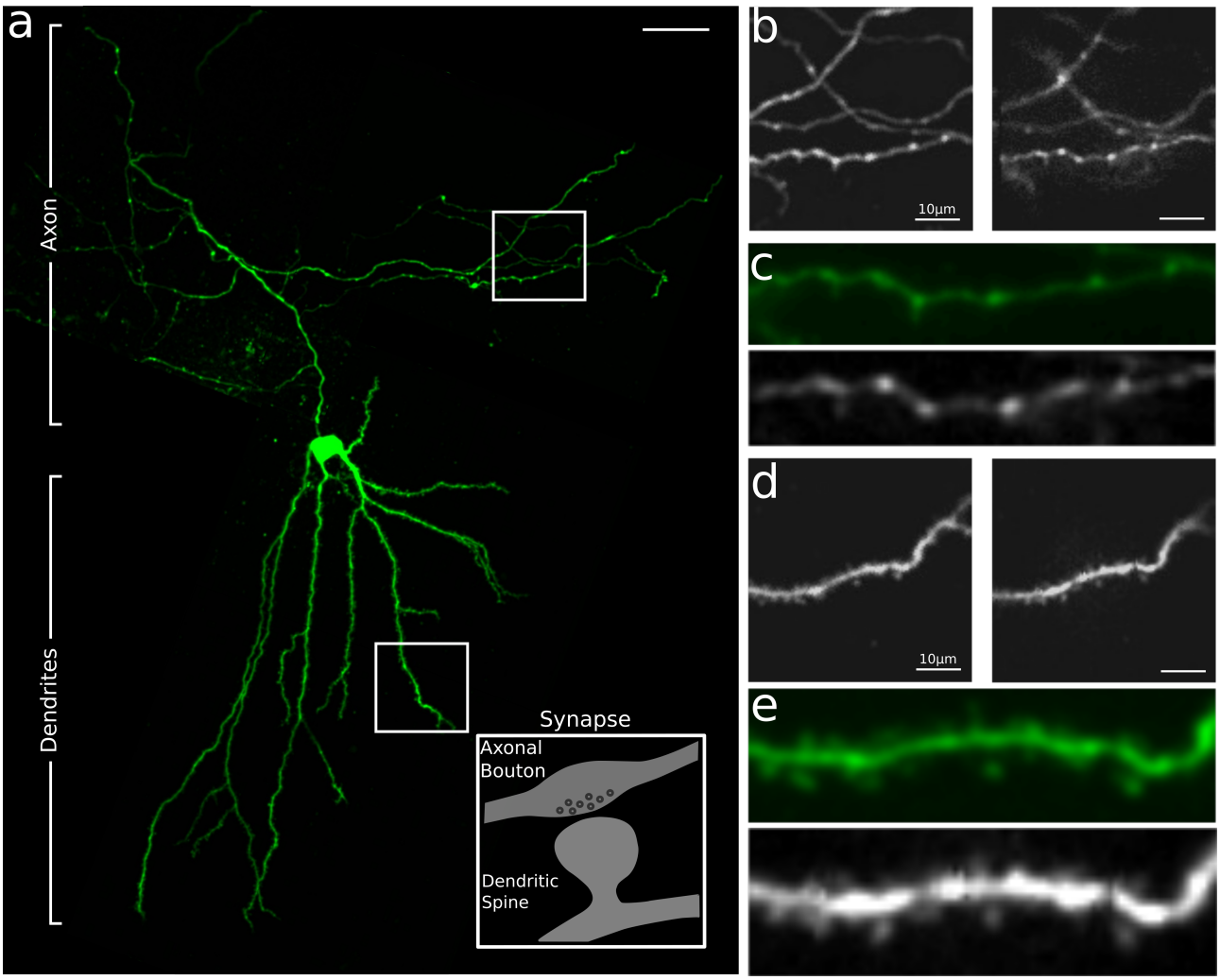

Figure 3.9: Comparative structural study of the accuracy in the depiction of synaptic pre- and postsynaptic specialisations (**a**) Concatenated image of the projections of 4 Z-stacks acquired by means of a confocal microscope with a 60x water-immersion objective of a single dentate granule neuron in a organotypic hippocampal brain slice cultured and prepared from the rat hippocampus (scale bar 50µm) (**b**) Comparative image of the same section of the axonal arbours imaged by the confocal microscope (left) and the optic fibre system (right) (Scale bar 10µm) (**c**) Magnification of (b): axonal boutons can be individually distinguished and are structurally identical when compared between the two imaging modalities (**d**) Comparative image of the same section of the dendrites imaged by the confocal microscope (left) and the optic fibre system (right) (scale bar 10µm) (**e**) Magnification of (d): dendritic spines can be individually distinguished and are structurally identical when compared between the two imaging modalities (in total 5 experimental trials were performed, technical assistance by Dr. Zahid Padamsey)(Vasquez-Lopez, Koren et al. 2018)

distinguished with an accuracy comparable to that of a confocal microscope. This is especially noteworthy in the case of the axonal boutons, whose fluorescent yield is significantly lower than that of the dendritic spines (confocal image was enhanced for better visibility; Vasquez-Lopez, Koren et al. 2018). An increase in the sensitivity of the optic fibre system through the adjustment of the PMT current allowed for the registration of weakly labeled structures without appreciable loss of resolution. The MMF based system resolved slightly less structural variations within the dendrites than the confocal microscope. Hereby

however is of note that the confocal images are maximal intensity stack projections, which tendentiously over-accentuate contrasts at the expense of reliability of portrayal, thus artificially adding structural variability. In the end, every structure in the confocal images has its correlate in the optic fibre images, hence this experiment serves as a robust validation of the reliability of the MMF approach in the acquisition of fluorescent images in living tissue (Vasquez-Lopez, Koren et al. 2018). This reliability is further supported by the circumstance that this approach does not introduce granulous artefacts (Mahalati et al. 2013, Kim et al. 2017), that constitute a side-effect of many computational image reconstruction approaches (Vasquez-Lopez, Koren et al. 2018).

Most technical challenges with this experimental set-up arose from, firstly, the necessity to keep the cell healthy for the duration of the entire procedure (otherwise the structural integrity of the neuron could no longer have been guaranteed), and secondly, that the neuronal structures of interest, µ-meters in scale, had to be targeted repeatedly by a 50 µm wide optic fibre tip lowered into the tissue blindly, with little means of orientation in all three dimensions.

In this subchapter, the performance of the optical configuration was tested and optimised for image acquisition of fluorescently labelled neuronal structures in alive tissue ex vivo. The acquired images are unparalleled in their spatial resolution and guarantee the accuracy of the depiction of organic fluorescent structures and especially pre- and post-synaptic structural specialisations of neurons. Moving forward, these results will constitute a reference framework for the appraisal of subsequent imaging performance in vivo.

3.4) Proof of principle in vivo imaging

The purpose of the following sub-chapter is the demonstration of the first structural imaging conducted within sub-cortical structures in the brain of an anaesthetised mouse. Furthermore, the incurred damage to the overlying brain tissue will be assessed and preliminary results will be evaluated which might serve as a stepping stone for future advances in the development of this technology.

In vivo imaging

Once the performance of the optical configuration was optimised for imaging fluorescently labelled neuronal structures within alive tissue ex vivo, first proof of principle in vivo imaging was conducted within deep brain structures of an alive, anaesthetised mouse (Vasquez-Lopez, Koren et al. 2018). A transgenic mouse line (Thy1-eGFP-M), sparsely expressing eGFP in the HPc as well as the striatum, was anaesthetised and stereotaxically immobilised. A small craniotomy was drilled centred above the striatum (Fig 3.10.a; coordinates: 1.3 mm anterior and 1.0 mm lateral relative to the bregma). The meninges protecting the brain tissue were removed with a needle, thus exposing the cortex which was kept moisturised for the entire duration of the procedure. Subsequently, the calibration unit underneath the MMF (125µm in diameter, both core and cladding) was substituted with the head fixed mouse (the sample unit). The optic fibre was then lowered slowly into the brain tissue (approximately 20µm/min) (Vasquez-Lopez, Koren et al. 2018). Its advancement through the tissue was accompanied by the online image acquisition through the optic fibre in the brain. Hereby the realtime feedback signal of diffuse overall fluorescence was used as indicator of the proximity of any fluorescently labelled neuronal structures. Once such proximity was established the optic fibre was kept stationary. The structure was subsequently put in focus by adjusting the focal plane through the loading of the corresponding calibration

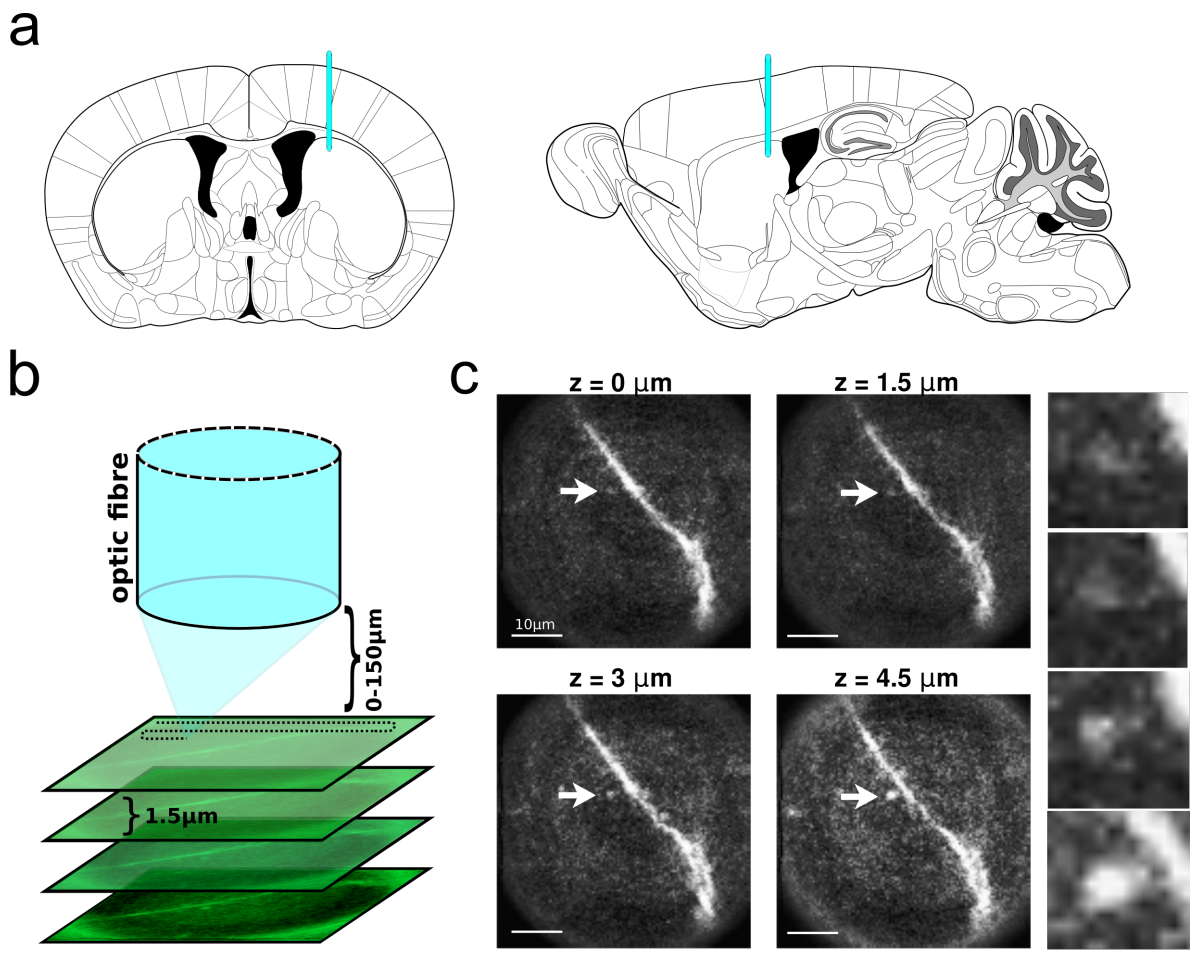

Figure 3.10: First proof of principle in vivo structural imaging of dendritic spines within the striatum of an anaesthetised mouse (**a**) Coronal and sagittal view of stereotaxic coordinates the optic fibre (MMF) was placed at for image acquisition (**b**) In advance of the imaging, repeated calibrations were undertaken while altering the distance from the distal fibre facet to the MO. Applied in succession, these calibrations allow the acquisition of a Z-stack (**c**) Dendritic spines are clearly discernible. Furthermore, structural characteristics of individual spines can be examined: their three-dimensional shape and relative coordination can be traced. Furthermore, the size of the spine head and -neck are distinguishable (in total experimental trials were performed on approx 12 mice; technical assistance by Dr. Sebastian Vasquez Lopez; scale bar 10 µm)(Vasquez-Lopez, Koren et al. 2018)

transformation matrix. Due to the use of the PMT during this process, the entire procedure of screening for fluorescently labeled cellular structures and imaging had to be undertaken in near complete darkness. The initial objective was the image acquisition within the nucleus accumbens (NAc) in the ventral striatum, however having traversed the cortical layers the clearest sub-cellular structure was found in the dorsal striatum (approximately 1.5 mm beneath the brain surface) in a distance of 25 µm from the distal fibre facet (judging by the respective focal plane calibration).

Hereby, multiple advantages of the optic fibre based system over comparative deep brain imaging approaches become evident. Firstly, the comparatively short distance between the optic probe facet and the imaged structure is indicative of the relative absence of organic debris usually accumulated at the tip of other invasive micro-endoscopes, which in the latter case necessitates the use of longer focal lengths. Secondly, the fact that imaging can be performed immediately after fibre insertion constitutes an advancement over larger probes, which cause cardiovascular and inflammatory responses that have to subside before the field of view is sufficiently cleared to permit image acquisition (commonly a matter of days to weeks). Lastly, in advance of the imaging experiment, repeated calibrations were undertaken while altering the distance from the distal fibre facet to the MO (from 0 up to approximately 100µm). Applied in succession, the virtual, holographic variation of the focal plane allowed for the acquisition of a Z-stack without varying the optic fibre's position (Fig 3.10). This constitutes a significant improvement over other optical probes, which commonly have an inert imaging plane (Vasquez-Lopez, Koren et al. 2018).

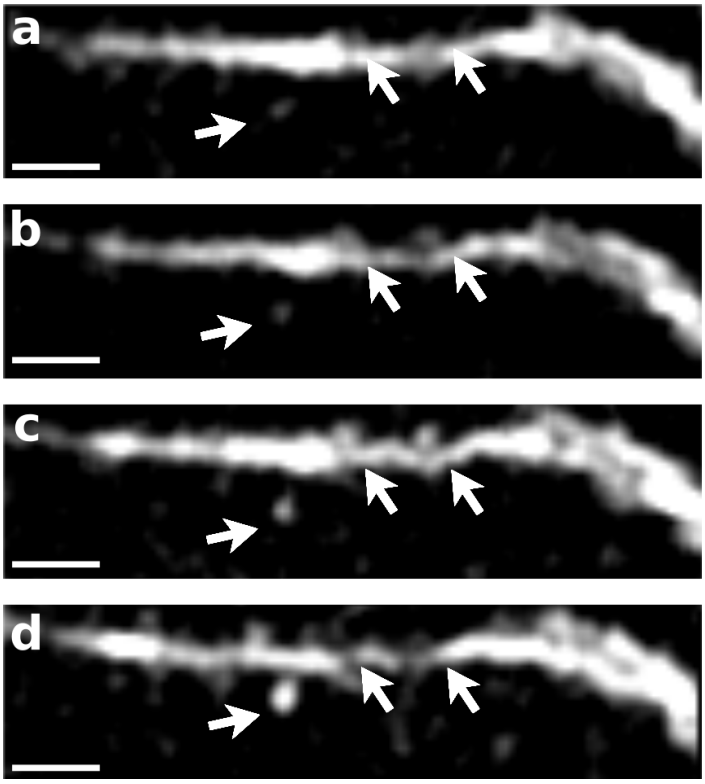

Figure 3.11: Processed, magnified and aligned dendritic spines. Applied in succession, the virtual, holographic variation of the focal plane allows for the acquisition of a Z-stack without varying the optic fibre's position (**a-d**) Single dendritic spines can be seen to ascend and descend out of focus despite the formerly delineated drawbacks of the single-photon set-up (scale bar 5 µm)(Vasquez-Lopez, Koren et al. 2018)

In the acquired images, dendritic spines are clearly discernible. Furthermore, structural characteristics of individual spines can be examined: their three-dimensional shape and

relative arrangement can be traced. Single dendritic spines can be seen to ascend and descend out of focus despite the formerly delineated drawbacks of the single-photon set-up (Fig 3.9). Furthermore, the size of the spine head and -neck are distinguishable. This may allow time-lapse chronic imaging studies in the future not only to investigate the turn-over of dendritic spines (generation and loss) but even the morphological changes in individual spines. The susceptibility to epi-fluorescent interference however did pose a serious constraint throughout the in-vivo imaging. This will have to be addressed through technical improvements in the future if deep brain imaging of neuronal structures of non-sparsely fluorescent labelling is to be achieved. Hereby, two recent advances in the field might prove instrumental: optic fibre based two-photon image acquisition through the successful compensation of the hereby occurring velocity dispersion effects (discussed later) and the development of optic fibre based digital confocal microscopy (Loterie et al. 2015). Notwithstanding this shortcoming, these results constitute the first ever deep brain structural imaging of neuronal synaptic specialisations in alive animals through a single optic fibre based micro-endoscope.

Histological study of the incurred damage

Following completion of the imaging procedure, the implanted probe was slowly retracted from the tissue. The mouse, kept under anaesthesia, was injected with pentobarbital and was subsequently transcardially perfused. The brain was extracted and sectioned (50 μm thick coronal slices) in order to verify the placement of the optic fibre (confirming the sub-cortical localisation of the acquired images) as well as to demonstrate the minimal invasiveness of the procedure by visualising the track of the fibre.

The sections were imaged by means of confocal microscopy and the track is visible on five different slices which allowed for a complete reconstruction of the fibre path through the cortical structure (Fig. 3.12a-e). The imaging site can be localised slightly beneath the lowest

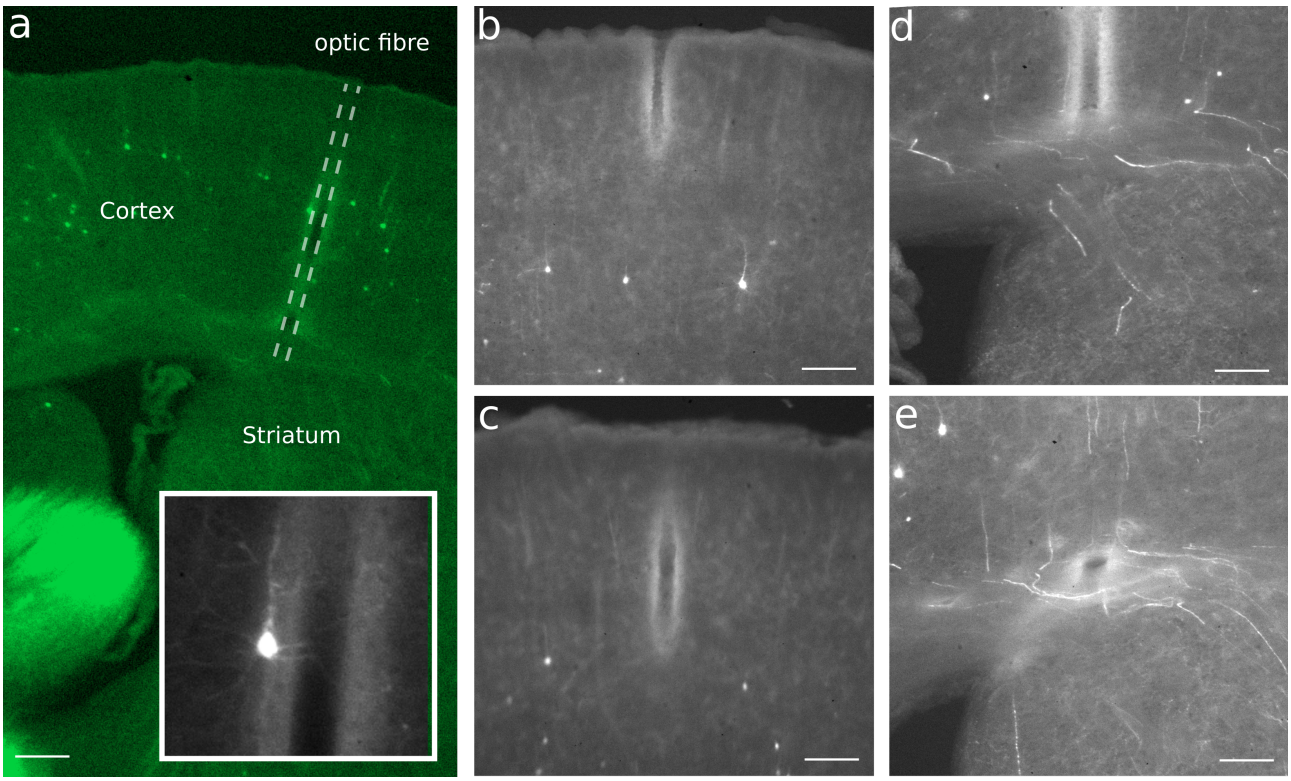

Figure 3.12: Histological study of tissue damage (**a**) Following completion of the imaging procedure, the implanted probe was slowly retracted from the tissue. The brain was extracted and sectioned (50 µm thick coronal slices) in order to verify the placement of the optic fibre (confirming the sub-cortical localisation of the acquired images) as well as to demonstrate the minimal invasiveness of the procedure by visualising the track of the fibre. By chance, one of the sections contained a fluorescently labeled cell in the cortex located in close proximity to the fibre track. This cell has maintained its morphological integrity and has even projections bordering and encompassing the pathway of the fibre (insert). (**b-e**) the track is visible on five different slices which allows for a complete reconstruction of the fibre path through the cortical structure. The imaging site can be localised slightly beneath the lowest fringes of the cortical layers within the dorsal striatum (scale bar 10 µm, technical assistance by Dr. Sebastian Vasquez Lopez) (Vasquez-Lopez, Koren et al. 2018)

fringes of the cortical layers within the dorsal striatum. Thereby, one of the stated objectives of the study, the proof of principle imaging in sub-cortical structures, was fulfilled. By chance, one of the sections contained a fluorescently labeled cell in the cortex located in immediate proximity to the fibre track (Fig. 3.12a). This cell has maintained its morphological integrity and has even projections bordering and encompassing the pathway of the fibre. This is remarkable, considering the hours-long duration of the experiment and that the fibre was continuously lowered and raised through the tissue µ-meters away from the cell body of this cell, thus inevitably causing mechanical stress. It illustrates that the structural integrity of the associated neuronal circuitry is not significantly impacted. Furthermore, it stands to reason, that the minimally invasive nature of this technology could reduce the ensuing immune

system response to the optic probe insertion in chronic preparations compared to other approaches (Tang et al. 2016, Xu et al. 2016).

Preliminary results on time-lapse chronic imaging in anaesthetised animals

Recent advances have been made in the correlation of structural changes in the circuit- and cellular architecture with animal behaviour. Whilst image acquisition in awake, behaving animals utilising the optic fibre system is not feasible yet (this possibility will be discussed later), time lapse chronic imaging might allow such correlations to be inferred. In the following, preliminary results will be discussed elucidating a putative strategy to achieve time lapse chronic image acquisition of sub cellular deep brain structures. In principle, two different approaches are conceivable to repeatedly attain optical access to the same neuronal deep brain structure over time. In the first scenario, a chronically implanted cannula could be used to provide a route for the recurrent lowering of an optical fibre into the brain. Hereby, the optic fibre utilised can be changed between imaging sessions. In the second scenario, a single optic fibre is chronically implanted, fixed to the scull and left stationary, suspended above the brain structure of interest.

In the first case, the cannula has to measure a slightly wider inner diameter than the optic fibre in order to repeatedly guide the optic fibre reliably towards the same imaging location. This method has multiple disadvantages. Firstly, it effectively increases the footprint of the optic probe. Secondly, the cannula has to be implanted blindly into the brain structure of interest, without knowledge whether any fluorescently labelled structure happens to be located underneath. Lastly, the flexible optic fibre has to be lowered through a rigid guiding cannula only marginally wider in diameter, while any perturbation or distortion in the fibre's shape would automatically invalidate the acquired transformation matrix calculated during calibration. This would necessitate the parallel sliding of two objects multiple centimetre in

length alongside each other, one attached to the mouse, the other to the optical set-up, while maintaining a constant microscopic distance between them. First trials of this approach have not proven fruitful (Dr. Sebastian Vasquez-Lopez; not shown here).

In the second scenario, the calibration of the optic fibre is conducted before the surgical procedure. This fibre is then chronically implanted into the brain structure of interest, whereby the positioning of the fibre can be accompanied by the online imaging feedback. This way, the imaging site can be optimised, which due to the limited window of view, owing to the small fibre radius (will be discussed later), is of importance. It is reasonable to assume that the shape of the optic fibre will not be subjected to distortions within the brain tissue, as it is incomparably more sturdy than tetrodes commonly used for electro-physiological chronic recordings over extended periods of time (see chapter 4). Once imaging is to be performed, the animal is anaesthetised and the initial calibration is used to image the neuronal structure underneath the optic fibre. The only difficulty hereby is that the proximal optic fibre facet has to be positioned microscopically precise at the same xyz orientation within the optical arm frame to match its position during the calibration. This may seem similarly challenging as the first strategy, however the normal functionality of the optical set-up can be reversed in order to provide a microscopic view of the proximate fibre facet throughout this process. During the calibration mode, the SLM is

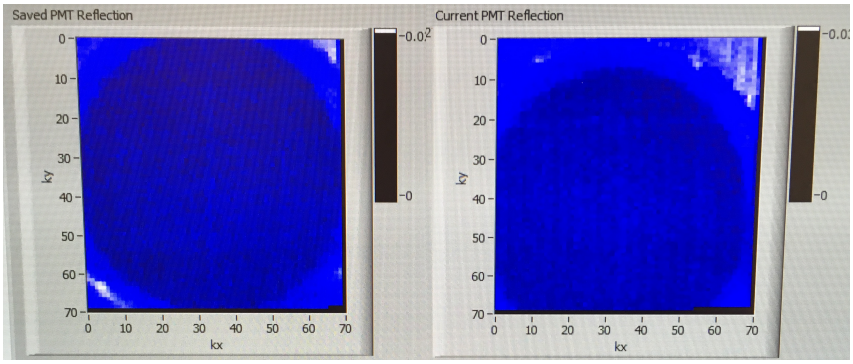

Figure 3.13: The point scanning over the proximate fibre facet is coupled to the signal intensity registration of the PMT and a blueprint image of the proximate fibre facet is generated while the fibre is implanted in vivo. This allows for a real time feedback and the precise microscopic xyz orientation of the fibre within the optical arm frame to match its position during the calibration (comparison left/right)

used to produce and scan a single diffraction limited focal point across the proximate end of the MMF, generating an orthogonal vector system of 50 by 50 that can be parameterised through x and y coordinates. During the imaging mode, the intensity of the transmitted response signal of the emitted fluorescence that is colluded and backtracked through the fibre is registered for each raster scan position by photo multiplier tubes (PMT). If the point scanning over the proximate fibre facet is coupled to the signal intensity registration of the PMT, a blueprint image of the proximate fibre facet is generated. Preliminary results are promising, although it has not quite been possible yet to recreate the initial high point quality of the diffraction limited point projected at the distal fibre facet after reinsertion of the fibre into the apparatus (Fig. 3.13).

The results presented in this subchapter constitute the first demonstration of high resolution imaging conducted through a single optic fibre endoscope within sub-cortical structures in vivo. They are furthermore a testament to the minimally invasive nature of this optical set-up as well as to the reliability in its depiction of synaptic structural specialisations of neurons. Finally, preliminary results introduced here might serve as a stepping stone for future advances in the development of this technology.

3.5) Discussion

This chapter showed the first full proof of principle in vitro and in vivo of a new minimally invasive high resolution deep brain imaging approach utilising adaptive optics and holographic light propagation through a single optical fibre, thinner than a human hair. Its diffraction limited resolution was confirmed on fluorescent beads and resolution gratings. Its accuracy in the depiction of organic fluorescent structures and especially pre- and post-synaptic structural specialisations of neurons was demonstrated in hippocampal organotypic slices and in the dorsal stratum of an anaesthetised mouse. In the following, the rational behind the individual experiments will be discussed.

While the first histological delineation of the dorsal hippocampal - ventral striatum circuitry and the functional study of its network physiology will be addressed in chapter 4, the HPc and the striatum served as target structures in the showcasing of the capabilities and limitations of the newly developed optical set-up for optic fibre based minimally invasive high resolution deep brain imaging.

In order to potentially investigate structural synaptic plasticity within this circuitry with minimal impact to the associated network structure in alive animals, a novel optical geometry was designed to enable in-vivo high resolution image acquisition through a single multimode optical fibre. The modular built set-up configuration and the functionality of this system was presented in detail in chapter 3.2. Then, in chapter 3.3, a standardised and controlled evaluation of the imaging capabilities of this optical system in vitro followed with the purpose of establishing a reference framework for future results achieved in vivo. Hereby, the lateral resolution theoretically achievable by the system was confirmed experimentally. Furthermore, it was confirmed that single pre- as well as postsynaptic neuronal membrane specialisations could be reliably visualised within alive tissue ex vivo. Although other attempts to image sub-

cellular neuronal structures in slices through multimode optic fibres had been made in the past (Papadopoulos et al. 2013), the results presented in this work constitute the first such demonstration to date of high enough quality to allow for the effective, controlled identification of single dendritic spines and axonal boutons.

Having established a reference framework for the appraisal of subsequent images acquired in vivo, the presentation of the first structural imaging conducted within sub-cortical structures in the brain of an anaesthetised mouse followed in chapter 3.4. Hereby, single dendritic spines were shown to be identifiable and discernible in their three dimensional arrangement. These images constitute the first visualisation of synaptic specialisation in vivo acquired through a single multimodal optic fibre. Moreover, various advantages of this technology over established approaches were discussed, such as the real time online visual feedback during implantation, the possibility of image acquisition immediately following surgery or the variation of the imaging plane without the need for physical movement of the distal fibre facet. Nevertheless, at the first glance, the hereby achieved imaging performance might as such seem inadequate for the daily practical use of this technology in the exploration of structural plasticity in vivo. This notion, while justifiable, nonetheless fails to account for the rapid pace in the improvement of this technology, and its future potential. GRIN lenses might serve as a useful indicator in the extrapolation of the future potential of MMF based imaging and its technological progression. In the advent of GRIN lens technology, the resolution of single dendritic spines achieved in vivo (Barretto et al. 2009) was highly comparable to the results presented here. However, while it took nearly 10 years for the GRIN lens approach to advance enough to be widely implemented and used by the scientific community, this might not need to be the case for the MMF approach. An important distinction between those two technologies is the fact that rather than relying on the development of optical components, the

MMF approach is predominantly based on software and electrical hardware solutions. These tend to exhibit more rapid product innovation cycles. In support of this stance, a few improvements currently underway and potentially implementable in the very near future will be discussed in detail in the General Discussion.

Finally, in addition to the acquired synaptic spine images, the incurred damage to the overlying brain tissue was assessed. The incurred tissue damage is usually little spoken of in prominent publications that use invasive deep brain imaging techniques. A recently published images of a sliced brain implanted with a GRIN lens can hereby serve as reference (Tang et al. 2016). While, in the case of MMF based imaging, neurons and even their arborisations in immediate proximity of the fibre tract retain their structural integrity, the damage incurred by by established approaches is significant enough to raise questions about possible cognitive impediments suffered by the animal as a result; impediments which might affect its behaviour, or at the very least sub cellular physiological processes such as synaptic plasticity (Xu et al. 2016). A further issue elucidated in previous work is the inflammatory response of the immune system, which it stands to reason should be significantly lower in the case of a single optic fibre (Xu et al. 2016).

CHAPTER 4: NETWORK DYNAMICS IN THE DORSAL HIPPOCAMPUS - ACCUMBAL CIRCUITRY

4.1) Introduction

Pyramidal cells in the dorsal HPc have been demonstrated to provide a spatial representation of locomotion trajectories (O'Keefe et al. 1971, Morris et al. 1982, Pfeiffer et al. 2013). The dorsal HPc projects to the NAc, which mediates the translation of higher-order motivational and intentional states into affective behavioural output. The hippocampus-accumbal circuitry has been postulated to promote the acquisition, consolidation and reinstatement of context specific reward seeking behaviour (Lindon et al. 2010, Britt et al. 2012, Chersi et al. 2015; my Transfer Report 2015). In the following chapter, the network dynamics within the dorsal hippocampal CA1- accumbal circuitry will be investigated by means of large scale electrophysiological recordings, whereby action potentials discharged by individual neurons are extracted in awake, freely moving animals (McNamara et al. 2014) and optogenetic means. A small genetically identifiable cell cohort in the NAc will be established as a crucial juncture point in the information relay within the dorsal hippocampal accumbal circuitry. This will allow for the first mechanistic model of the integration and processing of the dCA1 input within the network physiology of the accumbal circuitry. Furthermore, this might shed light upon the computational architecture underpinning context dependent reward seeking behaviour. In the future this work might serve as a suggestion how different and parallel inputs within global neuronal circuits in the brain could be integrated by local networks (Trouche, Koren et al. 2019).

The aim of this work was to analyse whether systemic network interactions between distinct cell types in the dCA1 and the NAc could be delineated. A recently proposed method of electrophysiological cell type classification (Sharott et al. 2009) was adapted and applied in

order to allow for the correlation of dCA1 activity with the neural activity of distinct NAc cell types. The experimental objective was to examine this correlation while the dCA1-NAc projections as well as their post-synaptic target cells in the NAc were silenced and stimulated. In doing so, so the underlying hypothesis, we would be able to discern the principles underlying the translation of dCA1 input into NAc output modulation.

4.2) Cell classification of NAc cells

Pairwise firing rate and spike time correlations between indiscriminate, individual cells often are not enough to account for systemic network interactions between distinct cell types (Mizuseki et al. 2009). In a heterogenous neural network such as the NAc, if cell type specific interactions are to be delineated, those cell types have to be reliably identified. The purpose of this subchapter is to develop a means for such reliable identification of cell types in the NAc from electrophysiological recordings obtained in freely moving mice.

Experimental setting

Mice were implanted with a customised micro-drive with twelve independently moveable tetrodes (48 channels in total), six of which were targeting the nucleus accumbens in the ventral striatum and another six the dorsal hippocampal CA1 layer, both in the right hemisphere. Each recording day commenced with the cell screening process, the lowering of the tetrodes in search of extracellular voltage discharges indicating neuronal spikes. Following the recording, the amplified, band pass filtered and digitalised signal from each of the channels was concatenated and used to extract the spikes for each of the detected neurons per tetrode. This was done by means of principal component analysis (PCA) applied to the four channels of each tetrode, and automated clustering (KlustaKwik), followed by a manual sorting and delineation of the resulting cell clusters based on physiological features such as

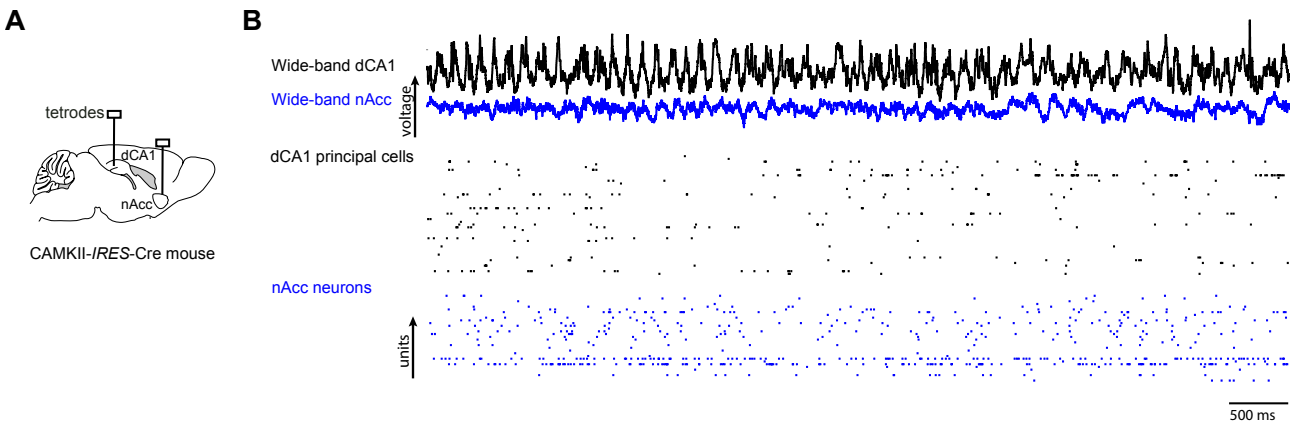

Figure 4.1: Simultaneous electrophysiological recordings in the hippocampal dorsal CA1 and NAc in freely moving, behaving mice. (**A**) A fully custom-made multichannel drive was implanted in mice targeting the two deep brain regions with 6 independently moveable tetrodes each. In the beginning of each experimental day the positioning of the tetrodes was altered in order to maximise the cell yield gained during the execution of the behavioural protocol. (**B**) Following the registration of the local field potential by the 4 channels of each tetrode, the signal was amplified, band pass filtered and digitalised. Single spike events were detected by means of high frequency filters, which were then assigned to different cell clusters through automated and manual clustering procedures, designating neuronal discharge activity of distinct individual cells (raster plots, scale bar 500 ms, n = 34 NAc neurons and 45 dCA1 PCs)

signal to noise ratio (indicated by the refractory period). The concomitantly extracted neuronal cell clusters in the NAc as well as the dCA1 were then analysed.

Waveform parameterisation

Published work suggests that distinct neuronal cell types in the NAc exhibit a spike waveform specificity which can be salvaged for the purpose of their identification from electrophysiological recordings (Sharott et al. 2009). The band-pass filtered (800 Hz to 5 kHz) and up-sampled (40 kHz) signal traces of every spike of each individual cell cluster, isolated as aforementioned, were aligned and averaged in order to gain the mean waveform for each channel of the recording tetrode. Subsequently, the average waveform with the highest amplitude (difference between highest and lowest voltage value within the designated time window) was chosen as representative of the cell. Although ideally, the relative positioning of the four channel wires of the tetrode to the cell should solely influence the amplitude but not the shape of the detected spike waveform in a predictable fashion (which disqualifies any waveform parameter that relies on the absolute value of the amplitude from being a suitable measure of cell type identity), certain recurrent alterations in the waveform between the

channels were observed, depending on their amplitude (not shown here). This might be caused by electrostatic forces between the separate channel wires and therefore, in order to maintain consistency and reproducibility with other published work, solely the dominant channel with the highest amplitude was utilised in the following.

The extracted average spike waveform, designated as the function of time w(t) (with w(t=0) being the global minimum of the function), was parameterised by three numerical measures: the duration of its first peak, duration of its second peak and the relative amplitude of the two. The duration of the first peak was defined as the time interval between the global minimum of w(t) (through of the spike; t=0) and the second zero intercept of the waveform (w(t)=0) to its left (Fig. 4.2a). The duration of the second peak was calculated analogous to the right of the spike through. The time constants of a neuronal discharge are considered to be associated with the intrinsic cellular features and largely independent of the distance between the cell and the recording tetrode wire.

$$DurationPeak_{1,2} = \begin{cases} t_{min} : \{t \mid w(t) = 0, w'(t) < 0\} & \text{if } t > 0 \\ -t_{min} : \{t \mid w(t) = 0, w'(t) > 0\} & \text{if } t < 0 \end{cases}$$

The relative amplitude of the two spikes was defined as the difference between the two peaks (local maxima w'(t)=0 between w(t1)=0 and w(t2)=0 left and right of the trough) over their sum (similar measure first implemented by Dr. Gido van de Ven in accordance with Royer et al. 2012; Weir et al. 2014):

$$spikeSymmetry = \frac{max(firstpeak)}{max(firstpeak) + max(secondpeak)}; spikeSymmetry \in (0; 1]$$

These measures presuppose, that the the global minimum of w(t) is preempted and succeeded by a zero intercept followed by a local maximum and a second zero intercept. Cell clusters,

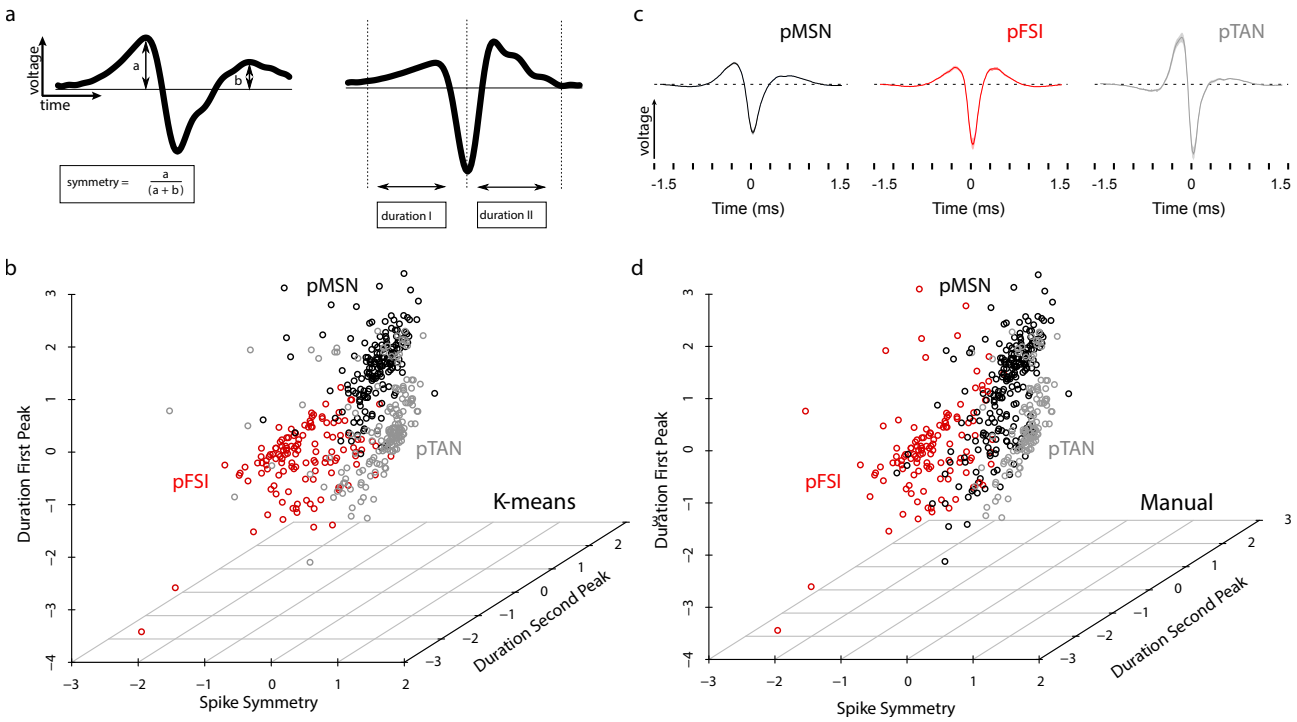

Figure 4.2: Cell type classification of recorded neurons in the NAc based solely on spike waveform parameters (**a**) The extracted mean spike waveform from the recording channel with highest amplitude, averaged over the entire recording duration, was parameterised through 3 numerical values: the duration of the first peak, the duration of the second peak and the relative amplitude of the two (spike symmetry) (**b**) In the 3-dimensional centred and scaled parameter space (centred to 0 and scaled to the interval (-4,4) at each axis for better visibility, no effect on clustering), three clusters emerge that can be verified through conventional supervised clustering algorithms (here: k-means). (**c**) The mean waveform of the cells attributed to the three clusters (with their respective corresponding cellular identity, which will be confirmed in chapter 4.4) are notably dissimilar (±SEM shaded area) (**d**) The manual classification of the spike waveforms in three groups by hand, which designates the optimal classification, has a similarity index of >90% with the clustering in (b) (n=418 neurons total, 169 MSNs and 125 FSIs and 124 TANs, from 2 mice and 18 recording days) (Trouche, Koren et al. 2019)

whose average waveform did not comply with this criterion were designated as "complex spikes" and excluded from any of the following analysis (approx. 10% of cell clusters, similar to Bakhurin et al. 2016). Such aberrations can be the result of a misplacement of the tetrode (especially in dendritic arbours) or due to a mismatch in the spike detection process.

For the purpose of this initial formal classification of cell types, 581 neuronal clusters in the NAc were extracted and parameterised (156 neurons were taken from an old recording data-set acquired by Dr. Stephanie Trouche in 2013, those cells were not included in any of the analysis following this subchapter). Similar to Sharott et al. 2009 and Bakhurin et al. 2016, all cell clusters were plotted against the three parameters: the duration of the first peak, duration of the second peak and the relative amplitude of the two. This method, first implemented by

Berke et al. 2004 (used a similar parametrisation), results in three distinct cell clusters within the three dimensional space. While some previous studies have used arbitrary cut-off criteria to assign cell type identity to the resulting clusters, here, in accordance with Sharott et al. 2009, a conventional k-means supervised clustering algorithm was used to allow for an automatic cell classification (Fig. 4.2b). The aim of this clustering method is to separate n elements in the d dimensional space into k clusters, so as to minimise the total distance between elements of the same cluster and to maximise the total distance between elements of different clusters. As such, through iterative adjustment of the group centroids (means), it tries to minimise the in-group variance, or

$$Var = \sum_{i=1}^{k} \sum_{j=1}^{n} ||x_i^j - c_i||^2,$$

whereby n is the number of NAc cells (n = 581), k is the expected number of NAc cell types (k = 3) and c is the centroid of the cluster i. This way, k-means clustering was used to subsume the individual cells under three clusters and assign them with a common cell identity (Fig. 4.2b, colour-coding will be adhered to through the entirety of chapter 4). Hierarchical clustering (Ward's minimum variance method) and density based clustering methods (dbscan) result in a very similar classification (not shown here).

The average spike waveform of all cells included in each of the clusters (Fig. 4.2c, shaded area depicts ±SEM) indeed reveals clear differences between the clusters. In order to provide a means of verification of the accuracy of the clustering method used here, this data-set was also clustered manually by hand (blindly). The similarity between the two classifications exceeds 90%. Owing to their waveform and in accordance with established terminology (Wilson et al. 1990; Kawaguchi 1993; Mallet et al. 2005; Sharott et al. 2009), the cell clusters

were classified as putative tonically active neurons (pTANs), fast spiking interneurons (pFSIs) and medium spiny neurons (pMSNs). Thus resulting classes exhibit marked distinctions in their spike train dynamics and firing properties (Trouche, Koren et al. 2019).

Spike train dynamics and firing properties

When the average waveforms of those three putative cell types are overlaid, it becomes apparent that each of the three parameters used, was designed to separate at least one cell type from the respective others. The duration of the first peak of pTANs is shorter compared to that of pMSNs and pFSIs. The same applies to the duration of the second peak of pFSIs relative to pTANs and pMSNs. pTANs are highly asymmetric with their first peak being strongly pronounced in comparison to the second, which is less the case for pMSNs. pFSIs finally, possess very symmetric waveform shapes, sometimes even exhibiting a spike symmetry reversal in favour of the second peak. These characteristics are in line with published literature and are hypothesised to be due to the intrinsic cellular characteristics of the different cell types (Bakhurin et al. 2016).

In order to validate the three cell clusters as correspondents of the different cell types, their spike train dynamics and firing properties had to be investigated and demonstrated to be distinct as well as compliant with precedingly published data. Firstly, the mean inter spike interval (ISI) distribution was computed for the three putative cell types. For added clarity within the lower frequency range, the logarithmic scale was applied to the time axis. The putative TANs have an unimodal ISI distribution, already described by others and owing to the rhythmic consistency and “tonic” character of their discharge dynamics (from now onwards tonically active neurons will no longer be denoted as “putative”). Interestingly, the average ISI distribution of pFSIs features a prominent rise at roughly 100 ms, which corresponds with the oscillatory frequency of the theta band. This observations will tie in with

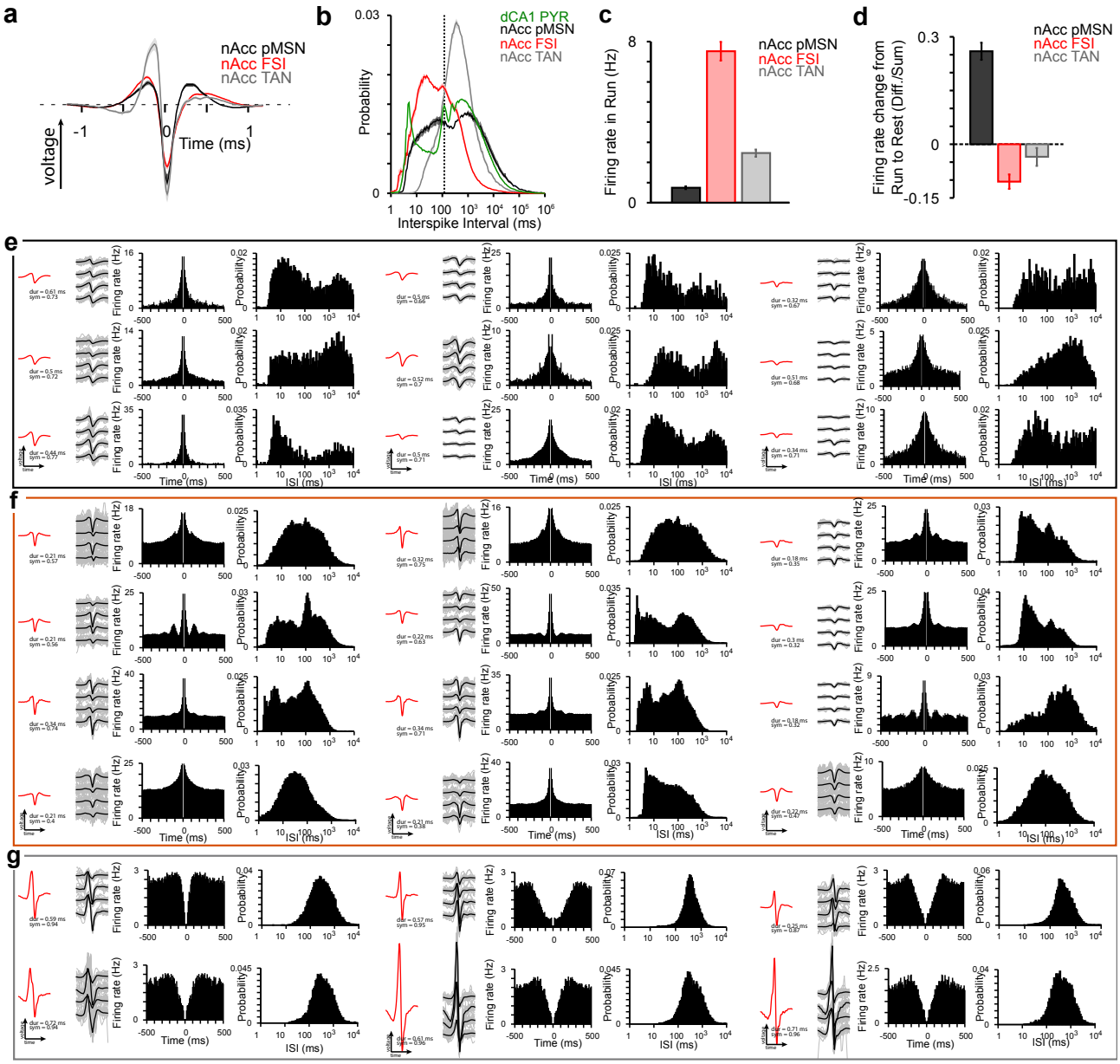

Figure 4.3: Physiological confirmation of the waveform based cell type classification in the NAc (**a**) The mean spike waveforms of all cells subsumed under the three clusters of cells (±SEM shaded area). These are designated as putative medium spiny neurons (pMSNs), fast spiking interneurons (FSIs) and tonically active neurons (TANs) in accordance with the nomenclature in the field, to be verified in the following (**b**) The normalised, average inter spike interval (ISI) distribution of the cells within the three classes on a logarithmic scale (±SEM shaded area). Marked distinction in the spike train dynamics of the three cell populations are apparent. Notably, TANs have a sharp single modal distribution which peaks close to the 1000ms mark. This attests to its strictly tonic activity profile and confirms among other indications this cell classes' designation as TANs. Also noteworthy is the distinct rise in the FSIs' probability to spike in theta rhythm (8-12 Hz), which is indicated by the dashed line that goes through the analogous sharp rise in the probability distribution of the dCA1 principal cells which is due to this cell types' well established coupling to this oscillatory frequency (the principal cells were included in this graph for this demonstrative reason only). This observation will gain further significance in the following subchapter. (**c**) Mean firing rate, averaged over the entire duration of the recording protocol, of the cells of each of the three classes (±SEM). The firing rate of FSIs is significantly higher than that of TANs and pMSNs, confirming among other indicators the identity of this class as fast spiking interneurons (**d**) Firing rate change between different behavioural states of the animal (active exploration vs. rest) (**e**) 9 representative example cells included in the cell cluster designated as putative MSNs. The mean waveform averaged over the entire recording from the channel with the highest amplitude is displayed (red) next to 40 randomly selected sample waveforms on each of the 4 tetrode channels with the corresponding averages during one recording session (typically 15 min in length). Next, the auto correlogram of the cell is shown as well as the ISI distribution. The individual mean waveforms as well as the ISI distributions match the overall average of the pMSN cell class and show remarkably little variance within the group as opposed to the other cell classes. (**f**) 12 representative example cells included in the cell cluster designated as FSIs exhibiting the characteristic properties of this class. (**g**) Similarly, 6 representative example cells included in the cell cluster designated as TANs (n=418 neurons total, 169 MSNs and 125 FSIs and 124 TANs, from 2 mice and 18 recording days) (Trouche, Koren et al. 2019)

the results in the subsequent subchapters. Secondly, the mean firing rate of each individual neuron was determined in Hz, regardless of the behavioural state of the animal and averaged within the respective cell cluster. Compatible with published results (Sharott et al. 2009, Bakhurin et al. 2016), the average firing rate of pFSIs is 7.5 Hz (from now onwards FSIs will no longer be denoted as "putative"), that of TAN 2.4 Hz and pMSN 0.8 Hz (graph includes ±SEM). Thirdly, the change in firing rate between awake and resting animal behaviour was calculated. FSIs decrease their activity during rest, pMSN increase their activity, whereas TANs were not significantly altered. Again, these results are in line with afore published data (Berke 2011). In conclusion, the physiological parameters of the cell clusters as distinguished solely by their spike waveform features have been shown to closely mirror previous descriptions of the three respective cell-types.

One point of contention might lie in the disproportionate number of FSIs and TANs in this data-set. According to histological studies (Tepper et al. 2010, Tepper and Bolam 2004, Gonzales et al. 2015), roughly 95% percent of all cells present in the dorsal striatum are MSNs, cholinergic interneurons (which are putative TANs) constitute to that effect about 1% and FSIs 2-3% (a more detailed analysis of the molecular make-up of the cell subpopulations described as FSIs will follow in a later subchapter). In the ventral striatum, though not as well described, the same proportions seem preserved. In comparison, this data-set, according to the described classification method, contains approximately 40% pMSNs, 30% FSIs and 30% TANs. The reason for the over-representation of the interneurons is multi-facetted. Firstly, cholinergic interneurons (which are putatively TANs) have a very expansive morphology and due to their widespread arborisations, their electric discharges can be picked up within a greater perimeter. This becomes especially apparent as individual TANs (verified by waveform and spike train dynamics) were recorded over many subsequent days, even though

the tetrodes were lowered intermittently. As for the FSIs, their high firing rate naturally biases the cell screening process in their favour in a brain region such as the NAc, which is known for its spareness of activity. Finally, most MSNs were shown to be silent at any given time point. This bias towards the recording of rare interneuron types which is owed to the technical idiosyncrasy of the recording method employed here, ultimately and rather fortunately enabled the in depth study of their role in the network dynamics of the dorsal hippocampal-accumbal circuitry, which is now to follow in the next subchapters.

In this subchapter, a means was developed for the reliable identification of cell types in the NAc from electrophysiological recordings obtained in freely moving mice. This approach allows for the further exploration of the functional interactions of distinct cell populations within the dorsal hippocampal-accumbal circuitry.

4.3) Activity of FSIs in the NAc is controlled by dCA1 principal cells

The purpose of the present subchapter is to analyse whether systemic network interactions between distinct cell types in the dCA1 and the NAc can be delineated through electrophysiological and optogenetic means.

Experimental setting

As already noted, direct projections from the dorsal hippocampal CA1 region reach the NAc of the ventral striatum (Fig. 4.4). In contrast to the input the NAc receives from the ventral HPc, this pathway however has not yet been the focus of attention. In order to explore the functional effect of the long range input from the principal cells of the dorsal CA1, CaMKII-Cre mice were injected with an adeno-associated virus vector (AAV) which encoded the protein Archaerhodopsin-T (ArchT) fused with the green fluorescent protein (GFP) under the control of a Cre-inducible promoter (CAG): AAV2-CAG-flex-ArchT-GFP. CamKII is the Ca^{2+}/calmodulin-dependent protein kinase II and is prominently expressed by the principal cells in the dorsal CA1 pyramidal layer. This physiologic expression drives the build-up of Cre recombinase, a tyrosine recombinase enzyme derived from bacteriophages. When the AAV vector is introduced into those cells, the Cre recombinase adheres to the LoxP recognition sites (flex) and activates the construct, which leads to the expression of ArchT-GFP in principal cells of the dCA1. ArchT is a outward proton pump protein derived from Archaea which is driven by yellow light (absorption peak at 580 nm) and causes a hyper-polarisation of the cell-membrane of a neuron, thus effectively silencing it by preventing the triggering or the propagation of a membrane discharge (Trouche, Koren et al. 2019). These animals were implanted with multichannel drives described in chapter 4.2, but in addition contained a stationary optic fibre positioned above the NAc. Between the injection of the virus and the recordings 4-6 weeks were passed in order to ensure that the ArchT proteins,

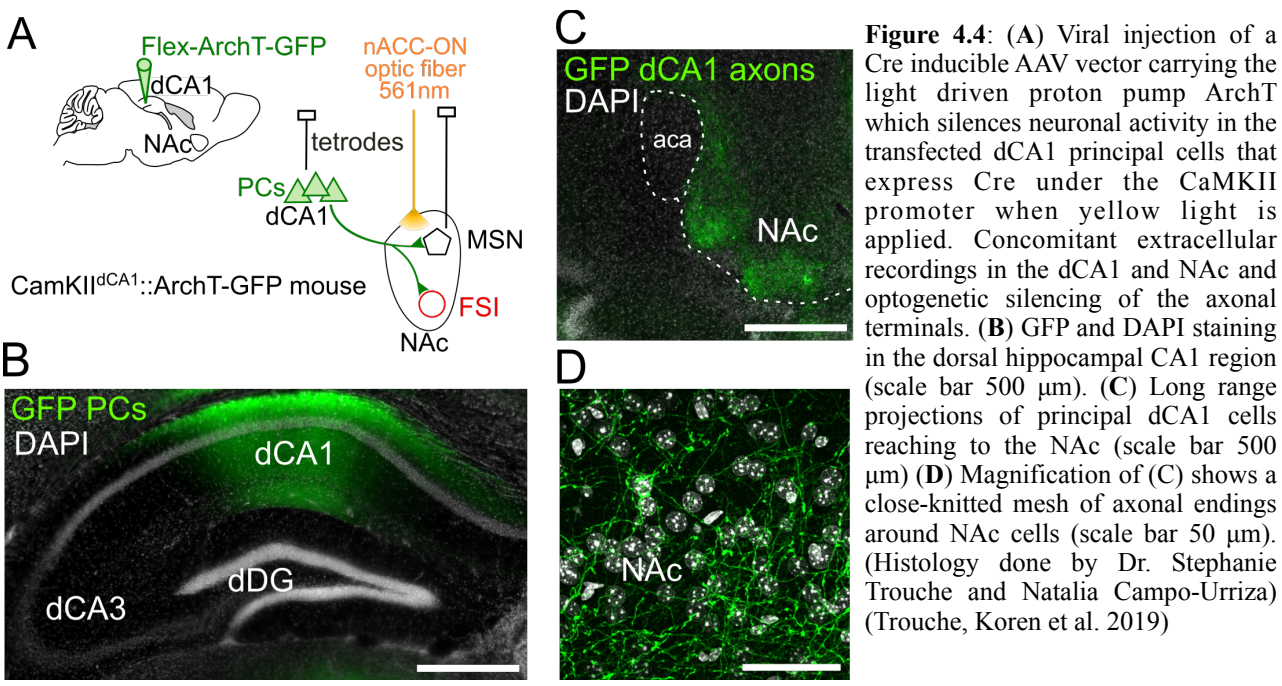

Figure 4.4: (**A**) Viral injection of a Cre inducible AAV vector carrying the light driven proton pump ArchT which silences neuronal activity in the transfected dCA1 principal cells that express Cre under the CaMKII promoter when yellow light is applied. Concomitant extracellular recordings in the dCA1 and NAc and optogenetic silencing of the axonal terminals. (**B**) GFP and DAPI staining in the dorsal hippocampal CA1 region (scale bar 500 µm). (**C**) Long range projections of principal dCA1 cells reaching to the NAc (scale bar 500 µm) (**D**) Magnification of (C) shows a close-knitted mesh of axonal endings around NAc cells (scale bar 50 µm). (Histology done by Dr. Stephanie Trouche and Natalia Campo-Urriza) (Trouche, Koren et al. 2019)

incorporated into the cell membrane of the dCA1 principal cells projecting to the NAc, would diffuse to their axonal terminals in the latter structure. During the concomitant recording of the cell activity in both brain regions, the NAc was flooded with yellow light, which allowed for the isolation of the NAc circuitry from the functional effect of dCA1 input (Fig. 4.4).

dCA1 principal cells selectively drive the activity of FSIs in the NAc

Any further analysis will exclusively concentrate on three cell types: principal cells in the dCA1, FSIs and pMSNs in the NAc (interneurons in the dCA1 as well as TANs in the NAc will be mentioned for supportive purposes only). In total 671 dCA1 pyramidal cells and 271 NAc neurons (including 169 MSNs and 65 FSIs) recorded from 5 behaving mice were used in this subchapter. Fig. 4.5a showcases representative examples of individual cells corresponding to those cell types. In line with the observation made in chapter 4.2 of the pronounced increase in the average ISI distribution of FSIs at the theta frequency band, the autocorrelation of the hereby exhibited cell (similarly to other examples in Fig. 4.3f) is modulated by theta oscillations. It is well established that theta oscillations can serve the purpose of synchronisation and organisation of information relay between different brain

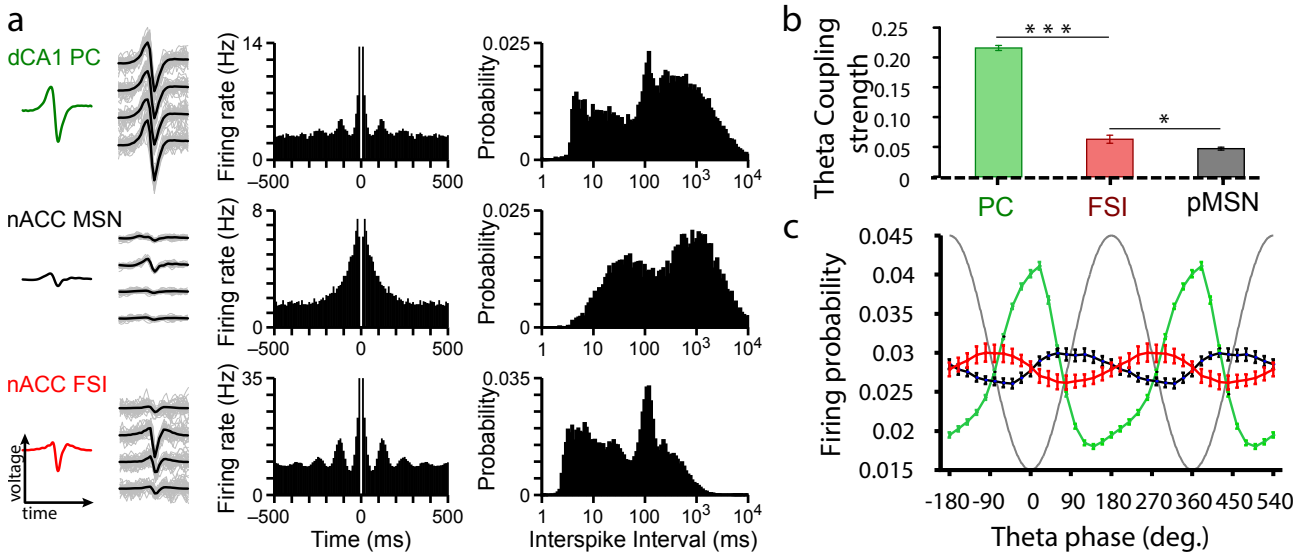

Figure 4.5: Cell-type specific activity coupling of NAc neurons to the dorsal hippocampal oscillations in theta band frequency (8-12 Hz) (**a**) Three representative example cells belonging to the designated classes of dCA1 principal cells and putative MSNs as well as FSIs in the NAc. Similar to Fig. 4.3 the mean spike waveform is displayed next to sample waveforms (grey) on each of the four channels of the recording tetrode with the respective averages (black). Furthermore, the auto-correlogram as well as the ISI distribution are presented. There is a noteworthy resemblance between the spike train dynamics of the principal cell and the FSI: both cells fire in bursts and their activity is paced by a rhythmicity which corresponds to theta band oscillations. (**b**) The average strength of the cell type's activity coupling to the theta band oscillations in the dCA1. (**c**) The normalised, mean theta phase distribution corresponding to all discharges of the cells within the three classes; only significantly modulated cells were included (n = 671 PYRs and 271 NAc neurons, including 169 MSNs and 65 FSIs, from two mice and 18 recording days) (Trouche et al. 2019)

structures as well as cell population communication within local networks. In order to investigate whether this might be the case with cell populations in the NAc in relation to the dCA1, the coupling of the activity of each NAc neuron to the hippocampal dCA1 theta frequency band oscillation phase was calculated. Importantly, theta band oscillations of the LFP in the NAc, comparably low in their power, do not necessarily phase-align with those in the dCA1, thus a coupling of NAc cells to dCA1 oscillations can't be taken for granted. The dCA1 LFP signal was band pass filtered (5–12 Hz theta, 4th order Butterworth filter) and a Hilbert transform was applied in order to recover the instantaneous theta power and phase during each cell discharge in the NAc. If the circular function of the distribution of theta phases corresponding to all discharges of an individual cell can be described as an oscillation significantly different from the uniform distribution, then the power and orientation of this cell's coupling to the dCA1 theta band can be concluded (implemented by Dr. Gido van de Ven, see DPhil thesis). Here, the average power of the respective cell type's activity coupling

to the instantaneous dCA1 theta oscillation is plotted in comparison with each other (Fig. 4.5b). In compliance with previously published data, principal cells of the dCA1 are strongly coupled to the local theta oscillations. Surprising however is the relative strength of the FSIs' coupling to the same rhythm as well as the less pronounced, but still significant coupling of the pMSN population. Having established that all three cell types couple to dCA1 theta oscillations, the next step was to explore whether they have characteristic cell type specific phase preferences relative to the oscillatory cycle of dCA1 theta. In order to do so, the average distribution of theta phases corresponding to all discharges of the cells within those classes was compared (Fig. 4.5c). Confirming published data, principal cells in the dCA1 preferentially discharge at the trough of the theta cycle. Interestingly, FSIs as well as pMSNs have a cell type specific phase preference as well, the former discharging during the descending phase of theta with the latter preferentially spiking during the ascending phase. Noteworthy is firstly the fact that the mean phase preference of FSIs occurs before the principal cells in the dCA1 spike and secondly that the FSI and the pMSN activity seemingly oscillate in anti-phase to each other relative to the dCA1 theta rhythm. Both observations will be of importance later on.

Having established the cell type specific oscillatory coupling of the NAc cell populations to the principal cells in the dCA1, the next step was to investigate whether there is evidence of a short latency spike time correlation between the two structures, which might provide indication of a direct monosynaptic activity drive imposed by the dCA1 principal cells over the network in the NAc. Pairwise firing rate and spike time correlations between individual cells in the dCA1 and NAc did not lead to conclusive results. The low firing rate of the cell types involved (specifically principal cells and pMSNs) in conjunction with the weakness of the driving forces, that necessarily has to be expected when two distant brain regions are

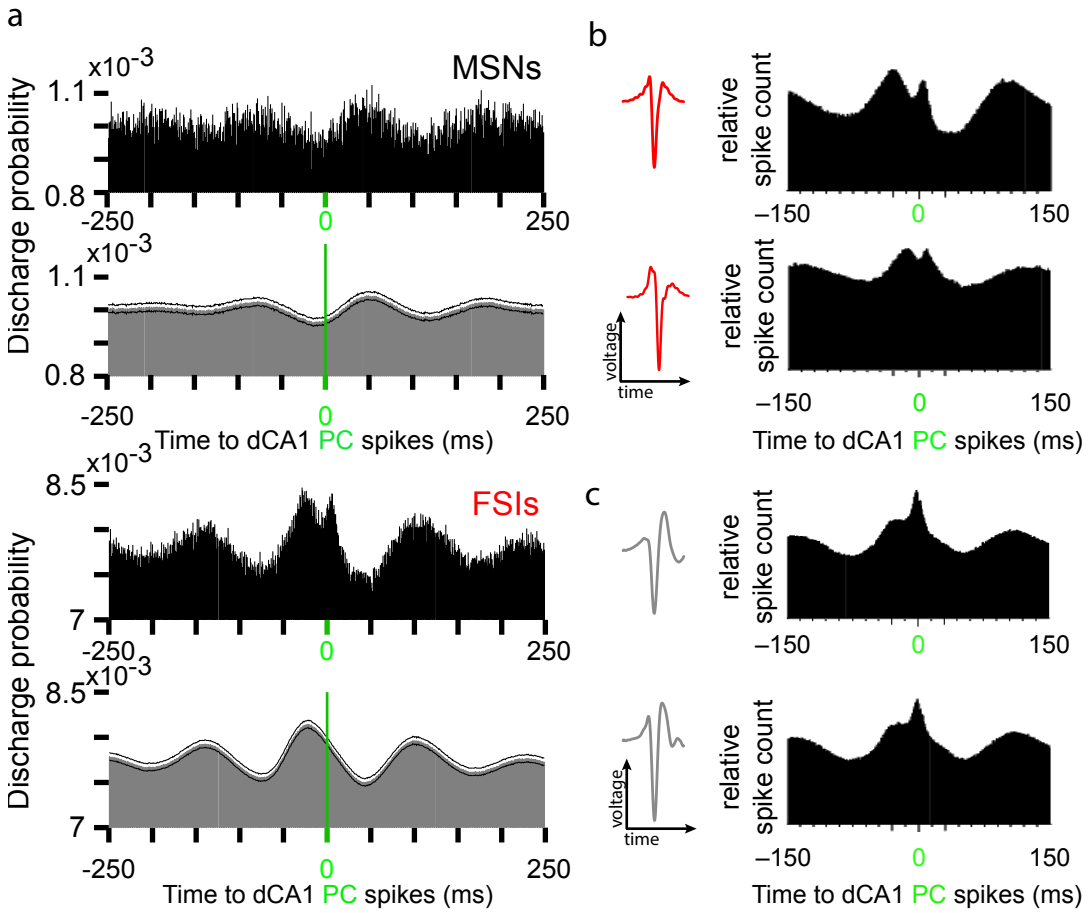

Figure 4.6: Population spike cross-correlograms relative to dCA1 principal cell spikes (**a**) For each reference dCA1 principal cell spike, the time locked cumulative neuronal response from the referred cell class (FSIs and pMSNs) was extracted and summed up (short latency PYR-to-FSI response offset: 3.2–8ms). As a control, each spike of the principal cells was randomly assigned to the same theta oscillatory phase of another theta cycle. (**b**) Examples of population cross correlograms of individual FSIs relative to concomitantly recorded cumulative PC spiking together with the corresponding average representative spike waveform of those cells. Furthermore, the oscillatory coupling of those cells' activity to the instantaneously extracted dCA1 theta band phase is depicted. (**c**) Similar to (b). Examples of population cross correlograms of individual dCA1 interneurons relative to concomitantly recorded PC spiking (methodology of separation of hippocampal principal neurons from interneuron see Csicsvari et al. 1998, 1999b, n = 671 PYRs and 271 NAc neurons, including 169 MSNs and 65 FSIs, two mice and 18 recording days) (Trouche, Koren et al. 2019)

connected through sparse projections, made an analysis indiscriminate of cell type identity challenging. In order to delineate systemic network interactions between the distinct cell types, the temporal relationship between single spike events of hippocampal and accumbal cell types was depicted through group cross-correlograms (analogue to Mizuseki et al. 2009). Only time periods of active exploratory behaviour (Thomson's multi-taper method) were considered. For each reference dCA1 principal cell spike, the time locked cumulative neuronal response from the referred cell class (FSIs and pMSNs) was extracted and summed up (Fig. 4.6a). As a control, each spike of the principal cells was randomly assigned to the

same theta oscillatory phase of another theta cycle in order to maintain the theta rhythm dynamics but break up any possible short latency spike time correlation between the reference and the referred cell type. Afterwards, the same time locked cumulative neuronal response from the referred cell class was calculated again, which was executed 1000 times in order to gain the confidence interval indicated in grey (a more elegant improvement over my own theta cycle trough triggered population spike response control, implemented by Dr. Vitor Lopes dos Santos). Two notable observations can be made hereby. Firstly, similar to the cell type specific oscillatory coupling of FSIs and pMSNs to the dCA1 theta rhythm, the cell type specific spiking in the NAc presents an oscillatory dynamic corresponding to theta frequency modulation. Moreover, these oscillations of the FSI activity are in anti-phase to the same of the pMSNs. Secondly, the FSI population exhibits a strong and brief, short latency discharge increase following the individual spiking of principal cells in the dCA1. When the timely relationship of principal cell discharges with the FSI neuronal activity (but not their correlation with the dCA1 theta rhythm) was perturbed, this effect dissipated, indicating a causality between the principal cells spiking events and the driven FSI activity. The time offset between the reference spikes in the dCA1 and the peak of the FSIs' short latency response was 3.2-8ms, allowing for the assumption of a monosynaptic driving influence that is exerted by the principal cells onto the FSIs, notably however not the MSNs. Furthermore, examples of population cross correlograms of individual FSIs with PCs (Fig. 4.6b) are shown to starkly resemble those of interneurons in the dCA1, which are well known to receive excitatory monosynaptic input form principal cells driving their activity (Fig. 4.6c).

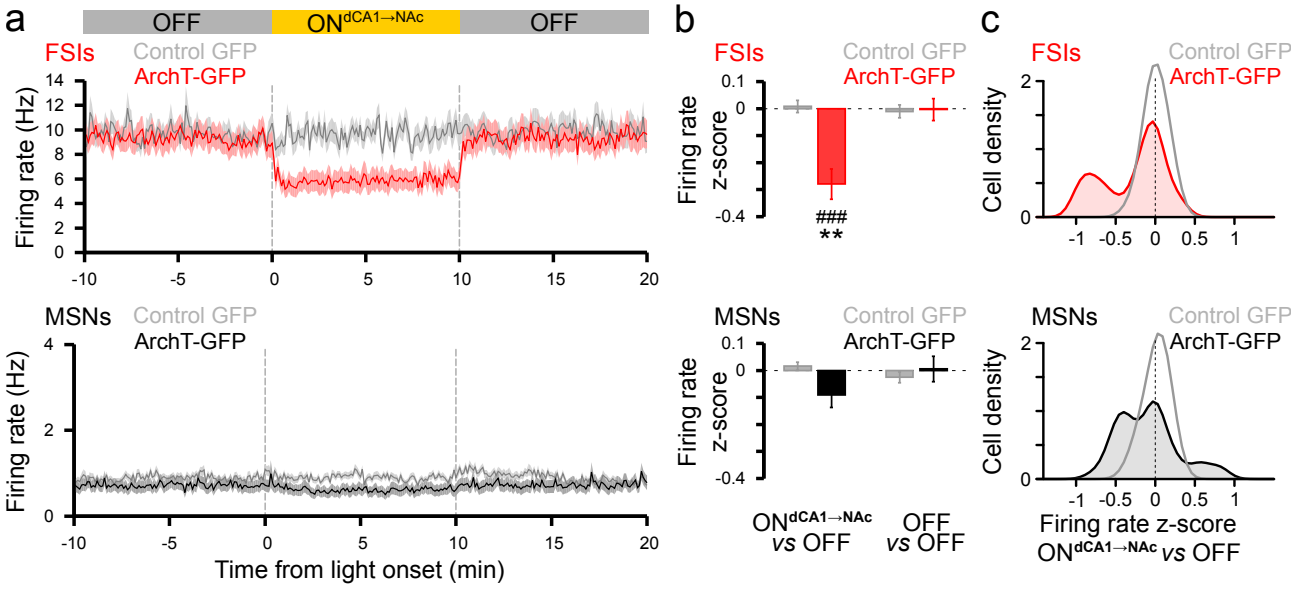

Figure 4.7: Effect of light induced silencing of dCA1 PC axonal projections on NAc population activity (**a**) Averaged firing rate response of distinct NAc cell type populations (FSIs, pMSNs, GFP Control in two mice) to a single prolonged 651 nm light pulse of 10 min (50-ms bins). (**b**) Average firing rate change of individual cells constituting the pMSN and FSIs cell cohorts from the Light OFF period preceding the light pulse relative to the following Light ON period as well as the Light OFF period thereafter. (mean ± SEM; **p<0.01 unpaired t-test MSNs versus FSIs, ### p<0.001 mean population rate change versus zero) (**c**) Density diagram of firing rate scores of individual cells constituting the pMSN and FSIs cell cohorts indicating the relative change of the Light OFF firing rate within the Light ON period (corresponding distributions of cell density estimated using a kernel density approach (Silverman, 1981)) (271 NAc neurons, including 169 MSNs and 65 FSIs from two ArchT-GFP mice and 18 recording days; n = 181 NAc neurons, including 107 MSNs and 35 FSIs from two GFP control mice and 12 recording days) (Trouche, Koren et al. 2019)

Synaptic input from dCA1 principal cells is necessary for the maintenance of the activity of a subgroup of FSIs

Once the systemic network communication between the principal cells in the dCA1 and the FSIs in the NAc was determined under physiological conditions, optogenetic means were used in order to disrupt it. The axonal terminals of long range projections from the dCA1 principal cells in the NAc were silenced by means of a single prolonged 561nm light pulse during the animal's exploratory behaviour (Light ON duration: 10 min). A few other published studies have demonstrated the effective silencing of axonal terminals using different molecular strategies (there is contention in the field as to which strategy is the most effective) (Wiegert et al. 2017), none of whom however has concomitantly recorded its postsynaptic effects on the targeted cell population in vivo. The effect of the light was a drastic decrease in average activity of the FSI population, whereas the mean activity of pMSN

as well as that of TANs (not shown, served as a control) was only weakly affected (Fig. 4.7a,b). Interestingly, in the beginning and after the end of the 10min laser pulse, a gradual adjustment of the mean FSI activity to the new base firing rate is observable, which is owed to the slow dynamics of the silencing mechanism of ArchT within axonal endings and confirms previous work of Dr. Mohamady El-Gaby on this subject (El-Gaby et al. 2016). A density diagram of the Light-OFF/Light-ON change in firing rate of all cells constituting the FSIs and pMSNs allowed further to differentiate the effect of the silencing. It shows that only a subset (roughly 30%) of FSIs was affected at all by the silencing of the hippocampal input, those however very strongly so, oftentimes being nearly entirely silenced (Fig. 4.7c). The pMSNs had a more differentiated response with one subgroup of cells being moderately silenced and another subgroups being strongly excited (TANs activity was inert, data not shown). This observation will tie in with the analysis and discussion in the following subchapters.

Consequently, the question arose, whether these silenced FSIs differed in any physiological parameter from the non-silenced FSIs and as such were discernible. Although similar in their waveform shape and spike train dynamics, one such difference became apparent when the average distribution of the extracted dCA1 theta phases corresponding to the discharges of those two cell cohorts was compared. Interestingly, preliminary evidence suggests (not shown), that non-silenced FSIs and silenced FSIs have different cell type specific phase preferences, the former discharging during the descending phase of dCA1 theta whereas the latter preferentially spiked during the ascending phase. Notably, this would mean that the FSIs, that were silenced when dCA1 principal cell input was inhibited, would have a physiological preference to spike after principal cells in the dCA1 theta cycle, whereas all other FSIs would spike before the principal cells and in anti-phase to the silenced FSIs.

Consequently, this raises the possibility of a feed-forward inhibition mechanism, that will be discussed later.

In this subchapter, electrophysiological and optogenetic means were used to analyse systemic network interactions between distinct cell types in the dCA1 and the NAc. It was established that dCA1 PCs selectively drive the activity of a subset of FSIs in the NAc and that functional input from dCA1 PCs is necessary for the maintenance of the activity of a subgroup of FSIs. This indicates that a subset of FSIs in the NAc might serve as a primary target for the PC input from the dCA1.

4.4) Optogenetic stimulation

The purpose of the following subchapter is to propose a molecularly defined group of NAc interneurons as a possible prospect capable of serving the translation of dCA1 input into a local network-wide response within the NAc.

Experimental setting

The main γ-Aminobutyric acid expressing (GABAergic) interneuron types in the striatum are parvalbumin (PV) positive, somatostatin (SST)/ neural protein (NPY) positive and calretinin (CR) positive cells. These three types constitute roughly 0.7%, 0.5% and 0.7% of all cells in the dorsal striatum and there is evidence to suggest that this is similarly the case in the ventral part (Tepper et al. 2010). Together, these three molecularly identifiable cell types make up the class of FSIs (Tepper and Koos 2010). In order to delineate the discrete contribution of any of these cell type subgroups to the network dynamics of the NAc, they had to be electrophysiologically marked. To this end, PV-Cre mice were injected into the NAc with a AAV vector which encoded for the protein Channelrhodopsin2 (hChR2) fused to an enhanced yellow fluorescent protein (EYFP) under the control of a Cre-inducible promoter (EF1a): AAV2:EF1a-DIO-hChR2(H134R)-EYFP-WPRE. When the AAV vector is introduced into Cre expressing cells, the Cre recombinase adheres to the LoxP recognition sites (DIO) and activates the construct, which leads to the expression of hChR2-eYFP in PV positive FSIs. hChR2 is a inward Calcium ion pump protein derived from algae which is driven by blue light (absorption maximum at 480 nm) and causes the depolarisation of the cell-membrane of a neuron, thus effectively triggering a membrane discharge (Trouche, Koren et al. 2019). These animals were implanted with the same multichannel drives containing an optic fibre positioned above the NAc described previously in chapter 4.2. Between the injection of the virus and the recordings 4 weeks were passed in order to ensure a sufficiently strong

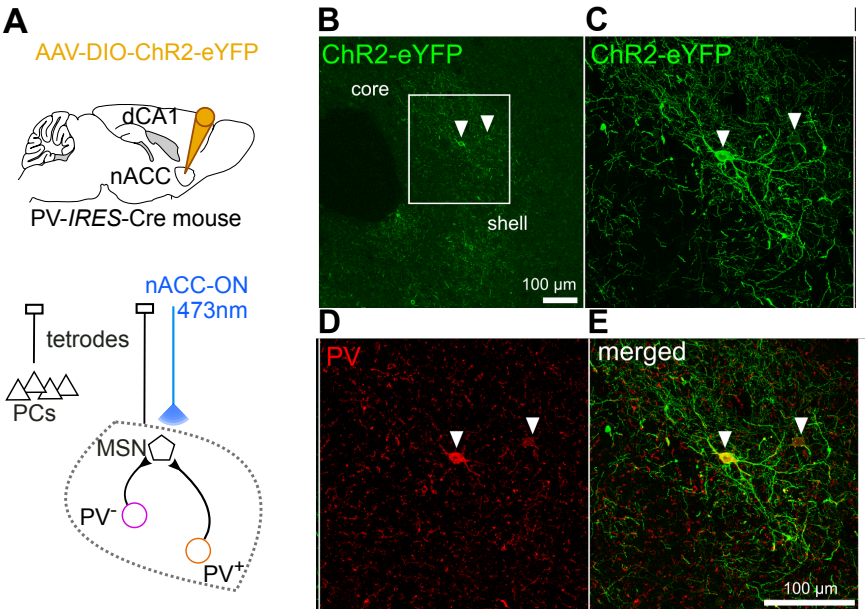

Figure 4.8: (**A**) Viral injection of a Cre inducible AAV vector carrying the light driven Calcium ion pump hChR2 which elicits neuronal activity in the transfected NAc PV+ interneurons when blue light is applied. Concomitant extracellular recordings in the dCA1 and NAc and optogenetic stimulation. (**B**) eYFP expression in the NAc. (**C**) magnification of (B) (**D**) PV staining in the NAc identifying PV+ interneurons (**E**) Co-localisation of PV staining and eYFP demonstrating the selectivity of the transfection method (Histology done by Dr. Stephanie Trouche and Natalia Campo-Urriza, scale bar 100µm) (Trouche, Koren et al. 2019)

expression and incorporation of the protein into the cell membrane. During the concomitant recording of the cell activity in both structures, the NAc was flooded with brief bursts of blue light, which allowed to study the functional effect of PV positive FSI activation on the local network dynamics as well as correlating thus identified cells' activity to the recordings in the dCA1 (Fig. 4.8).

PV positive interneurons are FSIs

The first purpose of this experiment was to investigate whether one can reliably and reversibly drive the activity of PV expressing interneurons through optogenetic means, thus allowing for their electrophysiological identification through simultaneous recording of their activity, and if so, whether they are indeed FSIs. To this effect, 500 light pulses of 10 ms in duration (the rationale for this particular duration will be elucidated in the following) were administrated to the animal in a partially randomised protocol over a 25 min long period of exploratory behaviour. In total, 4 different animals were recorded and 28 recording days were fully processed, which led to a whole of approx. 1800 cells being analysed, two thirds in the dCA1 and one third in the NAc. Eight of those NAc cells were unambiguously identified as

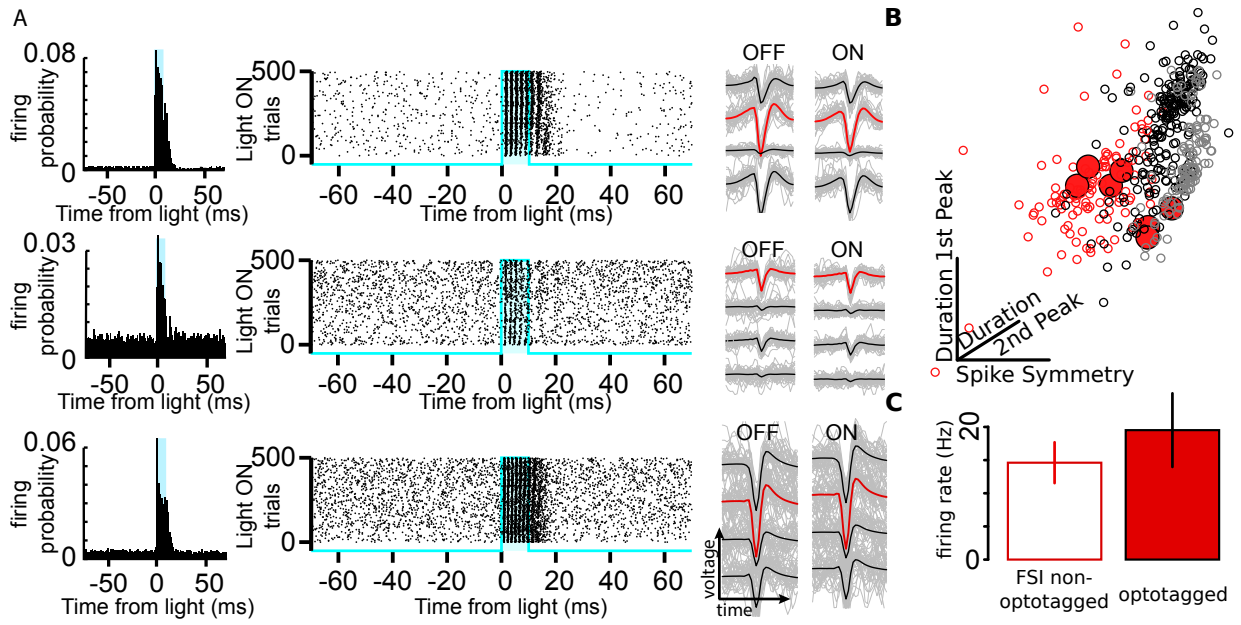

Figure 4.9: Light induced electrophysiological identification of PV positive interneurons in the NAc (**A**) 500 480 nm wavelength light pulses of 10 ms in duration in a partially randomised protocol over a 25 min long period of exploratory behaviour were administrated to four mice. The light onset triggered activity response of three representative examples of optotagged PV positive FSIs are presented by means of the firing probability concatenated over all trials as well as single spike responses over all individual trials. Furthermore, the average spike waveforms under ON- and OFF-Light conditions are compared. (**B**) The average spike waveforms of optotagged cells (n=8, filled red) were parametrised analogously to chapter 4.2 and demonstrated to cluster together with the other FSIs (**C**) The average overall firing rate of optotagged cells is compared with non-optotagged cells (n=8 optotagged FSIs and n=12 non-optotagged FSIs, recorded on the same tetrodes, from four mice and 28 recording days) (Trouche et al. 2019)

PV expressing interneurons, representative examples of which are seen in Fig. 4.9a. A few things are noteworthy hereby. Firstly, the averaged firing rate response of the thus optogenetically tagged cells triggered by the light is significantly higher than the cells' average base firing rate, thereby enabling a reliable identification. Secondly, the timing of the individual neuronal discharges within the activity bursts these cells exhibit in response to the light remains unvaried with every recurrent light pulse, leading to a seeming synchronisation when visualised over all trials simultaneously. This phenomenon indicates that, firstly, these cells' activity was driven to the maximum extent that was permitted by their intrinsic cellular and molecular constitution, and secondly, their cellular discharge mechanism recovered each time within seconds to its full potential to spike anew. A further observation lies in the continued activity of the PV positive interneurons in the milliseconds following the cessation of the light pulse, which can be explained by the cell membrane time constant which limits the pace it can recuperate the resting membrane potential after a complete depolarisation.

Lastly but importantly, the averaged spike waveform of those optogenetically tagged cells was similar during the light-ON periods compared to its counterpart during the remaining time. This further confirms that the cells‘ physiological condition during the burst activity was not detrimentally affected (the importance of which will become apparent in the following). In addition, it ensures that the spikes during the Light ON period do indeed belong to the respective cell and are not a fabricate of the data processing procedure (e.g. the manual spike sorting). Finally, in order to confirm that these cells are indeed FSIs, their average spike waveforms were parametrised analogously to chapter 4.2 and demonstrated to cluster together with the FSIs within the data set of that chapter (Fig. 4.9b). Moreover, the average firing rate of the optogenetically tagged cells was nearly 20 Hz, which does not significantly deviate from the firing rate of all non-optotagged FSIs, which were part of the data-set at hand (Fig. 4.9c).

Effect of activation of PV positive FSIs on the network

The duration of the blue light pulses applied to the NAc during the animal’s exploratory behaviour was chosen to be 10ms with the additional purpose to allow for a delineation of possible secondary effects of PV positive cell activity on the local network activity profile. On the one hand, the triggered response of those cells had to be of sufficient duration in order to ensure the possibility of postsynaptic hyper-polarisation of cells that were the monosynaptic targets of those GABAergic interneurons. On the other hand, the pulse length had to encompass the entire duration of a potential response latency between two such coupled cells accounting for the respective synaptic transmission. This was necessary to enable reproducibility over many Light-ON trials and eventually to allow the averaging over many cells which might lead to conclusions about the underlying connectivity pattern between the cell types responding to the light. Apart from the optotagged FSIs, there were other cells

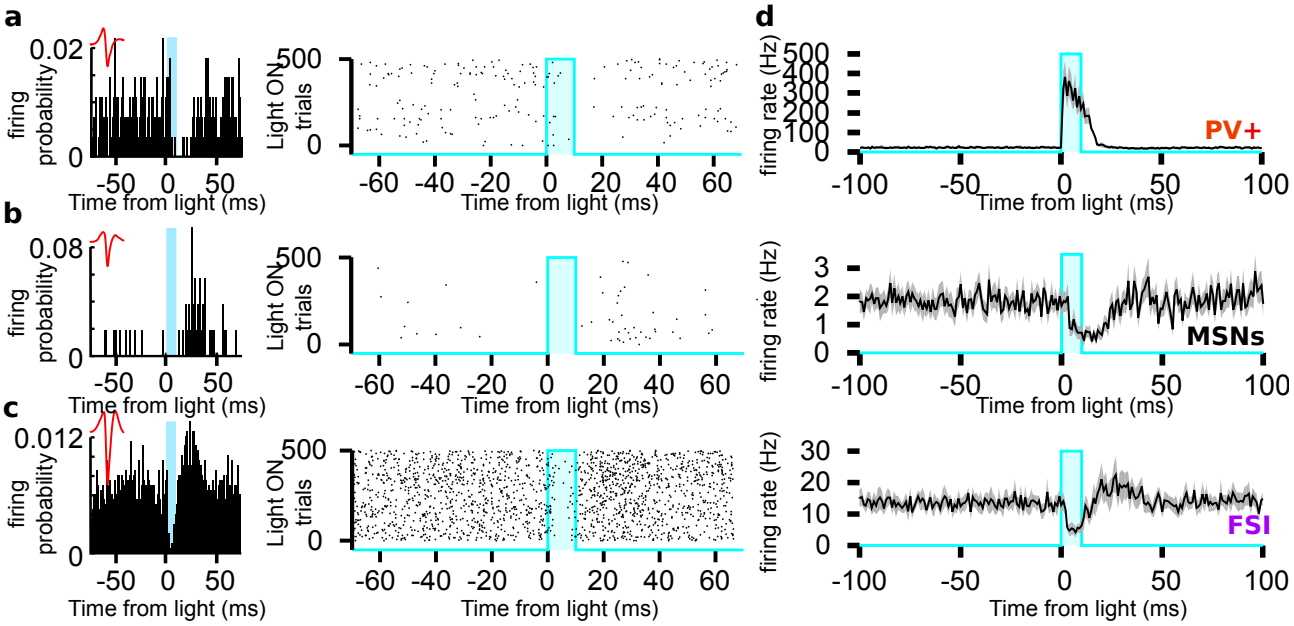

Figure 4.10: Secondary network effects of PV positive FSI activation (**a**) Representative example of silenced pMSN with its corresponding average spike waveform. The response is presented by means of the firing probability contaminated over all trials as well as single spike responses over all individual trials triggered by the light pulses. (**b**) Similar to (a) a representative example of an excited pMSN(**c**) Similar to (a), a representative example of a silenced FSI (**d**) The light pulse triggered firing rate response of three populations of cells in the NAc: optotagged FSI designated as PV positive (n=8), pMSNs (n=25, all light responding pMSNs were concatenated) as well as other, inhibited FSIs (n=6, mean ± SEM; 1ms bins; from four mice and 28 recording days) (Trouche, Koren et al. 2019)

identified to consistently react to the light induction. The reason, why they were not designated as PV expressing interneurons was either because they were inhibited or had a long response latency to the light. These cells were classified in line with the criteria established in chapter 4.2. Out of about 600 cells recorded in the NAc, 25 pMSNs were identified as strongly inhibited by the light, 3 pMSNs that were excited by the light and 6 FSIs that were strongly inhibited by the light (other, less affected cells, were not designated as "responding to light" in order to avoid false biasing of population averages). Three representative examples of these cases are presented in Fig 4.10a-c. Notably, the inhibited pMSN (Fig. 4.10a) is fully silenced by the light and remains so for an extended period of time before it recovers its activity, this reaction however does not follow immediately after the onset of the light but has a short latency period. In the case of the excited pMSN (Fig. 4.10b), its effect latency is even more pronounced, whereas the silenced FSI (Fig. 4.10c) has a very brief latency before being entirely silenced which is followed by a rebound effect, that one

would expect from an interneuron. When averaged out over all light responding cells of the three populations of cells (PV+ interneurons, pMSN and other FSIs), the latency can be studied further. It reveals, that while PV+ cells respond nearly immediately to the light with a sharp activity rise, pMSNs are inhibited approximately 3 ms thereafter and similarly so are other FSIs. This response latencies are in line with published results on monosynaptic response time latencies in the NAc and also match preliminary data in vitro in the lab (not shown). The excitation of the pMSN on a much longer time scale might be explained by a two synaptic mechanism of two inhibitory neurons, which would also explain why those cells were found so rarely. This might entail a FSI-FSI-MSN or a FSI-MSN-MSN cascade. Importantly, the average activity of the overall pMSN population is strongly modulated by the activation of nearby PV+ FSIs (silenced MSNs were predominantly found co-localised with PV+ FSIs on the same sub-set of tetrodes which were recurrently targeted to the same stereotaxic coordinates in the NAc, not shown).

Effect of activation of dCA1 axonal projections on the NAc network

One additional experiment was conducted with the aim to stimulate the dorsal CA1 projections within the NAc and to study their excitatory effect on the integrated network dynamics within the CA1-accumbal circuitry. This involved the injection into the dorsal HPc with a AAV vector which encoded for the protein Channelrhodopsin2 (hChR2) fused to an enhanced yellow fluorescent protein (EYFP) under the control of a CaMKII promoter: CaMKII-

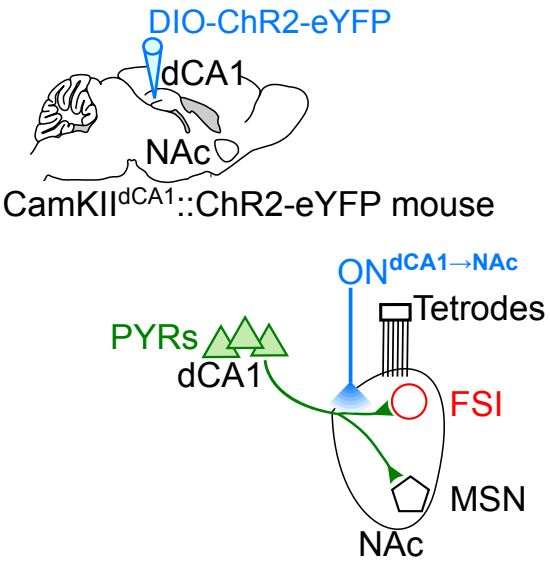

Figure 4.11: Stimulation of dCA1 projections within the NAc. An AAV vector was injected into the dorsal HPc encoding for the protein Channelrhodopsin2 (hChR2) fused to an enhanced yellow fluorescent protein (EYFP) under the control of a CaMKII promoter: CaMKII-hChR2(H134R)-EYFP. Subsequently, a multichannel drive with an optic fibre above the Nac was implanted (Trouche et al. 2019)

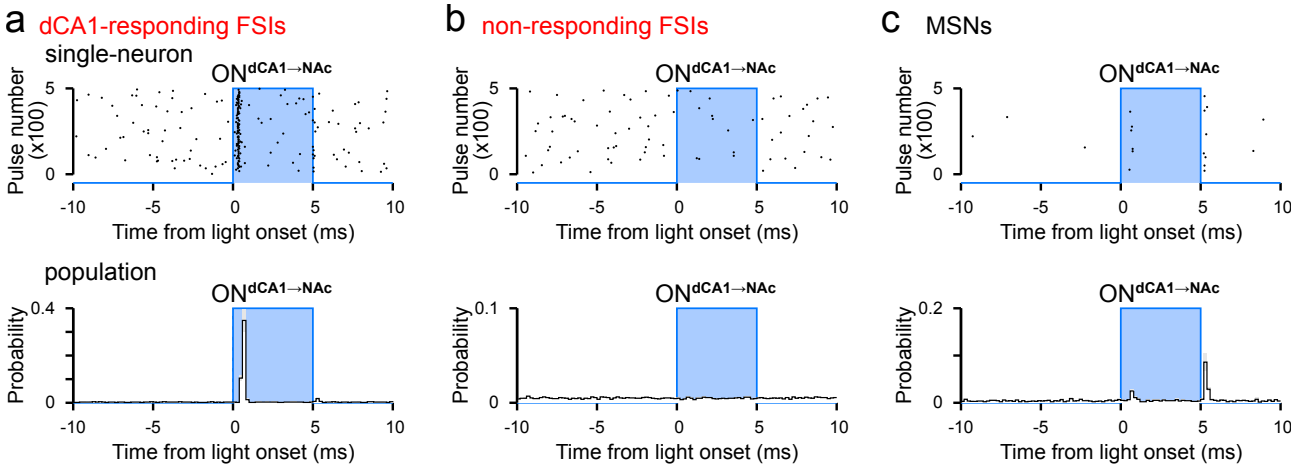

Figure 4.12: Concomitant recording of the cell activity, the NAc was flooded with randomised 5 ms long blue light pulses, in order to allow for enough time to study the effects of the activation of the axonal projections on the integrated network dynamics of the accumbal circuitry. (**a-c**) The responses of individual neurons are depicted designated as a light pulse responsive FSI, non-responsive FSI and a responsive pMSNS. The matching population responses of those cell populations, which were assigned their cell type identity in line with the criteria established in chapter 4.1, are seen (n = 222 NAc neurons including 128 MSNs and a total of 64 FSIs from two mice and 18 recording days, mean ± SEM, 0.2-ms bins, n = 12 dCA1-responding FSIs, n=52 non-responding FSIs, and n=128 MSNs) (Trouche, Koren et al. 2019)

hChR2(H134R)-EYFP. CaMKII is the Ca^{2+}/calmodulin-dependent protein kinase II and is prominently expressed by the principal cells in the dorsal CA1 pyramidal layer. This physiologic expression drives the build-up of Channelrhodopsin2 in these cells. These animals were implanted with the same multichannel drives containing an optic fibre positioned above the NAc described previously in chapter 4.2. Between the injection of the virus and the recordings 6 weeks in order to ensure a sufficient expression and incorporation of the protein in the cell membrane (Fig. 4.11; Trouche, Koren et al. 2019).

During the concomitant recording of the cell activity in both structures, the NAc was flooded with randomised 5 ms long blue light pulses, in order to allow for enough time to study the effects of the activation of the axonal projections on the integrated network dynamics of the accumbal circuitry (similar to chapter 4.2). Two animals were recorded this way for a total of 16 recording days. The effect of light stimulation on the various responsive cell type populations is seen in Figure 4.12. Hereby, the responses of individual neurons are depicted designated as a light pulse responsive FSI, non-responsive FSI and a responsive pMSN

(similarly to Fig.4.9 and 4.10). The matching population responses of those cell populations, which were assigned their cell type identity in line with the criteria established in chapter 4.2, are seen. Significantly, a subgroup of FSIs exhibits a strong short latency excitatory response within the first 1-2 ms following the light pulse induction. In the same time frame, pMSNs exhibit a very weak response, they do however respond strongly to the end of the laser pulse.

The results presented in this sub-chapter affirm firstly, that the dCA1 input exerts strong possibly mono-synaptic excitatory control over a subgroup of FSIs. They further confirm published data on the connectivity architecture within the NAc, notably that PV positive interneurons inhibit other FSIs, whereas pMSNs are inhibited by both parties. This architecture would theoretically put PV+ interneurons in an ideal position to relay information from the dCA1 to the MSNs that form the NAc output. In addition, dCA1 activity driven PV+ interneurons would be capable of supporting a putative feed-forward inhibition of other cell types in the NAc that was mentioned in chapter 4.3. and which will be further discussed later.

4.5) PV cells orchestrate MSN activity

Following the previous chapter's suggestion of PV positive interneurons as a possible primary target of the activity imposed by the dCA1 over the NAc, the purpose of this subchapter is to provide evidence that PV+ cells in the NAc are innervated by principal cells of the dCA1 as well to establish these cells as crucial junctures in the information relay within the dorsal hippocampal accumbal circuitry.

Experimental setting

This objective necessitated the development of a tool that would allow for the anatomical and electrophysiological identification of the subgroup of PV+ interneurons in the NAc that receives monosynaptic input from principal cells in the dCA1 as well as enabling the timely precise silencing of those cells' activity in order to allow for the study of their role in the integrated network dynamics of the overall circuitry. A new genetic strategy was conceptualised to meet those demands: a double-conditional Boolean logic transgene expression was designed in conjunction with the transsynaptic transfer of one of the two viral vectors (Zingg et al. 2017; Trouche, Koren et al. 2019). It required the initial in vitro verification (Fig. 4.13A,B) of a genetic tripartite system that would allow the expression of the proton pump ArchT (see chapter 4.3) exclusively in the presence of both the Cre and FlpO recombinases. Once confirmed in its efficacy it was implemented in vivo (Fig. 4.13C,D). An AAV vector carrying the FlpO transcript under the control of a Cre dependent promoter was injected into the dCA1 (pAAV-EF1a-DIO-FLPo-Myc), while an AAV vector encoding for the proton pump ArchT merged to an enhanced fluorescent marker EGFP under the control of a promoter whose expression was dependent on the presence of FlpO was injected into the NAc (pAAV-EF1a-fDIO-ArchT-EGFP) of a PV-Cre mouse (Trouche, Koren et al. 2019). Hereby, the transgene introduced into the dCA1 was packaged in a high-titre serotype 1 viral construct

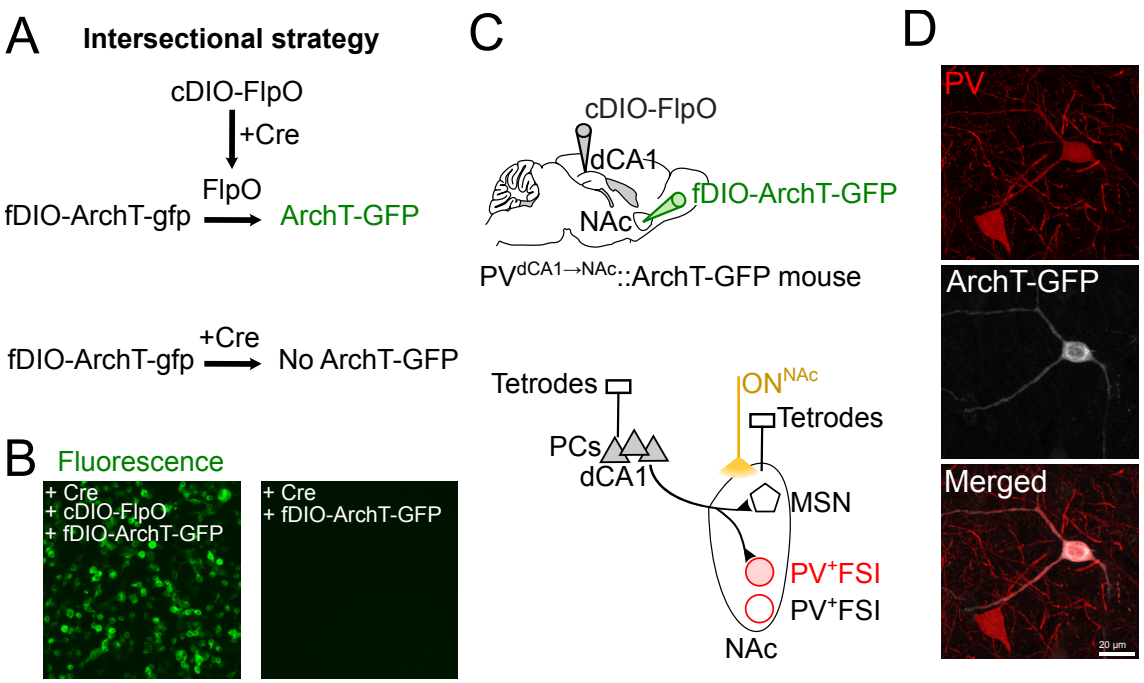

Figure 4.13: (**A**) Viral injection in the NAc of a Cre inducible AAV vector carrying the light driven proton pump ArchT fused with GFP which silences neuronal activity in the transfected NAc PV+ interneurons if FlpO is present and yellow light is applied. Viral injection in the NAc of a Cre inducible AAV vector carrying FlpO, which is capable of transsynaptic transfer. (**B**) In vitro specificity verification of genetic tripartite system (**C**) Concomitant extracellular recordings in the dCA1 and NAc and optogenetic silencing of PV+ interneurons in the NAc which are innervated by dCA1 PCs (**D**) PV staining in the NAc identifying PV+ interneurons. Co-localisation of PV staining and GFP demonstrating the selectivity of the transfection method (Design of intersectional strategy by Dr. Pavel Perestenko and Dr. Stephanie Trouche; Histology done by Dr. Stephanie Trouche and Natalia Campo-Urriza) (Trouche, Koren et al. 2019)

capable of anterograde cross-synaptic transfer. Consequently, PV positive interneurons in the NAc that were monosynaptic targets of dCA1 input, expressing the Cre recombinase due to their genotype background, were provided a Cre dependent FlpO recombinase and a FlpO dependent ArchT-eGFP construct. This led to the expression of ArchT-eGFP in solely those cells: any other cells outside of the NAc would not have received the FlpO dependent ArchT-eGFP construct, any PV negative cell in the NAc would not have had the intrinsic expression of Cre and any other PV positive interneuron in the NAc without the direct innervation from the dCA1 would not have been provided the Cre dependent FlpO recombinase (conceptualised mostly by Dr. Stephanie Trouche, engineered and implemented by Dr. Pavel Perestenko).

These animals were implanted with the same multichannel drives containing an optic fibre positioned above the NAc described previously in chapter 4.2. Between the injection of the

virus and the recordings 6 weeks were passed in order to ensure a sufficient expression and incorporation of the protein in the cell membrane. During the concomitant recording of the cell activity in both structures, the NAc was flooded with randomised 30 seconds long yellow light pulses, in order not to affect the PV positive cells irreparably while equally still allowing for enough time to study the effects of their silencing on the integrated network dynamics of the dCA1 accumbal circuitry.

NAc PV positive interneurons receive monosynaptic input from the dCA1

The identification of PV positive interneurons as a target of principal cell innervation from the dCA1 was achieved anatomically as well as electrophysiologically. It was confirmed through histological means that cells in the NAc expressing eGFP were in every case also expressing PV, however this was not true in reverse(Fig. 4.13D). The electrophysiological confirmation of these cells proved to be more challenging due to their very small quantity: a portion of the PV positive interneurons in the NAc were to be targeted which themselves constitute less than 1% of cells. Electrophysiologically, the cell yield of optotagged PV+ cells in chapter 4.4 can serve as a reference. In the present case however, not only were the cell numbers smaller as not all PV+ cells are innervated by dCA1 long range projections, but in addition those cells expressed ArchT instead of ChR2. This circumstance changes the efficacy of the cell screening process performed before each recording protocol drastically. Whereas in the case of ChR2, each time the tetrodes are lowered a brief flash of blue light could give indication whether an optotagged cell was in the proximity due to its strong response that can be seen by eye even in the unprocessed raw data, one can not detect by eye the absence of a transfected cell's activity when flashing yellow light for the activation of ArchT. Nevertheless, in spite of these difficulties Fig. 4.14 presents one such FSI that is effectively silenced by the light, ergo is a PV positive interneuron that receives monosynaptic input from the dCA1. Its firing rate

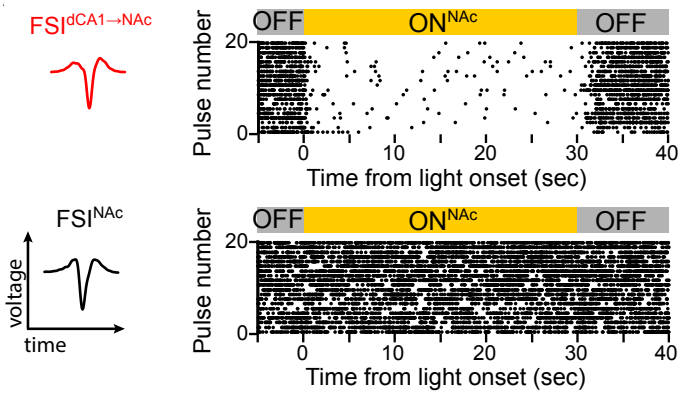

Figure 4.14 Examples of the effects of the light mediated silencing of PV^{+}FSI$^{dCA1->NAc}$ cells in the NAc. Two representative examples of FSIs responding to the 30 second long yellow light pulses. Light induction time triggered individual responses are visualised (individual discharges seen as dots) showing one FSI entirely silenced, hence designated as PV^{+}FSI$^{dCA1->NAc}$ cell and another non-responsive. Average spike waveforms are included (Trouche, Koren et al. 2019)

and average spike waveform are in line with the general description of FSIs in chapter 4.2 and its response to the light induction over many trials is consistent in its strength as well as reversible, which will be important in the following. Other FSIs responded with only very modest changes in their firing rates. MSNs responded towards the silencing of the subgroup of dCA1 innervated PV positive FSIs more differentially, either increasing or decreasing the activity (not shown).

dCA1 PCs shape the functional output of the NAc via PV+ FSIs

If PV+ cells which receive dCA1 input in the NAc were to be established as pivotal juncture points in the information relay within the circuitry, their activity had to be shown to be necessary for the meaningful local processing of the hippocampal input. This meant, their silencing had to perturb the relationship between the hippocampal input (principal cell activity) the NAc receives and the output it projects downstream (MSN activity). For this purpose it was paramount to quantify this relationship, which is possible through the application of a generalised linear model (GLM), a flexible generalisation of a regression model that allows for the disclosure of interrelated dependencies between any number of independent variables (in this case: spiking of individual principal cells in the dCA1) and so called dependent variables (spiking of individual pMSNs in the NAc) (Trouche, Koren et al. 2019). The aim is the generation of a numerical model that is capable to predict the activity

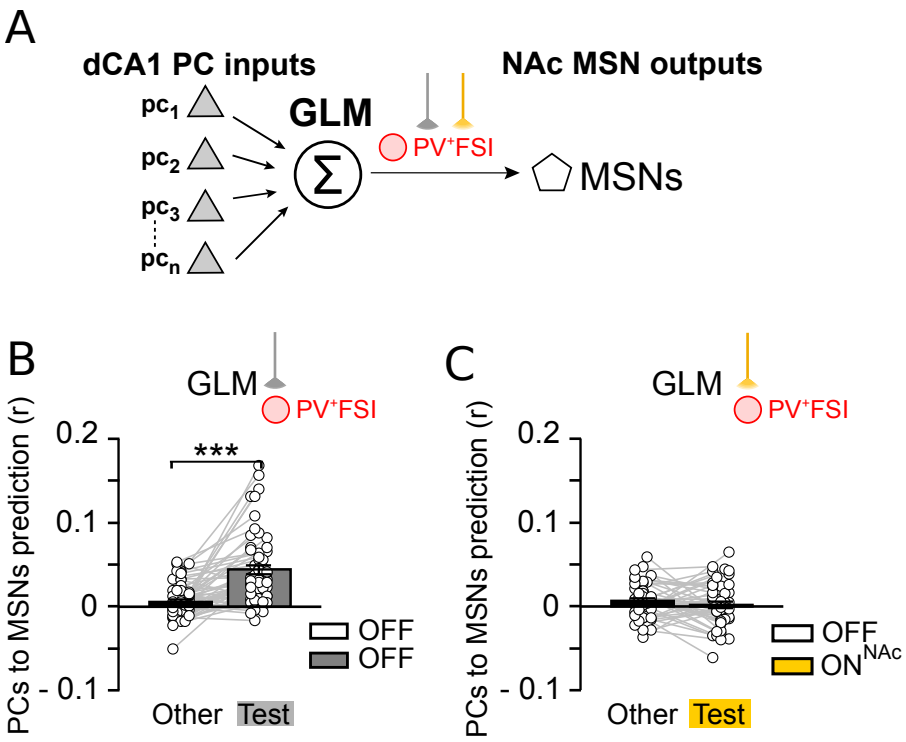

Figure 4.15: dCA1 PCs shape the functional output of the NAc via PV+ FSIs (**A**) Prediction of MSN activity based on PC spike trains with GLM (**B**) Under Light OFF conditions, the model was significantly better in predicting the MSN activity based solely on the dCA1 spike trains when the animal was re-exposed to the "Test" environment the model was trained on compared to the "Other" environment. (n = 58 MSNs from 30.25±3.98 PCs per GLM) (**C**) Under Light ON conditions however when $PV^{+}FSI^{dCA1->NAc}$ cells were optically silenced, the predictive power of the GLM was completely lost (n = 48 MSNs from 26.85±4.12 PCs per GLM). ***P<0.001 (from 4 mice) (Trouche, Koren et al. 2019)

profile of the pMSNs (NAc output) from a given activity profile of the principal cells in the dCA1 (NAc input).

In order to generate this model, the 4 animals were allowed to explore an environmental enclosure designated in the following as the "Test" context. During this exploratory behaviour the individual discharges of the cells concomitantly recorded in the dCA1 and the NAc were summed up within distinct time windows resulting in vectorised time binned spike trains. Similar to Buzsáki et al. 2010 those time windows were selected to correspond to the duration of the individual theta cycles extracted from the dCA1 local field potential, due to their physiological relevance in mnemonic computational processes as well as their role in pacing the NAc network response to the dCA1 input described earlier in this chapter (Trouche, Koren et al. 2019). Thus, each neuron's activity profile was represented by an array of numbers corresponding to its number of spikes within the entire succession of dCA1 theta cycles. The array, constituting the activity profile of all principal cells served as input to the GLM, while the activity profile of the NAc cells was to be predicted. The initial exposure to the "Test"

context allowed to train the model, i.e. to correlate the dCA1 input (PCs) to the NAc output (pMSNs). Each pMSN's spike number within a given theta cycle was modelled as dependent on the PC activity described through a linear superposition of their activity within that time period (Trouche, Koren et al. 2019):

$$MSN_n(\theta) = \alpha_0 + \sum_m \alpha_{PC_m} PC_m(\theta) + Error.$$

Hereby, α is a set of coefficients weighting the individual principal cell involvement in the prediction of a given MSN. The Error function denotes a distribution of variance between the linear model output and the actual MSN activity. In order to test the model, the animal was subsequently exposed to 2 distinct environmental enclosures: the same "Test" environment and the "Other". The linear regression between the vectorised predicted spike train of the pMSNs and their actual firing served hereby as a measure of accuracy of the prediction. Under Light OFF conditions, the model was significantly better in predicting the MSN activity based solely on the dCA1 spike trains when the animal was re-exposed to the "Test" environment the model was trained on compared to the "Other" environment (Trouche, Koren et al. 2019). This observation firstly confirms that the GLM is capable of making inferences about the NAc output based on the dCA1 input. Secondly, it shows that the NAc output is environment dependent. When the same experiment was conducted under Light ON conditions however, the predictive power of the GLM was completely lost. This means, that silencing those few PV+ FSIs in the NAc, that received monosynaptic input from dCA1 PCs was enough to erase any correlation between the dCA1 input and the NAc output, establishing them as crucial junctures in the information relay within the dorsal hippocampal accumbal circuitry.

In this subchapter NAc PV+ FSI were confirmed to receive monosynaptic input from the dCA1. Furthermore, dCA1 PCs have been shown to shape the functional output of the NAc via PV+ FSIs which thus play a crucial role in the information relay within the dCA1-accumbal circuitry.

4.6) Discussion

In this chapter, a means was developed for the reliable identification of cell types in the NAc from electrophysiological recordings. dCA1 PCs were established to selectively drive the activity of a subset of FSIs in the NAc. Furthermore, this synaptic input from the dCA1 was shown to be necessary for the maintenance of the activity of a subgroup of FSIs. It was further shown that PV+ FSIs receive monosynaptic input from the dCA1 and that the stimulation of dCA1 axons in the NAc leads to the entrainments of a subset of FSIs. Finally, dCA1 PCs were demonstrated to shape the functional output of the NAc via PV+ FSIs. These findings confirm PV+ FSIs to be a crucial juncture in the information relay within the dorsal hippocampal accumbal circuitry. In the following, the rational behind the individual experiments will be discussed (Trouche, Koren et al. 2019).

In order to address systemic network interactions within the dorsal CA1-accumbal circuitry, three prerequisites had to be fulfilled. Firstly, both deep brain regions had to be recorded simultaneously in awake, behaving animals. This excluded most contemporary approaches involving optical set-ups for deep-brain imaging, as these do not usually allow for multi site recordings in freely moving mice. Secondly, large scale recordings were necessary in order to delineate weak neural interactions, such as they had to be expected within a long range circuitry of sparse connectivity. This condition excluded techniques such as single cell juxta-cellular recordings due to the low achievable cell yield. And lastly, the cell type identity of the recorded cells had to be discerned if any account was to be made of systemic network

interactions within a circuitry that is highly heterogenous in its cellular architecture. Electrophysiological recordings do not allow for cell type identifications per se, hence a reliable method was developed and implemented for cell type discrimination. This methods is based solely on the parameterised spike waveform of the recorded cells and allows for the distinction between pMSNs, FSIs and TANs, thus enabling analysis that goes beyond merely the pairwise firing rate and spike time correlations between indiscriminate individual cells commonly applied in such cases.

In the following, this was used in order to examine whether long range projections of dCA1 principal cells exhibit any cell type specific effect within the NAc network. Firstly, FSIs as well as MSNs synchronise their activity to the theta band oscillations of the dCA1 (and hence the tact of principle cell firing) while firing rhythmically in anti-phase to each other. Secondly, the FSIs' activity is driven by principal cell spiking on a short timescale, which allows for the assumption of an underlying single-synaptic effect (which was later corroborated by the light driven activation of the dCA1 axons in chapter 4.4). This effect is not observed in MSNs. Thirdly, when the axonal input of the dCA1 projections is silenced, a subset of FSIs exhibits a stark drop in activity, while the activity profile of the rest of FSIs remains unchanged. The MSNs show a complex bimodal response, but weaker in it's extent of firing rate modulation. Lastly, there is indication that the FSIs silenced as a consequence of the light induction, are coupled to the ascending theta phase of the dCA1, whereas the non-silenced FSIs are coupled to the descending phase, and thus in anti-phase. This means, that the silenced FSIs become more active shortly after the activity of dCA1 principal cells peaks within the theta cycle. This suggests, that a subset of FSIs might serve as an nodal point for the relay of information from the dCA1 to the NAc.

Based on these findings and due to the heterogeneity of GABAergic interneuron types, that have been identified so far in the the NAc, the question arose, whether a molecularly defined group of interneurons could be proposed as a likely prospect for those cells. Interneurons expressing parvalbumin were chosen as the most likely candidate due to several reasons. Firstly, they have been shown to inhibit the other two types of GABAergic interneurons in the NAc as well as MSNs in in vitro experiments, while the other two types of FSIs have failed to do so. This is important, because not only would one expect those interneurons to have a strong capacity to modulate MSNs (the "output neurons" of the NAc), but also due to the putative FSI-FSI feed forward inhibition mechanism proposed in chapter 4.3. Secondly, preliminary results in the lab (not shown here, Trouche, Koren et al. 2019), suggest an anatomical co-localisation of the distribution of PV positive interneurons and dCA1 axonal terminals within the NAc, not observed in the case of the other FSI types. An optotagging experiment was devised in order to, firstly, confirm the classification of PV positive interneurons as FSIs, and secondly, to show that in vivo stimulation of PV positive FSIs was effective in silencing both, other GABAergic interneurons as well as MSNs. Although similar classifications have been presented in the past, this is the first time anybody was able to at least partially confirm this method through concomitant light induced stimulation (optotagging) of one cell-type and the study of its activity's effect on the network dynamics, which are in line with published data from in-vitro studies. In addition, these results constitute the first description of secondary effects of optotagging on different cell types in the local network architecture.

In order to provide further evidence, that PV+ cells in the NAc are mono-synaptically innervated by dCA1 principal cells as well as establish these cells as crucial junctures in the information relay within this circuitry, the last experiment was designed. Through an

intersectional trans-genetic strategy it was histologically as well as electrophysiologically shown that a small proportion of PV positive FSIs is indeed targeted by those projections. The silencing of these cells, which was shown to be very efficient, had a differential effect on the MSN population, either silencing or exciting them. In order to establish whether the computation of principal cell input into the output of the NAc was disrupted, a GLM model was calculated. It disclosed that the activity of this small amount of PV positive interneurons was necessary to maintain the predictability of the MSN output based on dCA1 activity. This means, that although it is not clear whether PV positive interneurons are the sole target of dCA1 long range projections among the interneurons in the NAc, they do perform a crucial role in the orchestration of MSN activity that is dependent on the dCA1 input.

CHAPTER 5: GENERAL DISCUSSION

5.1) Structural plasticity in the dorsal hippocampus - accumbal circuitry

The results presented in chapter 3 constitute the first full in vitro and in vivo proof of principle of a novel high resolution deep brain imaging approach utilising holographic control over light propagation through a single optical fibre. This technology reduces the footprint and thus resulting tissue damage by two orders of magnitude compared to other invasive techniques, which achieve similar, diffraction limited resolutions (Vasquez-Lopez, Koren et al. 2018). The resolution of this apparatus was confirmed on fluorescent beads and resolution gratings. It was further shown to reliably resolve axonal boutons and dendritic spines in hippocampal organotypic slices as well as in the dorsal stratum of an anaesthetised mouse. While not yet sufficiently advanced for routine use in the study of structural synaptic plasticity in deep brain structures, the application of adaptive optics to this end is promising nonetheless. In the following, an array of conservative predictions about the optic fibre system's potential technological advances over the next few years shall be made and discussed.

Functional imaging of neuronal activity

GRIN lens (Barretto et al. 2011, Resendez et al. 2016) as well as microscopy objective (Dombeck et al. 2010) set-ups are routinely used to record large scale neuronal population activity profiles both in head restrained and freely moving rodents (Sheffield et al. 2015, Jennings et al. 2015). This is done by means of genetically encoded calcium concentration indicators such as GCaMP, an engineered protein consisting of a per-mutated Green Fluorescent Protein, Calmodulin and M13 peptide. Calcium ions in solution bind reversely to the Calmodulin (CaM, calcium-modulated protein) section resulting in an conformational

change in the tertiary structure of GCaMP through its binding to the M13 peptide, which restores the fluorescence capacity of the Green Fluorescent Protein (GFP) peptide part. Therefore, action potential triggered calcium ion influx into the intracellular space of the active neuron triggers a spike in the fluorescence yield of this cell, which can be detected. In order to be able to do the same with the optic fibre based imaging set-up, some modification of the current system is necessary. The use of a liquid crystal based spatial light modulator (SLM) for the diffraction grating generation does not offer high enough refresh rates (204 Hz) to detect rapid spikes in neuronal activity. Recently however, acousto-optic deflectors (AOD; Cižmár et al. 2012) and digital micro-mirror devices (DMD; Conkey et al. 2012; Mitchell et al. 2016) were implemented by our collaborator Prof. Tomas Cizmar in optical geometries similar to the one presented here (Vasquez-Lopez, Koren et al. 2018). This allowed for a significant increase in sampling rates, by up to two orders of magnitude (acquisition speed up to 20 kHz or ~7-10 Hz for full image), which is sufficient for calcium imaging. That has very recently been demonstrated by Ohayon et al. 2017, who were able to image calcium transients in vitro with cellular resolution. It seems however, that this low spatial resolution impeded the application of this technology in vivo, as there was virtually no spatial specificity in the neural activity profile of different cells detected in vivo in this paper (each putative neuron in a given plane was shown to have a near identical response profile), therefore merely allowing the study of population activity. We are currently in the process of incorporating a DMD in our set-up (Turtaev et al. 2017), thus merging the unique spatial resolution presented in this thesis with the temporal precision necessary to resolve individual neuronal functional activity.

Two photon imaging

Single photon imaging of deep brain structures in vivo entails two main drawbacks. Firstly, high laser intensities necessitated by the optical set-up (emission signal has to be concatenated

back through the optic fibre which leads to loss) can lead to photobleaching (this became evident during the in vitro experiments in chapter 3.3). Secondly, the system design is susceptible to epi-fluorescent interference, i.e. excitation of out of focus fluorescence. This complication precludes the image acquisition in any but sparsely labelled fluorescent tissue, thus posing a significant obstacle in the routine application of the system. To address both issues, ideally, a two-photon system is needed. Recently, a first technical implementation of two photon imaging through a single optic fibre has been demonstrated by Morales-Delgado et al. 2015 and proof of principle image acquisition was achieved with fluorescent beads. Hereby, the group velocity dispersion effect, the focused femtosecond pulses are subjected to while travelling through the optic fibre, was compensated by stretching the light pulses through a simple optical prism geometry. Although the diameter of the optic probe used in that work was 350 μm, the same general principle can be applied to the optic fibre set-up described in chapter 3.2 and is indeed currently being implemented in the lab in collaboration with Prof. Dr. Martin Booth.

Imaging in awake, freely moving animals

For the purpose of static imaging in fixed brain tissue or anaesthetised head-fixed animals as presented in chapter 3, it sufficed to treat the MMF as a randomly diffuse optical medium. This was possible due to the availability of simultaneous optical access to the proximal as well as distal fibre facet, which allowed the preemptive empirical determination of the fibre specific transformation matrix. This allowed the acquisition of high resolution images as long as the physical integrity of the optic fibre itself was not affected during the procedure. This however would no longer be the case when imaging within awake and freely moving animals (Plöschner et al. 2015). If this is to be achieved, the TM would need to be adjusted in real time. Results recently published by our collaborator Prof. Tomas Cizmar demonstrate that

such online update might indeed be feasible (Plöschner et al. 2015). This is owed to the fact that optic fibres do exhibit a regularity of optical mode propagation due to their cylindrical symmetry. This circumstance can be exploited in the computational modelling and prediction of changes in the transformation matrix, something that has been formerly believed to be impossible due to the natural deviation of any real fibre from its theoretical, idealised properties. Plöschner et al. have shown that once the transformation matrix is calibrated beforehand, adjustments could then be applied in accordance with theoretical models. That permitted image reconstruction through a long optic fibre despite significant bending. These experiments were performed on fluorescent probes and beads. In conjunction with the results presented in this thesis, which open up the possibility of high resolution deep brain imaging in vivo, they might however lead the way toward imaging in freely moving animals.

Further developments underway

Multiple further technical improvements are already implementable or at least conceivable as part of the optical set-up presented in chapter 3.2. As mentioned before, there is no per se stipulation regarding some of the properties of the fibre. The diameter of the fibre, and hence the imaging area, can be altered at will which might prove beneficial if whole cell assemblies are to be imaged. The necessary changes to the set-up and software are indeed being currently implemented using a fibre with a core diameter of 100µm instead of 50µm. In addition, the numerical aperture of the optic fibre is being increased. This will allow for an improved resolution as well as increased gain, which might prove beneficial in the context of single photon imaging. Another potential expansion of this set-up's capabilities lies within multispectral imaging using different lasers. Already demonstrated by Ohayon et al. 2017, this entails the incorporation of a beam splitter into the light path and might potentially enable the efficient imaging of differently labeled cell populations, the simultaneous structural and functional imaging as well as the concomitant excitation or silencing of neurons. The latter, in

conjunction with the high spatial resolution presented in this thesis, might allow for the selective optical stimulation not only of individual cells, but also individual dendritic arbours and spines. Such capabilities would have a multitude of potential practical applications in the study of cell assembly processing and sub-cellular dendritic computing. As all these changes rely on modifications in the software and the exchange of different, mostly electric, components in the modular optical set-up, the improvement and technical advance of this technology in the future should prove relatively cost-effective as well as fast-paced.

5.2. Network dynamics in the dorsal hippocampus - accumbal circuitry

In chapter 4, a method of spike waveform classification was adapted for the reliable identification of cell types in the NAc from electrophysiological recordings. Based on this approach, dCA1 PCs were found to selectively drive the activity of a subset of NAc FSIs. Optogenetic silencing of those projections led to the inhibition of a subgroup of FSIs, while their stimulation allowed the entrainment of FSIs. The NAc circuit architecture suggests PV+ interneurons to be ideally poised to relay information from the dCA1 to the NAc and indeed they were shown to receive monosynaptic input from the dCA1. Finally, dCA1 PCs were shown to shape the MSN activity and thus the functional output of the NAc via PV+ FSIs (Trouche, Koren et al. 2019). Based on these results, a first mechanistic model of the network physiology in the dCA1-accumbal circuitry can be conceptualised that might serve as stepping stone for future investigations of this circuitry. What follows is an attempt to integrate the acquired knowledge about this network and to explain some phenomena that were observed.

Mechanistic model of network dynamics

Not all FSIs whose activity was driven by dCA1 PC spiking, and thus can be assumed as mono-synaptically innervated (chapter 4.3), were inhibited when dCA1 PC projections in the NAc were silenced (chapter 4.3). This observation might indicate that the dependency of mono-synaptically targeted NAc FSIs on the activity drive from the dCA1 might be multivariate. One factor that could influence whether a NAc FSI requires such input to maintain its activity at a given time could be the surrounding environment. Due to the strong place-dependence of the activity profile of PCs in the dCA1, it is reasonable to assume that the dCA1 input to the NAc, too, is context dependent. Indeed, preliminary results in the lab have shown “placeness” in MSN activity reminiscent of PCs in the dCA1. Furthermore, a

prediction model correlating dCA1 PC activity and NAc output was shown to lose its predictive power when the animal was placed in another environment (chapter 4.5). These findings suggest that FSIs could be selectively driven in an environmental context dependent manner.

Considering the strong inhibitory influence that PV+ FSIs have over the MSN population in the NAc (chapter 4.4), one might assume that the silencing of a proportion of PV FSIs would lead to a general increase in MSN activity. When however a proportion of FSIs was inhibited in response to the silencing of dCA1 PC projections in the NAc (chapter 4.3) as well as when a subset of PV+ FSI, which were mono-synaptically targeted by those projection, was silenced (chapter 4.5), this was not observed. In both cases, MSNs exhibited a bimodal response, being differentially inhibited and excited, while the overall population activity remained stable (chapter 4.3). This can be explained when taking into account the network dynamics within the MSN population itself. It has been shown firstly, that a large proportion of MSNs is silent at any given time point (Kiyatkin and Rebec 1996), and secondly, that this cell cohort has extensive recursive inhibitory connections, each MSN being innervated by approximately 1000 inhibitory synapses from other MSNs. According to theoretical models (Ponzi and Wickens 2013, Wickens and Arbuthnott 1993), this facilitates a “winner takes all”-activity profile of the population, whereby the small subset of MSNs, that is being active at a given time-point, inhibits the activity of any other MSN. Furthermore, interneurons within the NAc have been implicated to underpin the orchestration of the NAc output by facilitating the selective activity of those MSN subsets (Ponzi and Wickens 2013; Trouche, Koren et al. 2019).

In chapter 4.4, optogenetic stimulation of dCA1 axonal terminals in the NAc led to a stronger entrainment of FSIs compared to MSNs. Furthermore, optogenetic stimulation of PV+ FSIs in

the NAc led to an inhibition of MSNs. These findings fall short of proving feed forward inhibition of MSNs through PV+ FSIs. In order to conclusively test for such feed forward inhibition, acute ex vivo NAc slices were prepared in the lab (Dr. Tomas Ellender; Trouche, Koren et al. 2019). These were used in order to conduct whole cell patch clamp recordings on PV+ interneurons and MSNs while stimulating dCA1 projections in the NAc. In accordance with the results acquired in vivo, both PV+ interneurons and MSNs were shown to receive excitatory dCA1 input, while PV+ interneurons were more easily entrained than MSNs when stimulating dCA1 axons. Importantly, PV negative interneurons were not observed to receive such input. Furthermore, all responding MSNs exhibited not only excitatory postsynaptic potentials (EPSPs), but also inhibitory postsynaptic potentials (IPSPs). This indicates that MSNs that receive excitatory dCA1 input are subject to (probably PV+ interneuron mediated) feed forward inhibition (Trouche, Koren et al. 2019).

Based on the findings presented in this thesis, the following network dynamics model of information relay within the dCA1-accumbal circuitry can be conceptualised. The context dependent long range excitatory dCA1 PCs input, rhythmically coupled to hippocampal theta oscillations, could drive the activity of a cohort of FSIs (PV+ FSIs posing as likely candidates) and MSNs (chapter 4.3 and 4.4). These two cell populations in the NAc could thus be synchronised to the same dCA1 theta phase (chapter 4.3). These driven FSIs might subject other FSIs to feed forward inhibition (chapter 4.4), thereby synchronising them in anti phase to the MSNs (chapter 4.3). In this way, the dCA1 input would allow for the selection of a small context dependent set of FSIs to spike within the same short time frame as the MSNs. They would thus be in an ideal position to orchestrate NAc output (chapter 4.5) by facilitating the selective activity of a particular subset of MSNs in any given environmental context. It is well established that theta oscillations can orchestrate information relay between different brain structures by providing a time window for local network computation (Mizuseki et al.

2009; Trouche, Koren et al. 2019). As individual neurons in the NAc receive converging input from multiple brain regions (Floresco et al. 2014), such a temporal segregation of context dependent FSIs/MSNs cohorts, coupled to hippocampal theta oscillations, might allow the processing of spatial information with little interference from other upstream brain structures.

Behavioural relevance of the dCA1-NAc pathway

This network dynamics model might pose as a mechanism underpinning the translation of spatial representations into directives for appetitive behaviour. Behavioural results obtained in the lab (by Dr. Stephanie Trouche; Trouche, Koren et al. 2019), suggest that this might indeed be the case. The animals were performing in a standard conditioned place preference (CPP) task. The CPP apparatus consisted of two square compartments which contained two distinct contextual environments, one of which was associated with a sucrose reward, while the other contained water. When both the sucrose solution and water were removed, the animals still exhibited a preference toward the environmental context associated with the reward. This preference was abolished when the dCA1 axonal projections in the NAc were silenced (similarly to chapter 4.3) as well as when PV^{+} FSIs that were mono-synaptic targets of dCA1 projections were silenced (similarly to chapter 4.5). Finally, in order to

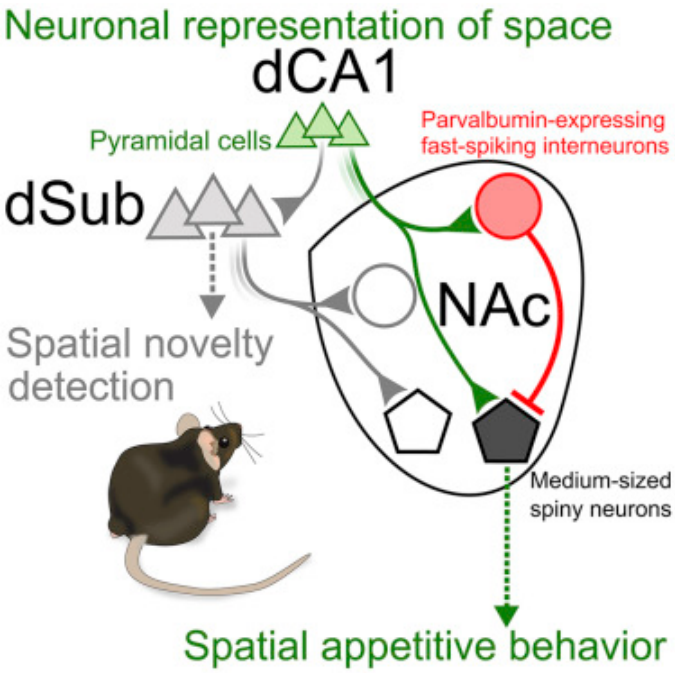

Figure 5.1: Dorsal HPc - accumbal circuitry. dCA1 PC long range projections mono-synaptically target MSNs as well as PV+ FSIs in the NAc. dCA1 shapes the functional output of the NAc through PV+ interneuron mediated feed forward inhibition of MSNs. This allows for the selective activity of context dependent MSN subsets and underpins the translation of neural representations of space into spatial appetitive behaviour. Furthermore, this process is independent of formerly described HPc-NAc projections such as the dSub-Nac pathway (Trouche, Koren et al. 2019)

further ascertain that the direct dCA1-NAc pathway is selectively responsible for the behavioural modulation within the CPP task, projections from the dorsal subiculum (dSub) to the NAc were silenced (described by Cembrowski et al. 2018). While silencing dCA1-NAc projections prevented conditioned place preference, silencing dSub-NAc axons did not (Trouche, Koren et al. 2019). This suggests firstly, that a functionally intact dCA1 input to the NAc is selectively necessary for the translation of the spatial representation of the environmental context encoded by PCs into the appetitive reward seeking behaviour geared towards this context. It shows secondly, that not only do PV positive interneurons, mono-synaptically targeted by dCA1 PC long range projections in the NAc, perform a crucial role in the orchestration of MSN activity that is dependent on the dCA1 input (chapter 4.5), but that they are also necessary for the expression of context dependent reward seeking behaviour (Fig. 5.1).

5.3 Conclusion

This thesis represents the first account of the dorsal CA1- accumbal circuitry in mice, which is ideally poised to be involved in the translation of spatial information into directives pertaining to reward seeking behaviour. Hereby, PCs in the dCA1 were established to drive the activity of PV+ FSIs in the NAc which in turn modulate NAc output through feed forward inhibition of MSNs. A first mechanistic model of the network dynamics in the dCA1-accumbal circuitry was presented here. These results might help to conceptualise, how the dCA1 is capable of projecting a comprehensive activity profile to the downstream network of the nucleus accumbens through sparse connectivity as well as how the accumbal network might potentially integrate multiple such inputs from different brain regions (Trouche, Koren et al. 2019). Furthermore, a new minimally invasive high resolution deep brain imaging approach utilising adaptive optics and holographic light propagation through a single optical fibre has been demonstrated. This technology's first full proof of principle in vitro and in vivo was presented here. This work might facilitate future investigations of structural synaptic plasticity in deep brain circuitries such as the hippocampal dCA1-accumbal pathway. It shall further serve as the first stepping stone in the ongoing progress of this technology and highlight a route to achieving minimally invasive high-resolution optical access to deep-brain sub-cellular structural and functional processes in living and possibly behaving animals (Vasquez-Lopez, Koren et al. 2018).

APPENDIX

Supplementary Table 1 Deep brain invasive imaging studies, included in Figure 3.4

Imaging approach	Resolution	Diameter
Aspiration		
Functional imaging of hippocampal place cells at cellular resolution during virtual navigation Daniel A Dombeck, Christopher D Harvey, Lin Tian, Loren L Looger & David W Tank Nature Neuroscience 03 October 2010	1.28μm	2.77 mm
High-Resolution In Vivo Imaging of Hippocampal Dendrites and Spines Adi Mizrahi, Justin C. Crowley, Eran Shtoyerman, and Lawrence C. Katz The Journal of Neuroscience, March 31, 2004	Diffraction limited	2.3 mm
Long-Term *In Vivo* Imaging of Dendritic Spines in the Hippocampus Reveals Structural Plasticity Ligang Gu, Stefanie Kleiber, Lena Schmid, Felix Nebeling, Miriam Chamoun, Julia Steffen, Jens Wagner, and Martin Fuhrmann Journal of Neuroscience 15 October 2014	Diffraction limited	3 mm
Projections from neocortex mediate top-down control of memory retrieval Priyamvada Rajasethupathy, Sethuraman Sankaran, James H. Marshel, Christina K. Kim, Emily Ferenczi, Soo Yeun Lee, Andre Berndt, Charu Ramakrishnan, Anna Jaffe, Maisie Lo, Conor Liston & Karl Deisseroth Nature 2015	0.98μm	3 mm
Internally Recurring Hippocampal Sequences as a Population Template of Spatiotemporal Information Vincent Villette,Arnaud Malvache,Thomas Tressard,Nathalie Dupuy,Rosa Cossart Neuron 2015	2 μm	3mm
Simultaneous cellular-resolution optical perturbation and imaging of place cell firing fields John Peter Rickgauer, Karl Deisseroth & David W Tank Nature Neuroscience 2014	Diffraction limited	2.77 mm
Calcium transient prevalence across the dendritic arbour predicts place field properties Mark E. J. Sheffield & Daniel A. Dombeck Nature 2015	Diffraction limited	2.77 mm
Dendritic Inhibition in the Hippocampus Supports Fear Learning Matthew Lovett-Barron, Patrick Kaifosh, Mazen A. Kheirbek, Nathan Danielson, Jeffrey D. Zaremba, Thomas R. Reardon, Gergely F. Turi, René Hen, Boris V. Zemelma, Attila Losonczy Science 2014	Diffraction limited	3 mm

Critical role of soluble amyloid-β for early hippocampal hyperactivity in a mouse model of Alzheimer's disease Marc Aurel Buschea, Xiaowei Chena, Horst A. Henninga, Julia Reichwaldd, Matthias Staufenbield, Bert Sakmanna,, and Arthur Konnertha PNAS 2012	Diffraction limited	2 mm
Distinct Contribution of Adult-Born Hippocampal Granule Cells to Context Encoding Nathan, B. Danielson, Patrick Kaifosh, JeffreyD. Zaremba, Matthew Lovett-Barron, Joseph Tsai, Christine A. Denny, Elizabeth M. Balough, Alexander R. Goldberg, Liam J. Drew, René Hen, Attila Losonczy , MazenA. Kheirbek Neuron 2016	Diffraction limited	1.5mm
Septo-hippocampal GABAergic signaling across multiple modalities in awake mice Patrick Kaifosh, Matthew Lovett-Barron, Gergely F Turi, Thomas R Reardon & Attila Losonczy Nature Neuroscience 2013	Diffraction limited	3-mm
GRIN lens		
Visualizing Hypothalamic Network Dynamics for Appetitive and Consummatory Behaviors Joshua H. Jennings, Randall L. Ung, Shanna L. Resendez, Alice M. Stamatakis, Johnathon G. Taylor, Jonathan Huang, Katie Veleta, Pranish A. Kantak1, Megumi Aita, Kelson Shilling-Scrivo, Charu Ramakrishnan, Karl Deisseroth, Stephani Otte, Garret D. Stuber 29 January 2015 Cell	2.5 μm	0.5 mm
In vivo fluorescence imaging with high-resolution microlenses Robert P J Barretto, Bernhard Messerschmidt & Mark J Schnitzer Nature Methods 2009	1.0 ± 0.2 μm	1.4 mm
Calcium imaging of sleep–wake related neuronal activity in the dorsal pons Julia Cox, Lucas Pinto & Yang Dan Nature Communications February 2016	2.5 μm	0.5 mm
Entorhinal Cortical Ocean Cells Encode Specific Contexts and Drive Context-Specific Fear Memory Takashi Kitamura, Chen Sun, Jared Martin, Lacey J. Kitch, Mark J. Schnitzer, Susumu Tonegawa Neuron September 23rd, 2015	2.5 μm	1.5mm
Distinct speed dependence of entorhinal island and ocean cells, including respective grid cells Chen Sun, Takashi Kitamura, Jun Yamamoto, Jared Martin, Michele Pignatelli, Lacey J. Kitch, Mark J. Schnitzer, Susumu Tonegawa PNAS July 13th, 2015	2.5 μm	1mm
Cell-Type-Specific Activity in Prefrontal Cortex during Goal-Directed Behavior Lucas Pinto, Yang Dan Neuron July 2nd, 2015	2.5 μm	1 mm
Neurons for hunger and thirst transmit a negative-valence teaching signal J. Nicholas Betley, Shengjin Xu, Zhen Fang Huang Cao, Rong Gong, Christopher J. Magnus, Yang Yu & Scott M. Sternson Nature April 27th, 2015	2.5 μm	0.6 mm

Long-term dynamics of CA1 hippocampal place codes Ziv Y., Burns L., Cocker E., Hamel E., Ghosh K., Kitch L., Gamal A., Schnitzer M. Nature Neuroscience February 10th, 2013	2.5 μm	2 mm
Miniaturized integration of a fluorescence microscope Ghosh K., Burns L., Cocker E., Nimmerjahn A., Ziv Y., Gamal A., Schnitzer M. Nature Methods September 11th, 2011	2.5 μm	2 mm
Impermanence of dendritic spines in live adult CA1 hippocampus Alessio Attardo, James E. Fitzgerald & Mark J. Schnitzer Nature 30 July 2015	1.0 ± 0.2 μm	1.8 mm and 2.4 mm
Time-lapse imaging of disease progression in deep brain areas using fluorescence microendoscopy Robert P J Barretto & Mark J Schnitzer Nature Medicine 2011	1.0 ± 0.2 μm and 1.84±0.1 μm	1.8-mm and 0.84-mm
High-speed, miniaturized fluorescence microscopy in freely moving mice Benjamin A Flusberg, Axel Nimmerjahn, Eric D Cocker, Eran A Mukamel, Robert P J Barretto, Tony H Ko, Laurie D Burns, Juergen C Jung & Mark J Schnitzer Nature Methods 2008	2.8–3.9 μm	2.5 mm
Dendritic encoding of sensory stimuli controlled by deep cortical interneurons Masanori Murayama, Enrique Pérez-Garci, Thomas Nevian, Tobias Bock, Walter Senn & Matthew E. Larkum Nature 2009	3.8 μm	0.5 mm
Fibrescope		
Overexpression of the Type 1 Adenylyl Cyclase in the Forebrain Leads to Deficits of Behavioral Inhibition Xuanmao Chen, Hong Cao, Amit Saraf, Larry S. Zweifel, and Daniel R. Storm 7 January 2015,J Neuroscience	3.3 μm	0.30mm
Disruption of Dopamine Neuron Activity Pattern Regulation through Selective Expression of a Human KCNN3 MutationMarta E. Soden, Graham L. Jones, Christina A. Sanford, Amanda S. Chung, Ali D. Güler, Charles Chavkin, Rafael Luján, Larry S. Zweifel, 20 November 2013, Neuron	3.3 μm	0.30mm
Organically modified silica nanoparticles: A nonviral vector for in vivo gene delivery and expression in the brain Dhruba J. Bharali, Ilona Klejbor, Ewa K. Stachowiak, Purnendu Dutta, Indrajit Roy, Navjot Kaur, Earl J. Bergey, Paras N. Prasad, and Michal K. Stachowiak PNAS June 13,2005	2.5 μm	0.35mm

Spatially Selective Holographic Photoactivation and Functional Fluorescence Imaging in Freely Behaving Mice with a Fiberscope Vivien Szabo Cathie Ventalon, Vincent De Sars, Jonathan Bradley, Valentina Emiliani Neuron 17 December 2014	3.3 μm	0.60 mm
Live imaging of neural structure and function by fibred fluorescence microscopy Pierre Vincent, Uwe Maskos, Igor Charvet, Laurence Bourgeais, Luc Stoppini, Nathalie Leresche, Jean-Pierre Changeux, Régis Lambert, Paolo Meda, and Danièle Paupardin-Tritsch EMBO Reports 2006	3.3 μm	0.65mm and 0.30mm
Circuit-dependent striatal PKA and ERK signaling underlies rapid behavioral shift in mating reaction of male mice Akihiro Goto, Ichiro Nakahara Takashi Yamaguchi Yuji Kamiok Kenta Sumiyam Michiyuki Matsud Shigetada Nakanishi, and Kazuo Funabiki PNAS 2015	3.5 μm	0.30 mm
Role of PKA signaling in D2 receptor-expressing neurons in the core of the nucleus accumbens in aversive learning Takashi Yamaguchi,a Akihiro Goto, Ichiro Nakahara, Satoshi Yawata,a Takatoshi Hikida, Michiyuki Matsuda, Kazuo Funabiki, and Shigetada Nakanishia PNAS 2015	3.5 μm	0.30 mm

REFERENCES

Abraham, W. C., Bliss, T. V. & Goddard, G. V. (1985). Heterosynaptic changes accompany long-term but not short-term potentiation of the perforant path in the anaesthetized rat. J. Physiol. 363, 335–349.

Adamantidis, A.R., Tsai, H.C., Boutrel, B., Zhang, F., Stuber, G.D., Budygin, E.A., Tourino, C., Bonci, A., Deisseroth, K., de Lecea, L. (2011). Optogenetic interrogation of dopaminergic modulation of the multiple phases of reward-seeking behavior. J. Neurosci. 31, 10829–10835.

Amaral, D.G., Witter, M.P. (1989). The three-dimensional organization of the hippocampal formation: a review of anatomical data. J. Neurosci. 31, 571-91.

Andersen, P., Sundberg, S. H., Sveen, O., Swann, J. W. & Wigström, H. (1980). Possible mechanisms for long-lasting potentiation of synaptic transmission in hippocampal slices from guinea-pigs. J. Physiol. 302, 463–482.

Annett, L.E., McGregor, A., and Robbins, T.W. (1989). The effects of ibotenic acid lesions of the nucleus accumbens on spatial learning and extinction in the rat. Behav. Brain Res. 31, 231–242.

Atasoy, D., Aponte, Y., Su, H. H., & Sternson, S. M. (2008). A FLEX switch targets Channelrhodopsin-2 to multiple cell types for imaging and long-range circuit mapping. J. Neurosci. 28, 7025–30.

Attardo, A., Fitzgerald, J. E. & Schnitzer, M. J. (2015). Impermanence of dendritic spines in live adult CA1 hippocampus. Nature 523, 592–596.

Auffret, A, Gautheron, V, Repici, M, Kraftsik, R, Mount, HT, Mariani, J, Rovira, C. (2009). Age-dependent impairment of spine morphology and synaptic plasticity in hippocampal CA1 neurons of a presenilin 1 transgenic mouse model of Alzheimer's disease. J Neurosci. 29, 10144–10152.

Axmacher, N., Cohen, M. X., Fell, J., Haupt, S., Duempelmann, M., Elger, C.E., Schlepper, T.E., Lenartz, D., Sturm, V., Ranganath, C. (2010). Intracranial EEG correlates of expectancy and memory formation in the human hippocampus and nucleus accumbens. Neuron 65, 541-9.

Bakhurin, K.I., Mac, V., Golshani, P., Masmanidis, S.C. (2016). Temporal correlations among functionally specialized striatal neural ensembles in reward-conditioned mice. J. Neurophysiol. 115, 1521-1532.

Bannerman, D.M., Grubb, M., Deacon, R.M., Yee, B.K., Feldon, J., Rawlins J.N. (2003). Ventral hippocampal lesions affect anxiety but not spatial learning. Behav Brain Res. 139, 197-213.

Barretto, R. P. J., Ko, T.H., Jung, J.C., Wang, T.J., Capps, G., Waters, A.C., Ziv, Y., Attardo, A., Recht, L., Schnitzer, M.J. (2011). Time-lapse imaging of disease progression in deep brain areas using fluorescence microendoscopy. Nat. Med. 17, 223–8.

Barretto, R. P., Messerschmidt, B. & Schnitzer, M. J. (2009). In vivo fluorescence imaging with high-resolution microlenses. Nat. Methods 6, 511–512.

Barrionuevo, G., Shottler, F. & Lynch, G. (1980). The effects of repetitive low-frequency stimulation on control and “potentiated” synaptic responses in the hippocampus. Life Sci. 27, 2385–2391.

Berke, J.D. (2011). Functional properties of striatal fast-spiking interneurons. Front Syst Neurosci. 5, 45.

Berke, J.D., Okatan, M., Skurski, J., Eichenbaum, H.B. (2004). Oscillatory entrainment of striatal neurons in freely moving rats. Neuron 43, 883-96.

Berridge, K.C., Robinson, T.E., Aldridge, J.W. (2009). Dissecting components of reward: 'liking', 'wanting', and learning. Curr Opin Pharmacol. 9, 65–73.

Betley, J. N., Xu, S., Cao, Z. F. H., Gong, R., Magnus, C. J., Yu, Y. & Sternson, S. M. (2015). Neurons for hunger and thirst transmit a negative-valence teaching signal. Nature 521, 180–185.

Bharali, D. J., Klejbor, I., Stachowiak, E. K., Dutta, P., Roy, I., Kaur, N., Bergey, E. J., Prasad, P. N., and Stachowiak, M. K. (2005). Organically modified silica nanoparticles: A nonviral vector for in vivo gene delivery and expression in the brain. Proceedings of the National Academy of Sciences 102, 11539-11544.

Björklund, A., Dunnett, S.B. (2007). Dopamine neuron systems in the brain: an update. Trends Neurosci. 30, 194-202.

Bliss, T. V. & Lømo, T. (1973a). Long-lasting potentiation of synaptic transmission in the dentate area of the anaesthetized rabbit following stimulation of the perforant path. J. Physiol. 232, 331–356.

Bliss, T. V. & Gardner-Medwin, A. R. (1973). Long-lasting potentiation of synaptic transmission in the dentate area of the unanaesthetized rabbit following stimulation of the perforant path. J. Physiol. 232, 357–374.

Bliss, T. V. P., Collingridge, G. L. & Morris, R. G. M. (eds Andersen, P., Morris, R. G. M., Amaral, D. G., Bliss, T. V. P. & O'Keefe, J.) in The Hippocampus Book. 343–474 (Oxford Univ. Press, New York, 2007)

Bosch, M. and Hayashi, Y. (2012). Structural plasticity of dendritic spines. Curr Opin Neurobiol. 22, 383–388.

Britt, J.P., Benaliouad, F., McDevitt, R.A., Stuber, G.D., Wise, R.A., and Bonci, A. (2012). Synaptic and behavioral profile of multiple glutamatergic inputs to the nucleus accumbens. Neuron 76, 790–803.

Brown, L. L., Schneider, J. S., & Lidsky, T. I. (1997). Sensory and cognitive functions of the basal ganglia. Current opinion in neurobiology. 7, 157-63.

Brown, S.P., Hestrin, S. (2009). Intracortical circuits of pyramidal neurons reflect their long-range axonal targets. Nature 457, 1133-6.

Buschea, M.A., Chena, X., Henninga, H.A., Reichwaldd, J., Staufenbield, M., Sakmanna, B., and Konnertha, A. (2012). Critical role of soluble amyloid-β for early hippocampal hyperactivity in a mouse model of Alzheimer's disease. PNAS 109, 8740-5.

Calipari, E.S., Bagot, R.C., Purushothaman, I., Davidson, T.J., Yorgason, J.T., Peña, C.J., Walker, D.M., Pirpinias, S.T., Guise, K.G., Ramakrishnan, C., Deisseroth, K., Nestler, E.J. (2016). In vivo imaging identifies temporal signature of D1 and D2 medium spiny neurons in cocaine reward. PNAS 113, 2726–31.

Caravaca-Aguirre, A. M., Niv, E., Conkey, D. B., and Piestun, R., (2013). Real-time resilient focusing through a bending multimode fiber. Opt. Express. 21, 12881-12887.

Cembrowski, M.S., Phillips, M.G., DiLisio, S.F., Shields, B.C., Winnubst, J., Chandrashekar, J., Bas, E., Spruston, N. (2018). Dissociable structural and functional hippocampal outputs via distinct subiculum cell classes. Cell. 173, 1280-1292

Cetin, A., Komai, S., Eliava, M., Seeburg, P.H., Osten, P. (2006). Stereotaxic gene delivery in the rodent brain. Nat Protoc. 1, 3166-73.

Chen, X., Cao, H., Saraf, A., Zweifel, L.S., and Storm, D.R. (2015). Overexpression of the Type 1 Adenylyl Cyclase in the Forebrain Leads to Deficits of Behavioral Inhibition. J Neurosci. 35, 339-51.

Chersi, F., & Burgess, N. (2015). The cognitive architecture of spatial navigation: hippocampal and striatal contributions. Neuron. 88, 64–77.

Chiara, D.G. (2002). Nucleus accumbens shell and core dopamine: differential role in behavior and addiction. Behav Brain Res. 137, 75-114.

Cho, Y.T., Fudge, J.L. (2009). Heterogeneous dopamine populations project to specific subregions of the primate amygdala. J. Neurosci. 165, 1501-18.

Christoffel, D.J., Golden, S.A., Dumitriu, D., Robison, A.J., Janssen, W.G., Ahn, H.F., Krishnan, V., Reyes, C.M., Han, M.H., Ables, J.L., Eisch, A.J., Dietz, D.M., Ferguson, D., Neve, R.L., Greengard, P., Kim, Y., Morrison, J.H., Russo, S.J. (2011). IkappaB kinase regulates social defeat stress-induced synaptic and behavioral plasticity. J. Neurosci. 31, 314–21.

Ciocchi, S., Passecker, J., Malagon-Vina, H., Mikus, N., and Klausberger, T. (2015). Brain computation. Selective information routing by ventral hippocampal CA1 projection neurons. Science. 348, 560–563.

Cižmár, T. & Dholakia, K. (2012). Exploiting multimode waveguides for pure fibre-based imaging. Nat. Commun. 3, 1027.

Cohen, M.X., Axmacher, N., Lenartz, D., Elger, C.E., Sturm, V., Schlepper, T.E. (2009). Neuroelectric signatures of reward learning and decision-making in the human nucleus accumbens. J. Neuropsychopharmac. 34, 1649-58.

Conkey, D. B., Caravaca-Aguirre, A. M. & Piestun, R. (2012). High-speed scattering medium characterization with application to focusing light through turbid media. Opt. Express. 20, 1733.

Cox, J., Pinto, L. & Dan, Y. (2016). Calcium imaging of sleep–wake related neuronal activity in the dorsal pons. Nat. Communications. 7, 10763.

Crowe, S. E. & Ellis-Davies, G. C. R. (2014). Longitudinal in vivo two-photon fluorescence imaging. J. Comparative Neurology 522, 1708–27.

Dan, Y. & Poo, M. M. (2004). Spike timing-dependent plasticity of neural circuits. Neuron. 44, 23–30.

Danielson, N.B., Kaifosh, P., Zaremba, J.D., Lovett-Barron, M., Tsai, J., Denny, C.A., Balough, E.M., Goldberg, A.R., Drew, L.J., Hen, R., Losonczy, A., Kheirbek, M.A. (2016). Distinct contribution of adult-born hippocampal granule cells to context encoding. Neuron. 90, 101-12.

Dudek, S. M. & Bear, M. F. (1992). Homosynaptic long-term depression and effects of N-Methyl-D-aspartate receptor blockade. PNAS 89, 4363–4367.

Dudek, S. M. & Bear, M. F. (1993). Bidirectional long-term modification of synaptic effectiveness in the adult and immature hippocampus. J. Neurosci. 13, 2910–2918.

Dupret, D., O'Neill, J., Pleydell-Bouverie, B. & Csicsvari, J. (2010) The reorganization and reactivation of hippocampal maps predict spatial memory performance. Nat. Neurosci. 13, 995–1002.

Dombeck, D., Harvey, C. D., Tian, L., Looger, L. L. & Tank, D. W. (2010). Functional imaging of hippocampal place cells at cellular resolution during virtual navigation. Nat. Neurosci. 13, 1433–40.

Dombeck, D.A., Harvey, C.D., Tian, L., Looger, L.L. & Tank, D.W. (2010). Functional imaging of hippocampal place cells at cellular resolution during virtual navigation. Nat. Neurosci. 11, 1433-40.

El-Gaby, M., Zhang, Y., Wolf, K., Schwiening, C.J., Paulsen, O., Shipton, O.A. (2016). Archaerhodopsin selectively and reversibly silences synaptic transmission through altered pH. Cell Reports. 16, 2259-2268.

Engert, F. & Bonhoeffer, T. (1999). Dendritic spine changes associated with hippocampal long-term synaptic plasticity. Nature. 399, 66–70.

Evans, A. E., Kelly, C. M., Precious, S. V., and Rosser, A. E., (2012). Molecular regulation of striatal development: a review. Anatomy Research International, Article ID 106529, 14 pages.

Everitt, B. J. and Robbins, T. W. (2005). Neural systems of reinforcement for drug addiction: from actions to habits to compulsion. Nat. Neurosci. 8, 1481– 1489.

Fadok, J.P., Dickerson, T.M., Palmiter, R.D. (2009). Dopamine is necessary for cue-dependent fear conditioning. J. Neurosci. 29, 11089-11097.

Farovik, A., Dupont, L.M., Eichenbaum, H. (2010). Distinct roles for dorsal CA3 and CA1 in memory for sequential nonspatial events. Learn Memory. 17, 12–17.

Felix-Ortiz, A.C., Tye, K.M. (2014). Amygdala inputs to the ventral hippocampus bidirectionally modulate social behavior. J. Neurosci. 34, 586-95.

Flagel, S.B., Clark, J.J., Robinson, T.E., Mayo, L., Czuj, A., Willuhn, I., Akers, C.A., Clinton, S.M., Phillips, P.E., Akil, H. (2011). A selective role for dopamine in stimulus-reward learning. Nature. 469, 53–57.

Floresco, S.B. (2014). The nucleus accumbens: an interface between cognition, emotion, and action. Annu Rev Psychol. 66, 25-52.

Floresco, S.B., Blaha, C.D., Yang, C.R., Phillips, A.G. (2001b). Modulation of hippocampal and amygdalar-evoked activity of nucleus accumbens neurons by dopamine: cellular mechanisms of input selection. J. Neurosci. 21, 2851–60.

Flusberg, B.A., Nimmerjahn, A., Cocker, E.D., Mukamel, E.A., Barretto, R.P.J., Ko, T.H., Burns, L.D., Jung, J.C. & Schnitzer, M.J. (2008). High-speed, miniaturized fluorescence microscopy in freely moving mice. Nat. Methods. 5, 935-8.

French, S.J., Totterdell, S. (2003). Individual nucleus accumbens-projection neurons receive both basolateral amygdala and ventral subicular afferents in rats. J. Neurosci. 119, 19–31.

Freund, T.F., Antal, M. (1988). GABA-containing neurons in the septum control inhibitory interneurons in the hippocampus. Nature. 336, 170-3.

Ghosh, K., Burns, L., Cocker, E., Nimmerjahn, A., Ziv, Y., Gamal, A., Schnitzer, M. (2011) Miniaturized integration of a fluorescence microscope Nat. Methods 8, 871-8.

Gillies, A., Arbuthnott, G. (2000). Computational models of the basal ganglia. Movement Disorders. 762–770.

Glimcher, P. W. (2011). Understanding dopamine and reinforcement learning: the dopamine reward prediction error hypothesis. PNAS 108, 15647-54.

Gonzales, K.K., & Smith, Y. (2015). Striatal Cholinergic interneurons in the dorsal and ventral striatum: anatomical and functional considerations in normal and diseased conditions. Annals of the New York Academy of Sciences. 1349, 1–45.

Goto, A., Nakahara, I., Yamaguchi, T., Kamiok, Y., Sumiyam, K., Matsud, M., Nakanishi, S., and Funabiki, K. (2015). Circuit-dependent striatal PKA and ERK signaling underlies rapid behavioral shift in mating reaction of male mice. PNAS 112, 6718-23.

Goto, Y., and O'Donnell, P. (2001). Synchronous activity in the hippocampus and nucleus accumbens in vivo. J. Neurosci. Off. J. Soc. Neurosci. 21, 131.

Gray, J.A. (1982). The neuropsychology of anxiety: an enquiry into the functions of the septo-hippocampal system. Oxford Univ. Press: Oxford, U.K.

Greba, A., Kokkinidis, L. (2000). Peripheral and intraamygdalar administration of the dopamine D1 receptor antagonist SCH 23390 blocks fear-potentiated startle but not shock reactivity or the shock sensitization of acoustic startle. Behav. Neurosci. 114, 262-272.

Greba, A. Gifkins, L. Kokkinidis (2001). Inhibition of amygdaloid dopamine D2 receptors impairs emotional learning measured with fear-potentiated startle. Brain Res. 899, 218-226.

Groenewegen, H.J., Vermeulen-Van der Zee, E., Kortschot, A., Witter, M.P. (1987). Organization of the projections from the subiculum to the ventral striatum in the rat. A study using anterograde transport of phaseolus vulgarus leucoagglutinin. J. Neurosci. 23, 103–20.

Groenewegen, H.J., Mulder, A.B., Beijer, A.V.J., Wright, C.I., Lopes da Silva, F.H., Pennartz, C.M.A. (1999). Hippocampal and amygdaloid interactions in the nucleus accumbens. Psychobiology. 27, 149–64.

Groenewegen, H.J., Berendse, H.W., Meredith, G.E., Haber, S.N., Voorn, P. (1991). Functional anatomy of the ventral, limbic system-innervated striatum. In The Mesolimbic Dopamine System pp. 19–59. New York: Wiley & Sons

Gruart, A., Munoz, M. D. & Delgado-Garcia, J. M. (2006). Involvement of the CA3-CA1 synapse in the acquisition of associative learning in behaving mice. J. Neurosci. 26, 1077–1087.

Gu, L., Kleiber, S., Schmid, L., Nebeling, F., Chamoun, M., Steffen, J., Wagner, J. and Fuhrmann, M. (2014) Long-term in vivo imaging of dendritic spines in the hippocampus reveals structural plasticity. J. Neurosci. 34, 13948-13953.

Gu, L. Kleiber, S., Schmid, L., Nebeling, F., Chamoun, M., Steffen, J., Wagner, J., Fuhrmann, M. (2014). Long-term in vivo imaging of dendritic spines in the hippocampus reveals structural plasticity. J. Neurosci. 34, 13948–13953.

Guarraci, F.A., Frohardt, R.J., Kapp, B.S. (1999). Amygdaloid D1 dopamine receptor involvement in Pavlovian fear conditioning. Brain Res. 827, 28-40.

Guarraci, F.A., Frohardt, R.J., Falls, W.A., Kapp, B.S. (2000). The effects of intra-amygdaloid infusions of a D2 dopamine receptor antagonist on Pavlovian fear conditioning. Behav. Neurosci. 114, 647-651.

Han, X. (2017). Role of dopamine projections from ventral tegmental area to nucleus accumbens and medial prefrontal cortex in reinforcement behaviors assessed using optogenetic manipulation. Metab. Brain Dis. 32, 1491-1502.

Harris, K.M., Stevens, J.K. (1989). Dendritic spines of CA1 pyramidal cells in the rat hippocampus: serial electron microscopy with reference to their biophysical characteristics. J. Neurosci. 9, 2982–2997.

Hasselmo, M. E., and Schnell, E. (1994). Laminar selectivity of the cholinergic suppression of synaptic transmission in rat hippocampal region CA1: computational modeling and brain slice physiology. J. Neurosci. 14, 3898-3914.

Hasselmo, M. E., and Wyble, B. P. (1997). Free recall and recognition in a network model of the hippocampus: simulating effects of scopolamine on human memory function. Behav Brain Res. 89, 1-34.

Hasselmo, M. E. (2011). Models of hippocampus Scholarpedia 6, 1371.

Heimer, L., Wilson, R.D. (1975). The subcortical projections of allocortex: similarities in the neuronal associations of the hippocampus, the piriform cortex and the neocortex. In Golgi Centennial Symposium Proceedings: Perspectives in Neurobiology, ed. M Santini, 173–93.

Hope, J., Kesner, R. (2007). Role of CA3 and CA1 subregions of the dorsal hippocampus on temporal processing of objects. Neurobiol Learn Mem. 88, 225–231.

Huff, M.L., Miller, R.L., Deisseroth, K., Moorman, D.E., LaLumiere, R.T. (2013). Posttraining optogenetic manipulations of basolateral amygdala activity modulate consolidation of inhibitory avoidance memory in rats. PNAS. 110, 3597-602.

Hyman, S.E., Malenka, R.C., Nestler, E.J. (2006). Neural mechanisms of addiction: the role of reward-related learning and memory. Annu Rev Neurosci. 29, 565-98.

Ikemoto, S., Bonci, A. (2014). Neurocircuitry of drug reward. Neuropharmacology. 76, 329-341.

Ilango, A., Kesner, A.J., Keller, K.L., Stuber, G.D., Bonci, A., Ikemoto, S. (2014). Similar roles of substantia nigra and ventral tegmental dopamine neurons in reward and aversion. J. Neurosci. 34, 817–822.

Jennings, J.H., Ung, R.L., Resendez, S.L., Stamatakis, A.M., Taylor, J.G., Huang, J., Veleta, K., Kantak, P.A., Aita, M., Shilling-Scrivo, K., Ramakrishnan, C., Deisseroth, K., Otte, S., Stuber, G.D. (2015). Visualizing hypothalamic network dynamics for appetitive and consummatory behaviors. Cell. 160, 516-27.

Ji, X. and Martin, G.E. (2012). New rules governing synaptic plasticity in core nucleus accumbens medium spiny neurons. Eur J. Neurosci. 36, 3615–3627.

Johansen, J.P., Hamanaka, H., Monfils, M.H., Behnia, R., Deisseroth, K., Blair, H.T., LeDoux, J.E. (2010). Optical activation of lateral amygdala pyramidal cells instructs associative fear learning. PNAS. 107, 12692-7.

Kahn, I., Shohamy, D. (2013). Intrinsic connectivity between the hippocampus, nucleus accumbens, and ventral tegmental area in humans. Hippocampus 23, 187-92.

Kaifosh, P., Lovett-Barron, M., Turi, G.F., Reardon, T.R. & Losonczy, A. (2013). Septo-hippocampal GABAergic signaling across multiple modalities in awake mice. Nat. Neurosci. 16, 1182-4.

Kauer, J.A., Malenka, R.C. (2007). Synaptic plasticity and addiction. Nat Rev Neurosci. 8, 844-58.

Kawaguchi, Y. (1993). Physiological,morphological, and histochemical characterization of three classes of interneurons in rat neostriatum. J. Neurosci. 13, 4908 – 4923.

Kesner, R.P. (1998). Neural mediation of memory for time: role of hippocampus and medial prefrontal cortex. Psychological Bulletin Reviews. 5, 585–596.

Kim, K.M., Baratta, M.V., Yang, A., Lee, D., Boyden, E.S., Fiorillo, C.D. (2012). Optogenetic mimicry of the transient activation of dopamine neurons by natural reward is sufficient for operant reinforcement. PLoS One 7, 33612.

Kim, G. et al. (2017). Deep-brain imaging via epi-fluorescence Computational Cannula Microscopy. Sci. Rep. 7, 44791.

Kitamura, T., Sun, C., Martin, J., Kitch, L.J., Schnitzer, M.J., Tonegawa, S. (2015). Entorhinal Cortical Ocean Cells Encode Specific Contexts and Drive Context-Specific Fear Memory. Neuron. 87, 1317-1331.

Kiyatkin, E. A., Andrebec, C. G. (1996). Dopaminergic modulation of glutamate-induced excitations of neurons in the neostriatum and nucleus accumbens of awake, unrestrained rats. J. Neurophysiol. 75, 142–153.

Klausberger, T., Somogyi, P. (2008). Neuronal diversity and temporal dynamics: the unity of hippocampal circuit operations. Science. 321, 53-7.

Knutson, B., Adams, C.M., Fong, G.W., and Hommer, D. (2001). Anticipation of increasing monetary reward selectively recruits nucleus accumbens. J. Neurosci. 21, 159.

Koob, G.F., Volkow, N.D. (2010). Neurocircuitry of addiction. Neuropsychopharmacology. 35, 217-38.

Koos, T., Tepper, J.M., and Wilson, C.J. (2004). Comparison of IPSCs evoked by spiny and fast-spiking neurons in the neostriatum. J. Neurosci. 24, 7916-22.

Koós, T. and Tepper, J.M. (1999). Inhibitory control of neostriatal projection neurons by GABAergic interneurons. Nat. Neurosci. 2, 467-72.

LaLumiere, R.T. (2014). Optogenetic dissection of amygdala functioning Front Behav Neurosci. 8, 107.

Lansink, C.S., Jackson, J.C., Lankelma, J.V., Ito, R., Robbins, T.W., Everitt, B.J., and Pennartz, C.M.A. (2012). Reward cues in space: commonalities and differences in neural coding by hippocampal and ventral striatal ensembles. J. Neurosci. Off. J. Soc. Neurosci. 32, 12444–12459.

Leonga, A. T. L., Chana, R. W., Gaoa, P. P., Chanc, Y, Tsiab, K K., Yungd, W, and Wua, E X. (2018). Long-range projections coordinate distributed brain-wide neural activity with a specific spatiotemporal profile. PNAS 113, 8306-8315.

Leutgeb, S., Leutgeb, J.K., Barnes, C.A., Moser, E.I., McNaughton, B.L., and Moser, M.-B. (2005). Independent codes for spatial and episodic memory in hippocampal neuronal ensembles. Science. 309, 619–623.

Levy, W.B. (1996). A sequence predicting CA3 is a flexible associator that learns and uses context to solve hippocampal-like tasks. Hippocampus. 6, 579-90.

Lindon, C., Nigg, E. A., Pines, J., Williams, B. C., Mochida, S., Zhao, Y., ... Hunt, T. (2010). Cholinergic interneurons control local circuit activity and cocaine conditioning. Science. 1677–1682.

Lisman, J.E. (1999). Relating hippocampal circuitry to function: recall of memory sequences by reciprocal dentate-CA3 interactions. Neuron. 22, 233-42.

Loterie, D., Farahi S., Papadopoulos, I., Goy, A., Psaltis, D., and Moser, C. (2015). Digital confocal microscopy through a multimode fiber. Opt. Express. 23, 23845.

Loterie D., Psaltis D., and Moser C., (2017). Bend translation in multimode fiber imaging. Opt. Express. 25, 6263-6273.

Lovett-Barron, M., Kaifosh, P., Kheirbek, M.A., Danielson, N., Zaremba, J.D., Reardon, T.R., Turi, G.F., Hen, R., Zemelma, B.V., Losonczy, A. (2014). Dendritic inhibition in the hippocampus supports fear learning. Science. 343, 857-63.

Luscher, C.J. (2010). Drug-evoked synaptic plasticity in addiction: from molecular changes to circuit remodeling. Neuron. 69, 650–663.

MacAskill, AF., Little, JP., Cassel, JM., Carter, AG. (2012). Subcellular connectivity underlies pathway-specific signaling in the nucleus accumbens. Nat. Neurosci. 15, 1624-6.

Mahalati, R. N., Gu, R. Y. & Kahn, J. M. (2013). Resolution limits for imaging through multi-mode fiber. Opt. Express. 21, 1656.

Malenka, R. C. & Bear, M. F. (2004). LTP and LTD: an embarrassment of riches. Neuron. 44, 5–21.

Maletic-Savatic, M., Malinow, R. & Svoboda, K. (1999). Rapid dendritic morphogenesis in CA1 hippocampal dendrites induced by synaptic activity. Science. 283, 1923–1927.

Mallet, N., Le Moine, C., Charpier, S., Gonon, F. (2005). Feedforward inhibition of projection neurons by fast-spiking GABA interneurons in the rat striatum in vivo. J. Neurosci. 25, 3857–3869.

Manns, J.R., Howard, M.W. (2007). Gradual changes in hippocampal activity support remembering the order of events. Eichenbaum H Neuron. 56, 530-40.

Marr, D. (1971). Simple memory: A theory for archicortex. Phil Trans Roy Soc B. 262, 23-81.

McNamara, C.G., Tejero-Cantero, A., Trouche, S., Campo-Urriza, N. & Dupret, D. (2014). Dopaminergic neurons promote hippocampal reactivation and spatial memory persistence. Nat. Neurosci. 17, 1658–1660.

McNaughton, B. L., and Morris, R. G. M. (1987). Hippocampal synaptic enhancement and information storage within a distributed memory system. Trends Neurosci. 10, 408-415.

Mendoza, M.L., Anderson, E.M., Kourrich, S., and Eisch, A.J. (2016). A NAc for Spinal Adjustments After Cocaine or Stress. Biol Psychiatry. 79, 872–874.

Meredith, G. E.; Pennartz, C. M.A.; Groenewegen, H. J. (1993). The cellular framework for chemical signalling in the nucleus accumbens. Chemical Signalling in the Basal Ganglia. Progress in Brain Research. 99, 3–24.

Meredith, G.E.; Agolia, R.; Arts, M.P.M.; Groenewegen, H.J.; Zahm, D.S. (1992). Morphological differences between projection neurons of the core and shell in the nucleus accumbens of the rat. J. Neurosci. 50, 149–62.

Misgeld, T., Kerschensteiner, M. (2006). In vivo imaging of the diseased nervous system. Nat Rev Neurosci. 7, 449-63.

Mitchell, K. J., Turtaev, S., Padgett, M. J., Čižmár, T. & Phillips, D. B. (2016). High-speed spatial control of the intensity, phase and polarisation of vector beams using a digital micro-mirror device. Opt. Express 24, 29269.

Mizrahi, A., Crowley, J.C., Shtoyerman, E., Katz, L.C. (2004). High-resolution in vivo imaging of hippocampal dendrites and spines. J. Neurosci. 24, 3147– 3151.

Mizuseki, K., Sirota, A., Pastalkova, E., & Buzsáki, G. (2009). Theta oscillations provide temporal windows for local circuit computation in the entorhinal-hippocampal loop. Neuron 64, 267–80.

Mogenson, G.J., Jones, D.L., and Yim, C.Y. (1980). From motivation to action: functional interface between the limbic system and the motor system. Prog. Neurobiol. 14, 69–97.

Montgomery, J. M. & Madison, D. V. (2002). State-dependent heterogeneity in synaptic depression between pyramidal cell pairs. Neuron 33, 765–777.

Moolman, D.L., Vitolo, O.V., Vonsattel, J.P., Shelanski, M.L. (2004). Dendrite and dendritic spine alterations in Alzheimer models. J Neurocytol. 33, 377-87.

Morris, R. G., Garrud, P., Rawlins, J. N. & O'Keefe, J. (1982). Place navigation impaired in rats with hippocampal lesions. Nature 297, 681–683.

Morales-Delgado, E. E., Farahi, S., Papadopoulos, I. N., Psaltis, D. & Moser, C. (2015). Delivery of focused short pulses through a multimode fiber. Opt. Express 23, 9109.

Muhammad, A., Carroll, C., Kolb, B. (2012). Stress during development alters dendritic morphology in the nucleus accumbens and prefrontal cortex. J. Neurosci. 216, 103–9.

Murayama, M., Pérez-Garci, E., Nevian, T., Bock, T., Senn, W. & Larkum, M.E. (2009). Dendritic encoding of sensory stimuli controlled by deep cortical interneurons. Nature 457, 1137-41.

Nader, K., LeDoux, J.E. (1999). Inhibition of the mesoamygdala dopaminergic pathway impairs the retrieval of conditioned fear associations. Behav. Neurosci, 113, 891-901.

Nestler, E.J. (2001). Molecular basis of long-term plasticity underlying addiction. Nat Rev Neurosci. 2, 119-28.

Neves, G., Cooke, S.F. & Bliss, T.V.P. (2008). Synaptic plasticity, memory and the hippocampus: a neural network approach to causality. Nat. Reviews Neurosci. 9, 65–75.

Norman, K.A., O'Reilly, R.C. (2003). Modeling hippocampal and neocortical contributions to recognition memory: a complementary-learning-systems approach. Psychol Rev. 110, 611-46.

Norrholm, S.D., Bibb, J.A. Nestler, E.J., Ouimet, C.C., Taylor, J.R., and Greengard, P. (2016). Cocaine-induced proliferation of dendritic spines in nucleus accumbens in dependent on the activity of cyclin-dependent kinase J. Neurosci. 116, 19-22.

O'Donnell, P., Grace, A.A. (1994). Tonic D2-mediated attenuation of cortical excitation in nucleus accumbens neurons recorded in vitro. Brain Res. 634, 105–12.

Ohayon, S., Aguirre, A.M.C., Piestun, R., DiCarlo, J.J. (2017). Deep brain fluorescence imaging with minimally invasive ultra-thin optical fibers. bioRxiv 116350.

O'Keefe, J. & Dostrovsky, J., (1971). The hippocampus as a spatial map. Preliminary evidence from unit activity in the freely-moving rat. Brain Research, 34, 171–175.

O'Keefe, J. (1976). Place units in the hippocampus of the freely moving rat. Exp Neurol. 51, 78-109.

Okun, M., Steinmetz, N. A., Cossell, L., Iacaruso, M. F., Ko, H., Bartho, P., Harris, K. D. (2015). Diverse coupling of neurons to populations in sensory cortex. Nature 521, 511–515.

Omar, J. A. and Mayank, R. M. (2009). The hippocampal rate code: anatomy, physiology and theory. Trends in Neurosci. 32, 329-38.

O'Neill, J. et al. (2010). Play it again: reactivation of waking experience and memory. Trends in Neurosci. 33, 220–9.

O'Neill, J., Senior, T.J., Allen, K., Huxter, J.R. & Csicsvari, J. (2008). Reactivation of experience-dependent cell assembly patterns in the hippocampus. Nat. Neurosci. 11, 209–215.

Papadopoulos, I.N., Farahi, S., Moser, C., and Psaltis, D., (2013). High-resolution, lensless endoscope based on digital scanning through a multimode optical fiber. Biomed. Opt. Express 4, 260-270.

Pascoli, V., Terrier, J., Hiver, A., Luscher, C. (2015). Sufficiency of mesolimbic dopamine neuron stimulation for the progression to addiction. Neuron 88, 1054–1066.

Petralia, R.S., Esteban, J.A., Wang, Y.X., Partridge, J.G., Zhao, H.M., Wenthold, R.J., Malinow, R. (1999). Selective acquisition of AMPA receptors over postnatal development suggests a molecular basis for silent synapses. Nat. Neurosci. 2, 31–36.

Pfeiffer, B. E., & Foster, D. J. (2013). Hippocampal place-cell sequences depict future paths to remembered goals. Nature 497, 74–79.

Phillips, R.G, LeDoux, J.E. (1992). Differential contribution of amygdala and hippocampus to cued and contextual fear conditioning. Behav Neurosci. 106, 274–285.

Phillips, R.G., LeDoux, J.E. (1994). Lesions of the dorsal hippocampal formation interfere with background but not foreground contextual fear conditioning. Learn Mem. 1, 34–44.

Pinto, L., Dan, Y. (2015). Cell-type-specific activity in prefrontal cortex during goal-directed behavior. Neuron 87, 437-50.

Pitkänen, A., Stefanacci, L., Farb, C.R., Go, G.G., LeDoux, J.E., Amaral, D.G. (1995). Intrinsic connections of the rat amygdaloid complex: projections originating in the lateral nucleus. J Comp Neurol. 356, 288-310.

Pitkänen, A., Pikkarainen, M., Nurminen, N., Ylinen, A. (2000). Reciprocal connections between the amygdala and the hippocampal formation, perirhinal cortex, and postrhinal cortex in rat. Ann N Y Acad Sci. 911, 369-91.

Plöschner, M., Tyc, T., & Čižmár, T. (2015). Seeing through chaos in multimode fibres. Nat. Photonics 9, 529–535.

Plöschner, M., Cizmar, T. (2015). Compact multimode fiber beam-shaping system based on GPU accelerated digital holography. Opt. Lett. 40, 197–200.

Plöschner, M., Straka, B., & Dholakia, K. (2014). GPU accelerated toolbox for real-time beam-shaping in multimode fibres. Opt. Lett. 22, 10583–10590.

Plöschner, M., Tyc, T. & Čižmár, T. (2015). Seeing through chaos in multimode fibres. Nat. Photonics 9, 529–535.

Ponzi, A., Wickens, J.R. (2013). Optimal balance of the striatal medium spiny neuron network. PLoS Comput Biol. 9, 1002954.

Rajasethupathy, P., Sankaran, S., Marshel, J.H., Kim, C.K., Ferenczi, E., Lee, S.Y., Berndt, A., Ramakrishnan, C., Jaffe, A., Lo, M., Liston, C. & Deisseroth, K. (2015). Projections from neocortex mediate top-down control of memory retrieval. Nature 526, 653-9.

Rensing, N., Ouyang, Y., Yang, X.F., Yamada, K.A., Rothman, S.M., Wong, M. (2005). In vivo imaging of dendritic spines during electrographic seizures. Ann. Neurol. 58, 888–898

Resendez, S. L. et al. (2016). Visualization of cortical, subcortical and deep brain neural circuit dynamics during naturalistic mammalian behavior with head-mounted microscopes and chronically implanted lenses. Nat. Protoc. 11, 566–97.

Rickgauer, J.P., Deisseroth, K. & Tank, D.W. (2014). Simultaneous cellular-resolution optical perturbation and imaging of place cell firing fields. Nat. Neurosci. 17, 1816-24.

Robinson, T.E., Kolb, B. (1999). Alterations in the morphology of dendrites and dendritic spines in the nucleus accumbens and prefrontal cortex following repeated treatment with amphetamine or cocaine. Eur J Neurosci. 11, 1598-604.

Robinson, T.E., Gorny, G., Mitton, E., Kolb, B. (2001). Cocaine self-administration alters the morphology of dendrites and dendritic spines in the nucleus accumbens and neocortex. Synapse 39, 257-66.

Robinson, A.J. and Nestler, E.J. (2011). Transcriptional and epigenetic mechanisms of addiction. Nat. Reviews Neurosci. 12, 623–37.

Rolls, E.T., Kesner, R.P. (2006). A computational theory of hippocampal function, and empirical tests of the theory. Neurobiol. 79, 1-48.

Rolls, E.T. (2007). An attractor network in the hippocampus: theory and neurophysiology. Learn Mem. 14, 714-31.

Ron, D. and Barak, S. (2016). Molecular mechanisms underlying alcohol-drinking behaviours. Nat. Review 17, 576-91.

Russo, S.J., Dietz, D.M., Dumitriu, D., Morrison, J.H., Malenka, R.C., Nestler, E.J. (2010). The addicted synapse: mechanisms of synaptic and structural plasticity in nucleus accumbens. Trends Neurosci. 33, 267-76.

Russo, S.J. and Nestler, E.J. (2013). The brain reward circuitry in mood disorders. Nat. Reviews Neurosci. 14, 736.

Rutherford, H.J., Williams, S.K., Moy, S., Mayes, L.C., Johns, J.M. (2011). Disruption of maternal parenting circuitry by addictive process: rewiring of reward and stress systems. Front Psychiatry. 2, 37.

Schacter, G.B., Yang, C.R., Innis, N.K., and Mogenson, G.J. (1989). The role of the hippocampal-nucleus accumbens pathway in radial-arm maze performance. Brain Res. 494, 339–349.

Schermer, R., (2007). Mode scalability in bent optical fibers. Opt. Express 15, 15674-15701.

Schultz, W. (2007). Behavioral dopamine signals. Trends Neurosci 30, 203–210.

Schultz, W. (2013). Updating dopamine reward signals. Curr Opin Neurobiol 23, 229–238.

Sharott, A., Moll, C.K.E., Engler, G., Denker, M., Grün, S., Engel, A.K. (2009). Different subtypes of striatal neurons are selectively modulated by cortical oscillations. J. of Neurosci. 29, 4571-4585.

Sheffield, M. E. J. & Dombeck, D. A. (2015). Calcium transient prevalence across the dendritic arbour predicts place field properties. Nature 517, 200-4.

Sjulson, L., Peyrache, A., Cumpelik, A., Cassataro, D., and Buzsáki, G. (2017). Cocaine place conditioning strengthens location-specific hippocampal inputs to the nucleus accumbens. BioRxiv 105890.

Smith, Y., Villalba, R.M., Raju, D.V. (2009). Striatal spine plasticity in Parkinson's disease: pathological or not? Parkinsonism Relat Disord. 15, 156-61.

Soden, M.E., Jones, G.L., Sanford, C.A., Chung, A.S., Güler, A.D., Chavkin, C., Luján, R., Zweifel, L.S. (2013). Disruption of dopamine neuron activity pattern regulation through selective expression of a human KCNN3 Mutation. Neuron 80, 997-1009.

Sombers, L. A., Beyene, M., Carelli, R. M., Wightman, R. M. (2009). Synaptic overflow of dopamine in the nucleus accumbens arises from neuronal activity in the ventral tegmental area. J. Neurosci. 29, 1735–1742.

Spemann, H.; Mangold, Hilde (1924). Über Induktion von Embryonalanlagen durch Implantation artfremder Organisatoren. (Induction of Embryonic Primordia by Implantation of Organizers from a Different Species) Archiv für mikroskopische Anatomie und Entwicklungsmechanik (in German). 100, 599–638.

Staubli, U. & Lynch, G. (1990). Stable depression of potentiated synaptic responses in the hippocampus with 1–5Hz stimulation. Brain Res. 513, 113–118.

Steward, O., Scoville, S.A. (1976). Cells of origin of entorhinal cortical afferents to the hippocampus and fascia dentata of the rat. J Comp Neurol. 169, 347-70.

Stuber, G.D., Britt, J.P., and Bonci A. (2012). Optogenetic modulation of neural circuits that underlie reward seeking. Biol Psychiatry 71, 1061-7.

Sun, Y., Nguyen, A., Nguyen, J., Le, L., Saur, D., Choi, J., Callaway, E.M., and Xu, X. (2014). Cell-type specific circuit connectivity of hippocampal CA1 revealed through Cre-dependent rabies tracing. Cell Rep. 7, 269-80.

Sylvian, G. (2017). Optical microscopy aims deep. Nat. Photonics 11, 14-16.

Szabo, V., Ventalon, C., De Sars, V., Bradley, J. & Emiliani, V. (2014). Spatially selective holographic photoactivation and functional fluorescence imaging in freely behaving mice with a fiberscope. Neuron 1–13.

Tabuchi, E.T., Mulder, A.B., and Wiener, S.I. (2000). Position and behavioral modulation of synchronization of hippocampal and accumbens neuronal discharges in freely moving rats. Hippocampus 10, 717–728.

Takumi, Y., Ramirez-Leon, V., Laake, P., Rinvik, E., Ottersen, O.P. (1999). Different modes of expression of AMPA and NMDA receptors in hippocampal synapses. Nat Neurosci. 2, 618–624.

Tang, Q., Tsytsarev, V., Liang, C.P., Akkentli, F., Erzurumlu, R.S., Chen, Y. (2016). In vivo voltage-sensitive dye imaging of subcortical brain function. Sci Rep. 5, 17325.

Tepper, J.M., Bolam, J.P. (2004). Functional diversity and specificity of neostriatal interneurons. Curr Opin Neurobiol. 14, 685-92.

Tepper, J. M., Tecuapetla, F., Koós, T., & Ibáñez-Sandoval, O. (2010). Heterogeneity and diversity of striatal GABAergic interneurons. Frontiers in Neuroanatomy 4, 150.

Tepper, J.M. and Koos, T. (2010). GABAergic interneurons of the striatum. Handbook of Behavioral Neurosci. 20, 151-166.

Treves, A. (2004). Computational constraints between retrieving the past and predicting the future, and the CA3-CA1 differentiation. Hippocampus 14, 539-556.

Trouche, S., Koren, V., Doig, N. M., Ellender, T. J., El-Gaby, M., Lopes-dos-Santos, V., Reeve, H. M., Perestenko, P. V., Garas, F. N., Magill, P. J., Sharott, A., Dupret, D. (2019). A hippocampus-accumbens tripartite neuronal motif guides appetitive memory in space. Cell DOI:https://doi.org/10.1016/j.cell.2018.12.037

Tsien, J.Z., Chen, D.F., Gerber, D., Tom, C., Mercer, E.H., Anderson, D.J., Mayford, M., Kandel, E.R., Tonegawa, S. (1996a). Subregion- and cell type-restricted gene knockout in mouse brain. Cell 87, 1317–1326.

Turner, B.D., Kashima, D.T., Manz, K.M., Grueter, C.A., Grueter, B.A. (2018). Synaptic plasticity in the nucleus accumbens: lessons learned from experience. ACS Chem Neurosci. 9, 2114-2126.

Turtaev, S., Leite, I., Mitchell, K., Padgett, M., Phillips, D., and Čižmár, T., (2017). Comparison of nematic liquid-crystal and DMD based spatial light modulation in complex photonics. Opt. Express 25, 29874-29884.

Van Strien, N. M., Cappaert, N. L. M. and Witter, M. P. (2009). The anatomy of memory: an interactive overview of the parahippocampal– hippocampal network. Nat. Review 10, 272-82.

Vandecasteele, M., Glowinski, J., & Venance, L. (2005). Electrical synapses between dopaminergic neurons of the substantia nigra pars compacta. The J. of Neurosci 25, 291-8.

Varela, C., Weiss, S., Meyer, R., Halassa, M., Biedenkapp, J., Wilson, M., Goosens, K., Bendor, D. (2016). Tracking the time-dependent role of the hippocampus in memory recall using DREADDs. PLoS ONE. 11.

Vasquez-Lopez, S.A, Koren, V., Ploschner, M., Padamsey, Z., Cizmar, T., Emptage, N. J. (2018). Minimally invasive deep-brain imaging through a 50 μm-core multimode fibre. bioRxiv 289793.

Villette, V., Malvache, A., Tressard, T., Dupuy, N., Cossart, R. (2015). Internally Recurring Hippocampal Sequences as a Population Template of Spatiotemporal Information. Neuron 88, 357-66.

Villalba, R.M., Smith, Y.J. (2018). Loss and remodeling of striatal dendritic spines in Parkinson's disease: from homeostasis to maladaptive plasticity? Neural Transm (Vienna). 125, 431-447.

Vincent, P., Maskos, U., Charvet, I., Bourgeais, L., Stoppini, L., Leresche, N., Changeux, J.P., Lambert, R., Meda, P. and Paupardin-Tritsch D. (2006). Live imaging of neural structure and function by fibred fluorescence microscopy. EMBO Reports 7, 1154-61.

Voorn, P., Vanderschuren, L. J., Groenewegen, H. J., Robbins, T. W., and Pennartz, C. M. (2004). Putting a spin on the dorsal-ventral divide of the striatum. Trends Neurosci. 27, 468– 474.

Wickens, J, Arbuthnott, G. (1993). The corticostriatal system on computer simulation: an intermediate mechanism for sequencing of actions. In: Arbuthnott G, Emson P, eds. Progress in Brain Research, vol 99.

Wiegert, J.S., Mahn, M., Prigge, M., Printz, Y., Yizhar, O. (2017). Silencing Neurons: Tools, Applications, and Experimental Constraints. Neuron 95, 504-529.

Whitlock, J. R., Heynen, A. J., Shuler, M. G. & Bear, M. F. (2006). Learning induces long-term potentiation in the hippocampus. Science 313, 1093–1097.

Wilson, M.A., and McNaughton, B.L. (1993). Dynamics of the hippocampal ensemble code for space. Science 261, 1055–1058.

Wilson, C.J., Chang, H.T., Kitai, S.T. (1990). Firing patterns and synaptic potentials of identified giant spiny interneurons in the rat neostriatum. J Neurosci. 10, 508 –519.

Witten, I.B., Lin, S.C., Brodsky, M., Prakash, R., Diester, I., Anikeeva, P., Gradinaru, V., Ramakrishnan, C., Deisseroth, K. (2010). Cholinergic interneurons control local circuit activity and cocaine conditioning. Science 330, 1677–81.

Witten, I.B., Steinberg, E.E., Lee, S.Y., Davidson, T.J., Zalocusky, K.A., Brodsky, M., Yizhar O., Cho, S.L., Gong, S., Ramakrishnan, C., Stuber, G.D., Tye, K.M., Janak, P.H., Deisseroth, K. (2011). Recombinase-driver rat lines: tools, techniques, and optogenetic application to dopamine-mediated reinforcement. Neuron 72, 721–733.

Xia, L., Nygard, S.K., Sobczak, G.G., Hourguettes, N.J., Bruchas, M.R. (2017). Dorsal-CA1 Hippocampal Neuronal Ensembles Encode Nicotine-Reward Contextual Associations. Cell Rep. 19, 2143-2156.

Xu, H., Pan, F., Yang, G. & Gan, W. (2007). Choice of cranial window type for *in vivo* imaging affects dendritic spine turnover in the cortex. Nat. Neurosci. 10, 549–551.

Yamaguchi, T., Goto, A., Nakahara, I., Yawata, S., Hikida, T., Matsuda, M., Funabiki, K., and Nakanishia, S. (2015). Role of PKA signaling in D2 receptor-expressing neurons in the core of the nucleus accumbens in aversive learning. PNAS 112, 11383-8.

Yukihiko, S., Shigeyuki, C. (2006). Neurochemistry of the Nucleus Accumbens and Its Relevance to Depression and Antidepressant Action in Rodents. Current Neuropharmacology. 4, 277–91.

Zaborszky, L., Alheid, G.F., Beinfeld, M.C., Eiden, L.E., Heimer, L., Palkovits, M. (1985). Cholecystokinin innervation of the ventral striatum: a morphological and radioimmunological study. J. Neurosci. 14, 427–53.

Zahm, D.S., Heimer, L. (1990). Two transpallidal pathways originating in the nucleus accumbens. J. Comp. Neurol. 302, 437–46.

Zahm, D.S., Brog, J.S. (1992). On the significance of subterritories in the “accumbens” part of the rat ventral striatum. J. Neurosci. 50, 751–67.

Zahm, D.S. (2000). An integrative neuroanatomical perspective on some subcortical substrates of adaptive responding with emphasis on the nucleus accumbens. Neurosci. Biobehav. Rev. 24, 85–105.

Zahm, D.S. (2008). Accumbens in a functional-anatomical systems context. In The Nucleus Accumbens: Neurotransmitters and Related Behaviors. ed. HN David, 1–36.

Ziv, Y., Burns, L., Cocker, E., Hamel, E., Ghosh, K., Kitch, L., Gamal, A., Schnitzer, M. (2013). Long-term dynamics of CA1 hippocampal place codes. Nat. Neurosci. 16, 264-6.